Università degli Studi di Napoli Federico II

Dottorato di Ricerca in Fisica

Ciclo: XXXVI

Coordinatore: Prof. Vincenzo Canale

Quantum Gravity Theory and Gamma Ray Astrophysics

Settore Scientifico Disciplinare: FIS/02

Dottorando

Domenico Frattulillo

Tutor

Prof. Giovanni Amelino-Camelia

Prof. Flavio Mercati

Anni: 2020/2024

Abstract

In this dissertation many of the main results I achieved during my Ph.D. are presented. Specifically, I dealt with both theoretical and phenomenological aspects of quantum gravity.

In the first part of this thesis we investigate some conceptual aspects that emerge when we consider quantum spacetimes whose relativistic symmetries are deformed at Planck-scale. In particular, we first study the properties of Noether charges in quantum spacetimes focusing on first-quantized particles described within a Hamiltonian framework, finding that their definition is strictly related to the form of the interaction potential. Then, we explore how deformations of symmetries can affect the role of observers and the properties of reference frames by focusing on a quantum group toy model. In particular, we deal with a simplified model in which two observers are just interested in the relative orientation among their frames assuming that the rotational invariance of spacetime is described by the quantum group $SU_q(2)$. Within this framework, we show the quantizazion of one of the Euler angles and a novel paradigm of agency-dependence of spacetime emerges, namely the properties of spacetime points depend on some choices made by the observer.

In the second part of this thesis, we present an in-depth study of in-vacuo dispersion in quantum spacetimes that is the most active area of quantum-gravity phenomenology. It is indeed well understood that cosmological distances are huge amplifier for the tiny Planck-scale effects, such that they can be within the reach of our current sensitivity. We present the most general formula for the time of flight of particle in DSR-deformed expanding spacetimes of FLRW type, that admits just three possible forms of redshift dependence and we discuss some noteworthy special scenarios. Finally, we conclude this dissertation with a novel analysis of in-vacuo dispersion through gamma ray bursts, also including data coming from the recently observed GRB221009A, obtaining intriguing indications on the possibility of having a non-monotonic dependence of the time delay on the redshift distance of the source.

Papers discussed in this thesis

- G. Amelino-Camelia, **D. Frattulillo**, G. Gubitosi, G. Rosati and S. Bedic, "Phenomenology of DSR-relativistic in-vacuo dispersion in FLRW spacetime," [arXiv:2307.05428 [gr-qc]](accepted for publication in JCAP).

- G. Amelino-Camelia, G. Fabiano and **D. Frattulillo**, "Total momentum and other Noether charges for particles interacting in a quantum spacetime," [arXiv:2302.08569 [hep-th]].

- G. Amelino-Camelia, V. D'Esposito, G. Fabiano, **D. Frattulillo**, P. A. Höhn, and F. Mercati, "Quantum euler angles and agency-dependent spacetime," Progress of Theoretical and Experimental Physics, p. ptae015, 01 2024

Other papers

- M. Arzano, A. D'Alise and **D. Frattulillo**, "Entanglement entropy in conformal quantum mechanics," JHEP **10** (2023), 165

- A. D'Alise, G. Fabiano, **D. Frattulillo**, S. Hohenegger, D. Iacobacci, F. Pezzella and F. Sannino, "Positivity conditions for generalized Schwarzschild space-times," Phys. Rev. D **108** (2023) no.8, 084042

- A. D'Alise, G. De Nardo, M. G. Di Luca, G. Fabiano, **D. Frattulillo**, G. Gaudino, D. Iacobacci, M. Merola, F. Sannino and P. Santorelli, *et al.* "Standard model anomalies: lepton flavour non-universality, g − 2 and W-mass," JHEP **08** (2022), 125

- A. Addazi, *et al.* (**COST CA18108 collaboration**) "Quantum gravity phenomenology at the dawn of the multi-messenger era—A review," Prog. Part. Nucl. Phys. **125** (2022), 103948

- R. Loll, G. Fabiano, **D. Frattulillo** and F. Wagner, "Quantum Gravity in 30 Questions," PoS **CORFU2021** (2022), 316

- R. Alves Batista, *et al.* (**COST CA18108 collaboration**) "White Paper and Roadmap for Quantum Gravity Phenomenology in the Multi-Messenger Era," [arXiv:2312.00409 [gr-qc]].

- P. Bosso, G. Fabiano, **D. Frattulillo** and F. Wagner, "Fate of Galilean relativity in minimal-length theories," Phys. Rev. D **109** (2024) no.4, 046016.

Contents

Chapter 1

Introduction

The work presented in this dissertation deals with both theoretical and phenomenological aspects of quantum gravity.

Our current description of Nature is based on two of the most successful theories of the history: quantum mechanics and general relativity.

The former is a theory that provides an accurate description of the microscopic world applying relativistic quantum field theory. In particular, it is formulated in a flat spacetime background where all the gravitational effects are neglected.

On the other side, general relativity is the present description of gravity at large length scales and it is a classical theory which neglects all the quantum properties of particles.

Even if these two theories are very successful in their own regime of validity, after about a century of research, we still don't know how to apply them in a regime in which both gravitational and quantum aspects should be taken into account, like for example a collision between two particles with impact parameter comparable with the Planck-length ℓ_p and energies of the order of the Planck-energy E_p:

$$E_p = \sqrt{\frac{\hbar}{G_N}} \simeq 1.2 \cdot 10^{19} GeV, \qquad \ell_p = \sqrt{\hbar G_N} \simeq 1.6 \cdot 10^{-35} m \tag{1.1}$$

where $\hbar$ is the Planck constant, G_N is the gravitational constant and the speed of light $c = 1$ in our units.

We could attempt to apply both theories simultaneously in such physical regime, but it is widely acknowledged that such endeavors do not yield any meaningful results.

For about one hundred years people addressed this quantum gravity problem thinking that indications from experiments would never come. In fact, Planck-energy is too above the highest energies we are presently able to reach at particle accelerators, and achieving energies of that magnitude is certainly completely outside our (near future) capabilities. Hence, it appeared unavoidable for theorists to base their studies only on certain conceptual criteria and over the years many candidates for a quantum gravity theory have been proposed in literature. Among such theories, the most famous approaches are String Theory [1–4], Loop Quantum Gravity [5–8] and some models based on non-commutative spacetimes [9–12], but many other approaches to the quantum gravity problem has been recently proposed [13–21]. But of course, to achieve significant progress in addressing the quantum gravity problem, some experimental indications are necessary.

In this direction, few decades ago, the possibility of a quantum gravity phenomenology has emerged and it is recently becoming more and more concrete [22–24]. This research program is based on the attempt of considering physical effects which should be low-energy remnants of the Planck-scale physics, and could be within the reach of our current sensitivity. Specifically, some candidate theories of quantum gravity give some predictions for the Planck-scale physics which, at the energy scales presently accessible in the experiments, leave some detectable traces. The main idea of this line of research is to look for amplifiers enlarging the tiny effects expected from quantum gravity, making them measurable through our present apparata.

The largest area of the quantum gravity phenomenology research concerns possible departures from Lorentz invariance at Planck-scale, focusing in particular on possible modifications of the energy-momentum relations. These are suggested by many approaches to the quantum gravity problem [25–28]. In this context we can distinguish between two scenarios. A first one in which relativistic invariance is broken (LIV), giving rise to a preferred frame picture, while another possibility is that relativistic invariance is merely deformed (DSR), preserving the equivalence of reference frames but requiring a deformation of relativistic laws of transformation among observers (see section 1.3.1).

Possible modifications of the energy-momentum dispersion relation at first order in the quantum gravity scale (the first order is sufficient for phenomenological purposes) can be written as:

$$m^2 \simeq E^2 - p^2 \pm p^2 \left(\frac{E}{E_{QG}}\right) , \tag{1.2}$$

where E_{QG} is the quantum gravity scale, expected to be around the Planck-energy, $\pm$ refers to the sign of the deformation, E, p and m are respectively the energy, the momentum and the mass of the particle.

One of the most studied effect in this framework is "in-vacuo-dispersion" according to which the speed of light in vacuum becomes energy dependent as a consequence of deformations of dispersion relations:

$$v \sim \left(1 \mp \frac{E}{E_{QG}}\right) , \tag{1.3}$$

where the sign $\mp$ refers to the subluminal and superluminal scenarios.

Of course, this offers a very attractive opportunity for phenomenology as suggested for the first time in [29]. In fact, even if the speed of light receives small corrections, that at

leading order are proportional to the ratio of the energy of the particle and the quantum gravity scale, measurable effects can be obtained considering, for instance, corrections to the time of flight of astrophysical particles. The cosmological distances, indeed, can be a huge amplifier for such effects making them within the reach of our sensitivity:

$$\Delta t \sim \frac{\Delta E}{E_{QG}} T \,, \tag{1.4}$$

where T is the time distance of the source and ΔE the energy difference of the two particles considered (see fig. 1.1).

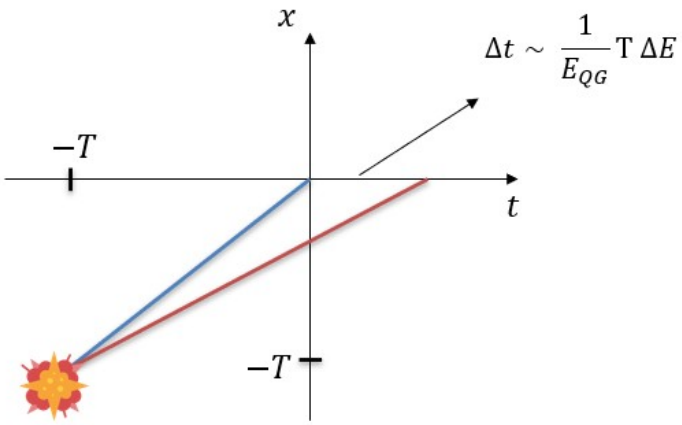

Figure 1.1: Two photons emitted simultaneously and with different energies by a distant source will arrive with a time delay to our telescopes. Assuming to be in the subluminal scenario, in blue we have the worldline of a low-energy photon for which Planck-scale corrections are negligible and in red the one of an high-energy photon.

Other relevant opportunities to test the Planck-scale physics are connected with studies of threshold conditions for certain particle physics processes [30, 31]. In particular, threshold anomalies can be thought as kinematic modifications of the special relativity description of interactions. A most relevant example for phenomenological purposes is electron-positron pair production from the interaction between very high-energy and very low-energy photons, such as those from the cosmic microwave background (CMB) or extragalactic background light (EBL) that can lead to a possible modification of the transparency of the universe to high-energy gamma rays [32–34]. When we study these threshold anomalies, we have to distinguish between the LIV

and the DSR scenarios since they lead to quite different predictions. Specifically, at leading order, modifications for the special-relativistic threshold $E_{\rm th}^{\rm SR}$ ($E_{\rm th}^{\rm SR} = \frac{m_e^2}{\epsilon}$) of this process in the LIV and DSR scenarios can be written as [24, 31]

$$E_{\rm th}^{\rm LIV} \approx \frac{m_e^2}{\epsilon}\left(1+\alpha\frac{m_e^4}{\epsilon^3 E_{QG}}\right) = \left(1+\alpha\frac{m_e^2}{\epsilon^2}\frac{E_{\rm th}^{\rm SR}}{E_{QG}}\right)E_{\rm th}^{\rm SR}\,, \tag{1.5}$$

$$E_{\rm th}^{\rm DSR} \approx \frac{m_e^2}{\epsilon}\left(1+\beta\frac{m_e^2}{\epsilon E_{QG}}\right) = \left(1+\beta\frac{E_{\rm th}^{\rm SR}}{E_{QG}}\right)E_{\rm th}^{\rm SR}, \tag{1.6}$$

where α and β are real parameters characterizing the deformations, ϵ is the energy of the CMB (or EBL) photon and m_e is the mass of the electron.
In this case we have a different kind of amplifier with respect to the time delay expression, namely the ratio between the mass of the electron and the energy of the low-energy photon. Furthermore it is important to notice that the correction to the threshold condition in the DSR scenario is much smaller than the one obtained in the LIV case.
Finally, other recent experimental searches of quantum gravity induced effects are connected with the deep infrared regime. In fact, there are some quantum spacetime models that present Infrared/Ultraviolet mixing (IR/UV mixing) [35, 36], a mechanism that produces non trivial effects also in the deep infrared regime even if only an ultraviolet new physics scale is introduced. Interesting phenomenological opportunities to test these effects come from high-precision table-top experiments. These include cold-atom interferometry measurements, where the ratio between the mass of the particle and its momentum is a huge amplifier for the Planck scale effects [37–39].

1.1 The Planck-scale

As already mentioned previously, the physical regime where both quantum and gravitational effects become not negligible, is expected to be around the Planck-scale E_p:

$$E_p = \sqrt{\frac{\hbar}{G_N}} \simeq 1.2\cdot 10^{19} GeV\,. \tag{1.7}$$

To understand why we expect that both quantum properties and gravitational effects should be taken into account around the Planck-scale we present a famous gedanken-experiment (see [40]). Suppose that we want to localize a particle of mass m within a region of radius r. According to general relativity its Schwarzschild radius:

$$r_S = 2G_N m \tag{1.8}$$

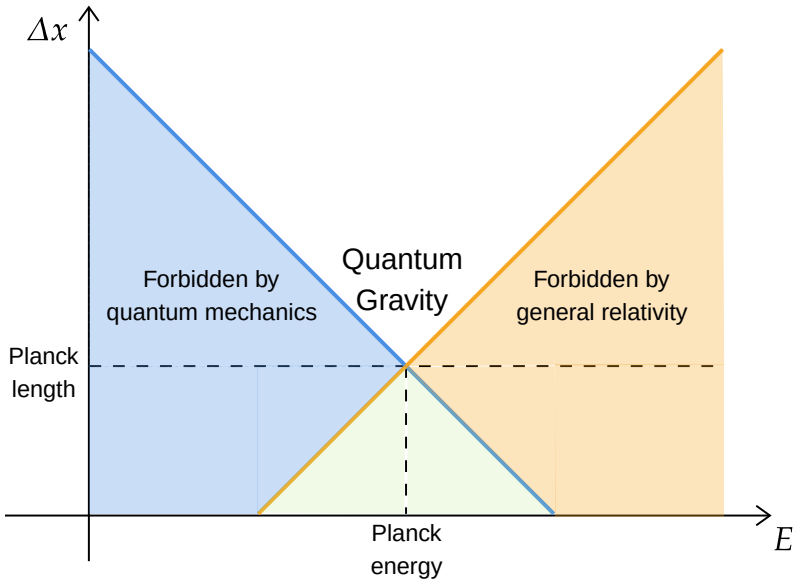

Figure 1.2: The Schwarzschild radius and the Compton radius identify two regions prohibited respectively by general relativity and quantum mechanics and they intersect around the Planck-scale.

gives a fundamental obstruction to localize the mass into too small regions since the production of a black holes is predicted.
On the quantum mechanics side a fundamental limit on the localizability of a particle is given instead by its Compton radius:

$$r_C = \frac{h}{m}\,. \tag{1.9}$$

This restriction arises from the necessity for the injected energy into the system to be lower than the amount needed to create another particle of the same type, leading to the disruption of the measurement process.
Consequently, the Schwarzschild radius and the Compton radius identify two regions prohibited respectively by general relativity and quantum mechanics and their intersection ouccurs around the Planck-scale (see fig. 1.2):

$$r = r_S = r_C \to r \sim \ell_p\,. \tag{1.10}$$

This heuristic argument thus suggests the possibility of having a fundamental lower limit to the localization measurement of a particle around the Planck-scale.

1.2 Quantum spacetimes

A natural way to implement a lower limit to the localization procedure of a particle is by introducing spacetime non-commutativity in the same way as quantum mechanics introduces some limitations for procedures intending to obtain a combined determination of both position and momentum admitting the following non-trivial commutator:

$$[x, p] = i\hbar\,. \tag{1.11}$$

With spacetime non-commutativity we assume that spacetime coordinates do not commute among themselves, producing some restrictions for the combined determination of more than one spacetime coordinate. Formally, a non-commutative spacetime is a non-commutative and associative algebra generated by a set of spacetime operators x^μ. Non-commutative spacetimes are also frequently called "quantum spacetimes" and they offer a mathematical description of the concept that around the Planck scale, it is plausible that the spacetime in not described as usual as a differentiable manifold.
One of the most studied examples of non-commutative spacetimes is the so called θ Moyal-Weyl spacetime (or canonical non-commutative spacetime) [10, 41] defined by the following commutation relations between spacetime coordinates:

$$[x_\mu, x_\nu] = i\theta_{\mu\nu}\,, \tag{1.12}$$

where $\theta_{\mu\nu}$ is a skew-symmetric matrix with the dimensions of a length squared in which is encoded the new ultraviolet physics scale.
Finally, another relevant class of non commutative spacetimes is given by the Lie algebraic type defined, in general, by the following commutator:

$$[x_\mu, x_\nu] = ic^\rho_{\mu\nu}x_\rho\,. \tag{1.13}$$

Among the non-commutative spacetimes of Lie algebra type, the most studied one is the so called κ-Minkowski spacetime [42, 43]. It is a deformation of the algebra of complex-valued functions on Minkowski spacetime into the non-commutative algebra $\mathcal{A}$ generated by coordinate functions satisfying the following commutation relations:

$$[x_\mu, x_\nu] = \frac{i}{\kappa}\left(v_\mu x_\nu - v_\nu x_\mu\right)\,, \tag{1.14}$$

where v_μ is a set of four real numbers and κ is an inverse-length scale, expected to be of the order of the Planck energy. The above relations close a Lie algebra, known as

an(3) of which $\mathcal{A}$ is the universal enveloping algebra.
We can also classify the κ-deformations according to the sign of $||v|| = v_\mu \eta^{\mu\nu} v_\nu$ in the following way [44–46]:

- time-like deformations if $||v|| > 0$,
- light-like deformations if $||v|| = 0$,
- space-like deformations if $||v|| < 0$.

where $\eta^{\mu\nu}$ =diag$(1, -1, -1, -1)$ is the standard Minkowski metric.

1.3 The fate of Lorentz invariance

From a quantum spacetime perspective, it is reasonable to expect departures from Lorentz invariance around the Planck-scale. For example, if we consider the commutator (1.14), this equation is in general not covariant under the action of standard Lorentz transformations:

$$x'_\mu = \Lambda^\nu_\mu x_\nu + a_\mu \,, \tag{1.15}$$

where Λ^ν_μ is a classical Lorentz matrix and a_μ is a translation parameter. Specifically, if we adopt (1.15), in general we will obtain:

$$[x'_\mu, x'_\nu] \neq \frac{i}{\kappa} \left(v_\mu x'_\nu - v_\nu x'_\mu \right) \,. \tag{1.16}$$

Therefore, it is reasonable to expect that the introduction of quantum features in the structure of spacetime would also impacts the fate of Lorentz symmetries.

In particular, two different possibilities about the fate of Lorentz invariance at Planck-scale can arise and these are discussed in the next subsection.

1.3.1 Lorentz Invariance Violation (LIV) vs Doubly Special Relativity (DSR)

In this subsection we discuss the fate of Lorentz invariance. In a physical theory Poincarè symmetry has to surely emerge at low energy with respect to the Planck-

scale but departures from Lorentz invariance could arise around the Planck-scale and these can occur in two different ways.

A first possibility is that Lorentz symmetry is broken and relativistic invariance is lost, giving rise to a preferred-frame picture, and the principle of relativity of inertial frames must be abandoned (LIV) [25, 47, 48].

The second possibility is that relativistic symmetries are instead deformed in order to accommodate a new invariant scale of energy, expected to be around the Planck-scale, in such a way that the relativistic nature of the theory is preserved. In such theories two invariant scales are thus present, namely the speed of light c and the Planck energy E_p and for this reason they are called Doubly Special Relativity (or Deformed Special Relativity) theories (DSR) [49–51]. The existence of an invariant scale of energy is clearly incompatible with the boost sector of the Poincarè algebra due to the well known length contraction phenomenon predicted by special relativity. Therefore, it must be deformed in such a way that boost transformations saturate at Planck-scale [52].

Finally, in order to guarantee the relativistic picture of such models, also the composition laws of momenta have to be typically deformed [53, 54] in a non-linear way to be compatible with deformed relativistic transformations:

$$p_\mu + k_\mu \to (p \oplus k)_\mu \,, \tag{1.17}$$

where $\oplus$ denotes the deformed composition law of momenta.
This is similar to what happens in the transition from Galilean relativity to special relativity, where Lorentz boosts preserve the invariance of the speed of light c and this invariance also requires that the usual sum of velocities is replaced by a non-trivial one:

$$\vec{v} \oplus \vec{u} = \frac{1}{1 + \frac{\vec{v}\cdot\vec{u}}{c^2}} \left(\vec{v} + \frac{\vec{u}}{\gamma_v} + \frac{1}{c^2} \frac{\gamma_v}{1+\gamma_v} (\vec{v}\cdot\vec{u})\vec{v} \right) \,, \quad \text{where } \gamma_v = \sqrt{1 - \frac{v^2}{c^2}} \,. \tag{1.18}$$

This composition law is non-commutative and non-associative and it plays a fundamental role in the consistency of special relativity. In fact, also the law of composition of velocities has to be compatible with the principle of relativistic invariance of the speed of light c.

In order to take into account the non-linear aspects introduced by the Planck-scale, DSR deformed symmetries are typically described in terms of Hopf algebras and quantum groups that represent some natural candidates for this purpose. A rigorous description of such mathematical structures is given in the next chapter 2.

1.4 The relative locality regime

We conclude this introductory chapter presenting the Relative Locality regime [55, 56]. It is a "classical and non gravitational" regime of quantum gravity in the sense that both $\hbar$ and G_N are negligible but their ratio is fixed:

$$\hbar \to 0, \qquad G_N \to 0, \quad \text{but fixed} \quad \sqrt{\frac{\hbar}{G_N}} = M_p \,. \tag{1.19}$$

In this physical regime both gravity and quantum mechanics are thus switched off but we have non trivial effects due to the Planck mass which parametrizes non linearities in momentum space. The idea that momentum space could have a non trivial geometry when quantum gravity effects are taken into account was originally proposed by Max Born [57] who, in 1938, introduced what is now known as Born reciprocity principle according to which an equivalence between spacetime and momentum space is expected. However, the introduction of gravity breaks this symmetry between spacetime and momentum space because the former is now curved while the latter is flat. In this perspective, allowing the momentum space geometry to be curved is a natural way to reconcile gravity with quantum mechanics.
The relative locality framework is therefore dual to the general relativity one since, now, momentum space is curved while spacetime is flat (see fig. 1.3).
Specifically, in this framework, the mass of a particle is interpreted as the geodesic distance from the origin of the momentum space providing the following dispersion relation:

$$D^2(p, 0) = m^2 \,, \tag{1.20}$$

where $D(p, 0)$ is the distance between p_μ and the origin of the momentum space.
Also a non-trivial affine connection is needed in order to produce non-linearities in the law of composition of momenta, which is in general used to formulate the conservation of momentum:

$$(p \oplus q)_\mu = p_\mu + q_\mu + \frac{1}{M_p}\Gamma_\mu^{\alpha\beta} p_\alpha q_\beta + \mathcal{O}\left(\frac{1}{M_p^2}\right), \tag{1.21}$$

where we are considering only the the leading order in $\frac{1}{M_p}$ and $\Gamma_\mu^{\alpha\beta}$ is the affine connection evaluated at the origin of the momentum space [55, 56].
We can show how having a non trivial geometry for the momentum space affects the notion of locality, a concept that in special relativity is observer independent due to the fact that the composition law for momenta is linear. To see this let us consider a

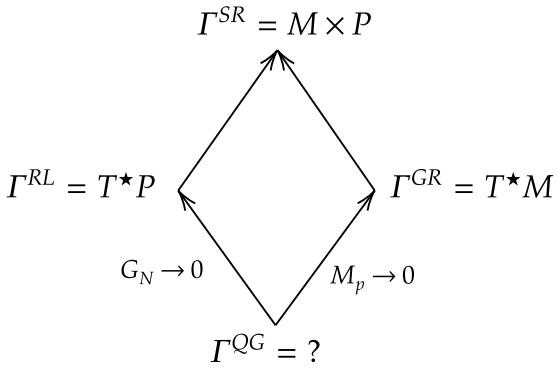

Figure 1.3: General relativity and relative locality are dual theories. In general relativity spacetime is curved but momentum space is flat. The opposite is the case in relative locality. Starting from an unknown quantum theory of gravity, one can move to special relativity through two paths. Taking $\hbar \to 0$ but keeping G_N fixed (so that M_p also goes to 0) one ascends on the right to general relativity. But keeping M_p fixed while taking $G_N \to 0$ (and hence also $\hbar \to 0$) leads to the relative locality regime on the left [56].

multi-particle system and suppose that x_a^μ are the positions of the particles according to Alice. The total momentum of the system generates translations. Suppose that a second observer, Bob, is separated by a vector s^μ from Alice. In special relativity the total momentum reads:

$$P_\nu^{tot} = \sum_a p_\nu^a \,. \tag{1.22}$$

Therefore we have:

$$\delta x_a^\mu = \{P_\nu^{tot} s^\nu, x_a^\mu\} = s^\mu \qquad \forall a \,. \tag{1.23}$$

What happens if the composition law is non linear as in (1.21) ?

$$\begin{aligned} \delta x_a^\mu = \{P_\nu^{tot} s^\nu, x_a^\mu\} = \left\{ \sum_b p_\nu^b s^\nu + \sum_{f<d} \frac{1}{M_p} \Gamma_\nu^{\alpha\beta} p_\alpha^f p_\beta^d s^\nu, x_a^\mu \right\} = \\ = s^\mu + \frac{1}{M_p} s^\nu \sum_{d>a} \frac{1}{M_p} \Gamma_\nu^{\mu\beta} p_\beta^d + \mathcal{O}\left(\frac{1}{M_p^2}\right) . \end{aligned} \tag{1.24}$$

Consequently we can see that how much a worldline of a particle is translated depends on the momenta carried by it and the particles it interacts with. The result is a feature

known as "relative locality" according to which the concept of locality becomes observer dependent (see fig. 1.4).

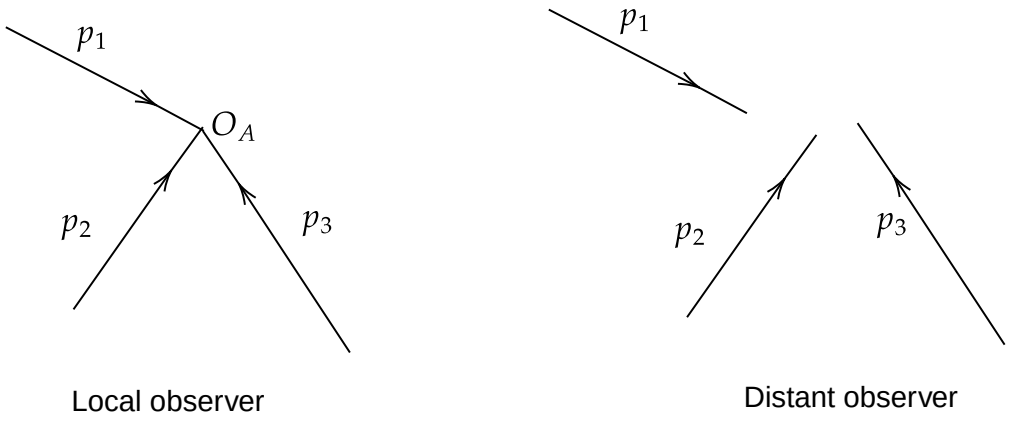

Figure 1.4: If the event is at the origin of an observer's coordinate system, then the event is described as local, as on the left. If the event is far from the origin of the observer's coordinates, the event is described as non-local, in the sense that the projections of the ends of the worldlines no longer meet at the point where the interaction takes place, as on the right [56].

Finally, some attempts to generalize the relative locality framework to scenarios in which spacetime curvature is not neglected have been recently made [58–60], trying to construct a theory where both momentum space and spacetime are curved.

Thesis Overview

In chapter 2 some mathematical preliminaries regarding Hopf algebras and quantum groups, which are the fundamental structures in order to describe symmetries of quantum spacetimes, are presented. Then, the following chapter 3 is devoted to the discussion about the fate of conserved charges in quantum spacetimes and in chapter 4 it is investigated the possible role of observers and the properties of reference frames in a quantum spacetime by focusing on a quantum group toy model.

Then we deal with the phenomenological part of this dissertation. Specifically, we start from chapter 5 in which it is discussed the phenomenology of in-vacuo dispersion

and the possibility of testing departures from Lorentz invariance through time of flight measurements. Finally, in chapter 6 a novel analysis of in-vacuo dispersion through gamma ray bursts is discussed and interesting preliminary results on the possibility of having a non-monotonic behaviour of the time delay as a function of the redshift distance of the source are obtained.

Chapter 2

Mathematical preliminaries

In this chapter we introduce some mathematical structures that are needed in order to describe symmetries of quantum spacetimes. In classical spacetimes symmetries are typically described in terms of Lie algebras and Lie groups, but in order to describe symmetries of quantum spacetimes we need to introduce new structures that take into account the non-linear aspects introduced by the Planck-scale. In this perspective Hopf algebras and quantum groups provide quite natural tools to describe quantum symmetries. These are discussed in this chapter, mainly following the approach in [61].

In the last part of this chapter we also present the θ Moyal-Weyl non-commutative spacetime and then we introduce the famous κ-Minkowski spacetime and discuss its deformed symmetries.

2.1 Algebras, Lie algebras and Universal enveloping algebras

2.1.1 Algebras

A unital associative algebra $\mathcal{A}$ is a vector space over a field $\mathbb{K}$ equipped with the product $\mu : \mathcal{A} \otimes \mathcal{A} \to \mathcal{A}$ and the unit $\eta : \mathbb{K} \to \mathcal{A}$, satisfying the following requirements:

$$\begin{aligned} \mu \circ (\mu \otimes id) &= \mu \circ (id \otimes \mu) \\ \mu \circ (id \otimes \eta) &= id = \mu \circ (\eta \otimes id) \end{aligned} \tag{2.1}$$

where id is the identity map. In fig. 2.1 the algebra axioms are expressed in terms of commutative diagrams.

2.1.2 Lie algebras

A Lie algebra $\mathcal{L}$ is an algebra over a field $\mathbb{K}$, with a product :

$$[\ ,\ ] : \mathcal{L} \otimes \mathcal{L} \to \mathcal{L} \tag{2.2}$$

called Lie bracket, which satisfies the following conditions:

$$\begin{aligned} &[a\, l_1 + b\, l_2, c\, l_3 + d\, l_4] = ac\,[l_1, l_3] + ad\,[l_1, l_4] + bc\,[l_2, l_3] + +bd\,[l_2, l_4] \qquad \forall a, b, c, d \in \mathbb{K},\ l_i \in \mathcal{L} \\ &[l_1, l_2] = -[l_2, l_1] \qquad l_i \in \mathcal{L} \\ &[l_1, [l_2, l_3]] + [l_3, [l_1, l_2]] + [l_2, [l_3, l_1]] = 0 \qquad l_i \in \mathcal{L} \end{aligned} \tag{2.3}$$

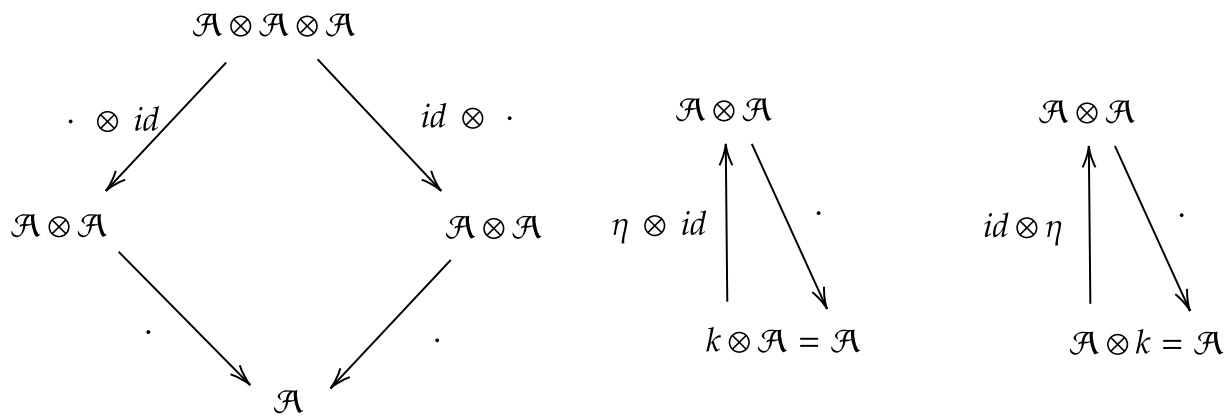

Figure 2.1: Algebra axioms expressed as commutative diagrams.

The first two conditions imply that the Lie bracket is a bilinear and skew-symmetric map, while the last condition is known as Jacobi identity.
Elements of a Lie algebra $\mathcal{L}$ form a basis of generators if they provide a maximal set of independent elements, which generate the whole Lie algebra by linear combinations. The dimension of a Lie algebra coincides with its dimension as a vector space. If $b_1, ..., b_n$ provide a basis for a Lie algebra we can introduce the notion of structure constants in the following way:

$$[b_i, b_j] = c_{ij}^k b_k \,, \tag{2.4}$$

where c_{ij}^k are the structure constants and they determine completely the Lie algebra.

2.1.3 Universal enveloping algebras

Starting from a Lie algebra we can construct its universal enveloping algebra. Specifically, we can first introduce the tensor algebra on the vector space of $\mathcal{L}$ as follows:

$$\mathcal{T}(\mathcal{L}) = \mathbb{K} \oplus \mathcal{L} \oplus (\mathcal{L}\otimes\mathcal{L}) \oplus ... \tag{2.5}$$

where $\otimes$ is the tensor product and $\oplus$ is the direct sum of vector spaces. Now, we have to "lift" the Lie bracket from the Lie algebra to the tensor algebra to obtain a map

defined on $\mathcal{T}(\mathcal{L}) \otimes \mathcal{T}(\mathcal{L}) \to \mathcal{T}(\mathcal{L})$ that is also bilinear, skew-symmetric and obeys the Jacobi identity. We can do this grade by grade starting from $[\ ,\ ] : \mathcal{L} \otimes \mathcal{L} \to \mathcal{L}$:

$$l_1 \otimes l_2 = [l_1, l_2] \tag{2.6}$$

and lifting this bracket to $\mathcal{T}^n(\mathcal{L})$ recursively by defining:

$$[l_1 \otimes l_2, l_3] = l_1 \otimes [l_2, l_3] + [l_1, l_3] \otimes l_2 \,. \tag{2.7}$$

If we now introduce the equivalence relation $\sim$, given by:

$$l_1 \otimes l_2 - l_2 \otimes l_1 = [l_1, l_2] \,, \tag{2.8}$$

then, the universal enveloping algebra $\mathcal{U}(\mathcal{L})$ can be defined as:

$$\mathcal{U}(\mathcal{L}) = \mathcal{T}(\mathcal{L}) / \sim \tag{2.9}$$

2.2 Coalgebras, bialgebras and Hopf algebras

2.2.1 Coalgebras

A coalgebra $\mathcal{C}$ is a vector space over a field $\mathbb{K}$, with two $\mathbb{K}$-linear maps, the coproduct $\Delta : \mathcal{C} \to \mathcal{C} \otimes \mathcal{C}$ and the counit $\epsilon : \mathcal{C} \to \Bbbk$ satisfying:

$$\begin{aligned} (\Delta \otimes id) \circ \Delta &= (id \otimes \Delta) \circ \Delta \\ (id \otimes \epsilon) \circ \Delta &= (\epsilon \otimes id) \circ \Delta \end{aligned} \tag{2.10}$$

Coalgebras are dual algebraic structures to the unital associative algebras, in fact their maps are the inverse of each other. This can be seen by considering their commutative diagrams. In fact, starting from the diagrams of an unital associative algebra (see fig. 2.1) and turning all arrows around, one obtains the axioms of coalgebras (see fig. 2.2):

We conclude this subsection introducing the famous Sweedler notation that is often used to represent coproducts. The most general form for the coproduct of an element a of a coalgebra is a sum of elements in $\mathcal{C} \otimes \mathcal{C}$ that can be indicated as:

$$\Delta(c) = \sum_i c^i_{(1)} \otimes c^i_{(2)} = c_{(1)} \otimes c_{(2)} \,, \tag{2.11}$$

where in the last equality indices and sum have been omitted.

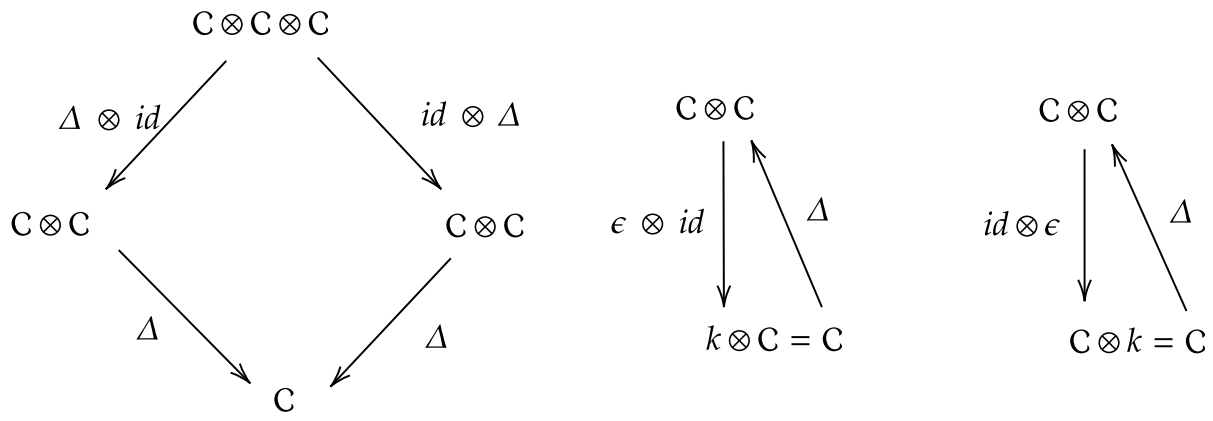

Figure 2.2: Coalgebra axioms expressed as commutative diagrams.

2.2.2 Bialgebras

A bialgebra $\mathcal{B}$ is a unital algebra and a coalgebra, whose coprdouct Δ and counity ϵ are algebra homomorphism with respect to the product and the identity:

$$\begin{aligned} &\Delta(a \cdot b) = \Delta(a) \cdot \Delta(b) \\ &\epsilon(a \cdot b) = \epsilon(a)\epsilon(b) \qquad\qquad \forall a, b \in \mathcal{B} \\ &\Delta(\mathbb{1}) = \mathbb{1} \otimes \mathbb{1} \\ &\epsilon(\mathbb{1}) = 1 \end{aligned} \tag{2.12}$$

where $\mathbb{1}$ is the neutral element of the algebra. In fig. 2.3 we show the diagrams relative to bialgebra axioms.
Finally in the next subsection we see how to make a bialgebra into an Hopf algebra.

2.2.3 Hopf algebras

An Hopf algebra $\mathcal{H}$ is a bialgebra over a field $\mathbb{K}$ with a $\mathbb{K}$-linear map $S : \mathcal{H} \to \mathcal{H}$, the antipode, which satisfy the following condition (also see fig. 2.4):

$$\mu \circ (S \otimes id) \circ \Delta = \mu \circ (id \otimes S) \circ \Delta = \eta \circ \epsilon \tag{2.13}$$

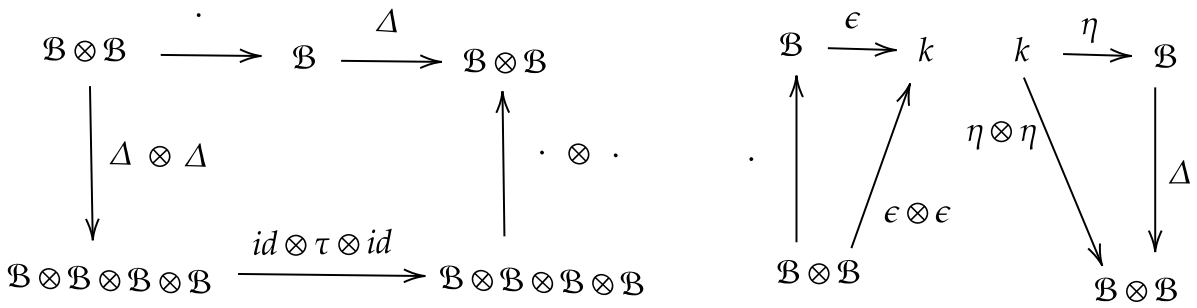

Figure 2.3: Diagrams relative to bialgebra axioms.

The role of the antipode si like that of an inverse but it has not to satisfy in general the relation $S^2 = id$. Moreover, the antipode of a Hopf algebra is unique and obeys

$$S(hg) = S(g)S(h) \tag{2.14}$$

$$S(\mathbb{1}) = \mathbb{1} \tag{2.15}$$

$$S \otimes S \circ \Delta h = \tau \circ \Delta \circ S(h) \tag{2.16}$$

$$\epsilon(S(h)) = \epsilon(h) \tag{2.17}$$

where τ is the flip map such that:

$$\tau(a \otimes b) = b \otimes a\,. \tag{2.18}$$

An Hopf algebra is commutative if it is commutative as an algebra. It is cocommuative if it is commutative as a coalgebra, namely if $\tau\Delta = \Delta$.

2.2.4 Examples of Hopf algebras

We here provide two simple examples of Hopf algebras that can help to understand the meaning of the structures we introduced in the previous sections.

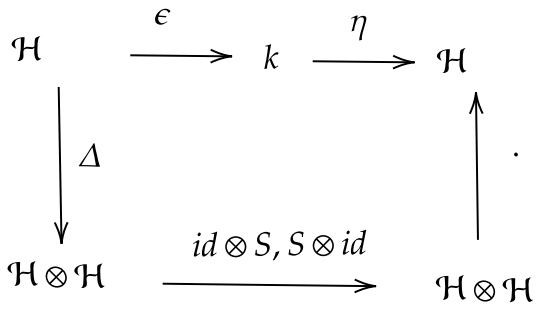

Figure 2.4: Additional axiom to make a bialgebra into an Hopf algebra.

• Let G be a Lie group and consider $C(G)$ the space of continuous functions on G, with the following definitions:

$$\begin{aligned}
&(f \cdot h)(g) = f(g)h(g), \qquad f, h \in C(g),\, g \in G \\
&\Delta f(g_1 \otimes g_2) = f(g_1 g_2) \\
&\eta(a) = a1, \qquad a \in \mathbb{C} \qquad 1(g) = 1 \\
&\epsilon(f) = f(e), \qquad e \text{ is the identity element of the group } G \\
&S(f)(g) = f(g^{-1})
\end{aligned} \tag{2.19}$$

With these structures $C(G)$ is an Hopf algebra realization. In particular, it is co-commutative if G is commutative as can been seen from the second line of (2.19).

Furthermore, from the algebra of function over a group we can also obtain the so-called quantum group. In particular, it can be defined by deforming the algebra of complex functions on the group in a non-commutative way.

• Let us now construct an Hopf algebra from the universal enveloping algebra $\mathcal{U}(\mathcal{L})$ of a Lie algebra $\mathcal{L}$. To do so we have to introduce the coalgebra structures and a notion of antipode S. We can do this in the following way:

$$\begin{aligned}
&\Delta(l_i) = l_i \otimes \mathbb{1} + \mathbb{1} \otimes l_i \qquad \forall l_i \in \mathcal{L} \\
&\Delta(\mathbb{1}) = \mathbb{1} \otimes \mathbb{1} \\
&\epsilon(l_i) = 0 \qquad \epsilon(\mathbb{1}) = 1 \\
&\eta(\lambda) = \lambda \mathbb{1} \qquad \forall \lambda \in \mathbb{K}
\end{aligned} \tag{2.20}$$

The coproducts in (2.20) are called primitive and we can prove their compatibility with the product of the algebra (the Poisson bracket) straightforwardly:

$$\Delta([l_i, l_j]) = \Delta(c_{ij}^k l_k) = c_{ij}^k (l_k \otimes \mathbb{1} + \mathbb{1} \otimes l_k) = [\Delta(l_i), \Delta(l_j)]\,. \tag{2.21}$$

To complete the Hopf algebra construction, it remains to define an antipode, that is easily found to be:

$$S(l_i) = -l_i \qquad S(\mathbb{1}) = \mathbb{1} \tag{2.22}$$

2.2.5 Dual Hopf algebras

Given two vector spaces A and B over $\mathbb{C}$ we say that they are dually paired if there exists a sesqulinear form:

$$\langle\ ,\ \rangle : A \otimes B \to \mathbb{C} \tag{2.23}$$

defining a non-degenerate scalar product between the two spaces.
Given a vector space V over $\mathbb{C}$, one can define its algebraic dual space V^* as the space of linear functionals over V as follows:

$$V^* = \mathrm{Lin}(V) \qquad \langle f, x\rangle = f(x) \qquad f \in V^*, x \in V \tag{2.24}$$

Two hopf algebras $\mathcal{H}$ and $\mathcal{H}^*$ are dually paired if the coalgebra of $\mathcal{H}$ defines the algebra of $\mathcal{H}^*$ and vice-versa as follows:

$$\begin{aligned}
&\langle a \cdot b, c\rangle = \langle a \otimes b, \Delta c\rangle \qquad \forall a, b \in \mathcal{H}^*, c \in \mathcal{H}\\
&\langle \mathbb{1}, c\rangle = \epsilon(c)\\
&\langle a, c \cdot d\rangle = \langle \Delta(a), c \otimes d\rangle \qquad \forall a \in \mathcal{H}^*, c, d \in \mathcal{H}\\
&\langle a, \mathbb{1}\rangle = \epsilon(a)\\
&\langle S(a), c\rangle = \langle a, S(c)\rangle
\end{aligned} \tag{2.25}$$

2.2.6 Action of an Hopf algebra over an algebra (coalgebra)

Given an Hopf algebra $\mathcal{H}$ and an algebra $\mathcal{A}$ a left action of $\mathcal{H}$ over $\mathcal{A}$ is a linear map:

$$\triangleright : \mathcal{H} \times \mathcal{A} \to \mathcal{A} \tag{2.26}$$

such that:

$$\begin{aligned}
&(h_1 \cdot h_2) \triangleright a = h_1 \triangleright (h_2 \triangleright a)\\
&h \triangleright \mathbb{1} = \epsilon(h)\mathbb{1}
\end{aligned} \tag{2.27}$$

Moreover the structures of $\mathcal{A}$ are preserved by the action of $\mathcal{H}$ (covariant action) if

$$h \triangleright (a \cdot b) = (h_{(1)} \triangleright a) \cdot (h_{(2)} \triangleright b) \tag{2.28}$$

In the same way we can define the left action of an Hopf algebra $\mathcal{H}$ on a coalgebra $\mathcal{C}$ and it is covariant if the following requirements are satisifed :

$$\Delta(h \triangleright c) = (h_{(1)} \triangleright c_{(1)}) \otimes (h_{(2)} \triangleright c_{(2)}) = \Delta(h) \triangleright \Delta(c) \tag{2.29}$$

and

$$\epsilon(h \triangleright c) = \epsilon(h)\epsilon(c)\,. \tag{2.30}$$

Analogously we can also define a right action $\triangleleft$ of $\mathcal{H}$ over $\mathcal{A}$ (or $\mathcal{C}$):

$$\triangleleft : \mathcal{A} \times \mathcal{H} \to \mathcal{A} \tag{2.31}$$

that is covariant if:

$$(a \cdot b) \triangleleft h = (a \triangleleft h_{(1)}) \cdot (b \triangleleft h_{(2)})\,. \tag{2.32}$$

Finally, if we now consider two dually paired Hopf algebras $\mathcal{H}$ and $\mathcal{H}^*$ the definition of a left action $\triangleright$ over an algebra defines a dual right action $\triangleleft$ over the dual algebra in the following way:

$$\langle a, h \triangleright b\rangle = \langle a \triangleleft h, b\rangle \tag{2.33}$$

2.2.7 Coaction of an Hopf algebra over an algebra

Given an Hopf algebra $\mathcal{H}$ and an algebra $\mathcal{A}$ a left coaction of $\mathcal{H}$ over $\mathcal{A}$ is a linear map:

$$\beta : \mathcal{A} \to \mathcal{H} \otimes \mathcal{A} \tag{2.34}$$

satisfying:

$$\begin{aligned} (id \otimes \beta) \circ \beta &= (\Delta \otimes id) \circ \beta \\ (\epsilon \otimes id) \circ \beta &= id \end{aligned} \tag{2.35}$$

Moreover the coaction is covariant if

$$\begin{aligned} \beta(a \cdot b) &= \beta(a)\beta(b) \\ \beta(\mathbb{1}) &= \mathbb{1} \otimes \mathbb{1} \end{aligned} \tag{2.36}$$

We are now ready to discuss symmetries of non-commutative spacetimes that is the subject of the next section.

2.3 Symmetries of non-commutative spacetimes

In this section we will discuss how the symmetries of a non-commutative spacetime can be naturally described in terms of Hopf algebras structures and quantum groups. In particular, we will focus first on the θ Moyal-Weyl spacetime (canonical non-commutativity) and then we discuss the famous κ-Minkowski spacetime.

2.3.1 Moyal-Weyl spacetime

As anticipated in the previous chapter, one of the most famous examples of non-commutative spacetimes is the so called θ Moyal-Weyl spacetime [10,41] that is defined by the following commutation relations:

$$[x_\mu, x_\nu] = i\theta_{\mu\nu}\,, \tag{2.37}$$

where $\theta_{\mu\nu}$ is a skew-symmetric matrix with the dimensions of a length squared in which is encoded the new physics scale.
These commutation relations are not covariant under the action of the standard Poincarè transformations and we want to find which transformations leave invariant this non-commutative spacetime. Specifically, we look for a deformation of the algebra of functions on the Poincarè group such that:

$$[x'_\mu, x'_\nu] = i\theta_{\mu\nu}\,, \tag{2.38}$$

where:

$$x'_\mu = \Lambda_\mu^{\ \alpha} \otimes x_\alpha + a_\mu \otimes 1\,, \tag{2.39}$$

Such request, as can been verified straightforwardly, is satisfied by considering the following deformed commutators:

$$[a_\mu, a_\nu] = i(\delta_\mu^{\ \rho}\delta_\nu^{\ \sigma} - \Lambda_\mu^{\ \rho}\Lambda_\nu^{\ \sigma})\theta_{\rho\sigma}\,, \quad [\Lambda_\mu^{\ \rho}, \Lambda_\nu^{\ \sigma}] = 0 = [\Lambda_\mu^{\ \rho}, a_\nu]\,, \tag{2.40}$$

but undeformed coproducts, antipodes and counits:

$$\begin{aligned} &\Delta(\Lambda_\nu^{\ \mu}) = \Lambda_{\ \rho}^{\mu} \otimes \Lambda_{\ \nu}^{\rho}, \quad S(\Lambda_\nu^{\ \mu}) = (\Lambda^{-1})_{\ \nu}^{\mu}, \quad \epsilon(\Lambda_\nu^{\ \mu}) = \delta_\nu^{\ \mu} \\ &\Delta(a^\mu) = \Lambda_{\ \rho}^{\mu} \otimes a^\rho + a^\mu \otimes 1, \quad S(a^\mu) = -(\Lambda^{-1})_{\ \rho}^{\mu} a^\rho, \quad \epsilon(a^\mu) = 0\,, \end{aligned} \tag{2.41}$$

where $\Lambda_{\ \rho}^{\mu}\Lambda_{\ \sigma}^{\nu}\eta_{\mu\nu} = \eta_{\rho\sigma}$. Consequently, in order to guarantee the covariance of the commutator (2.37), a non-commutativity among translation parameters is needed, reflecting the non-commutative nature of spacetime coordinates.

In the following we will discuss symmetries of κ-Minkowski spacetime, but let us first introduce the notion of Weyl maps and star product in the next subsection.

2.3.2 Weyl maps, star product and integration

Other mathematical tools useful to construct theories on non-commutative spacetimes are the Weyl maps (also see [62] for further details). In this section we briefly review how they can be defined in κ-Minkowski spacetime that we have already presented in the previous chapter, but for completeness we here report the commutation relations that define this non-commutative spacetime:

$$[x_\mu, x_\nu] = \frac{i}{\kappa}\left(v_\mu x_\nu - v_\nu x_\mu\right) , \tag{2.42}$$

where v_μ is a set of four real numbers and κ is an inverse-length scale, expected to be of the order of the Planck energy and the commutative picture is recovered by considering the limit $\kappa \to \infty$.
Weyl maps are linear maps Ω_κ from the space of commutative functions to the non-commutative algebra of functions generated by non-commutative coordinates. It is sufficient to specify the Weyl map on the plane-waves and extend it by linearity to a generic function $f(x)$, whose Fourier transform is $\tilde{f}(p) = \frac{1}{(2\pi)^4}\int f(x)e^{-ipx}d^4p$:

$$\Omega_\kappa(f(x)) = \int \tilde{f}(p)\Omega_\kappa(e^{ipx})d^4p\,, \tag{2.43}$$

Of course, a good definition of Weyl map has to reproduce the correct classical limit:

$$\Omega_\kappa(f(x)) \xrightarrow{\kappa\to\infty} f(x)\,. \tag{2.44}$$

There is no unique definition of Weyl maps and we here provide two examples of possible ways to define them. Specifically, we can consider the time-to-the-right-ordering Ω_R and the symmetrized one Ω_S defined as:

$$\begin{aligned}\Omega_R(e^{ipx}) &= e^{ip_i x^i}e^{ip_0 x^0}\\ \Omega_S(e^{ipx}) &= e^{ip_0 x^0/2}e^{ip_i x^i}e^{ip_0 x^0/2}\end{aligned} \tag{2.45}$$

Associated to each Weyl map it is also possible to introduce a star product $\star_\kappa$ in the following way:

$$\Omega_\kappa(f \star_\kappa g) = \Omega_\kappa(f)\Omega_\kappa(g)\,. \tag{2.46}$$

It reproduces the properties of the non commutative product of elements of κ-Minkowski but it is applied to commutative functions.

For completeness, we conclude this subsection introducing a notion of integration on non-commutative spacetimes. As in the commutative case, we define integrals as linear map associating functions on κ-Minkowski to complex numbers with the request that the integral must reduce to the integral of the corresponding commutative function when $\kappa \to \infty$. A natural way to define integrals is the following:

$$\int \Omega_\kappa(f(x))d^4x = \int \tilde{f}(p)d^4p \int \Omega_\kappa(e^{ipx})d^4x\,, \tag{2.47}$$

where as in the commutative case we define:

$$\int \Omega_\kappa(e^{ipx})d^4x = (2\pi)^4\delta^4(p)\,. \tag{2.48}$$

A notion of integration is of course a necessary ingredient in order to construct field theory over a non-commutative spacetime [36, 63].

2.3.3 Timelike κ-Minkowski spacetime

We are now ready to introduce the symmetries of κ-Minkowski spacetime focusing in particular on the so called timelike scenario that can be obtained from (2.42) choosing $v_\mu = \delta^0_\mu$. It is thus characterized by the following commutators between spacetime coordinates:

$$[x_0, x_i] = \frac{i}{\kappa}x_i \qquad [x_i, x_j] = 0\,. \tag{2.49}$$

The deformed symmetries associated to this non-commutative spacetime are described by the κ-Poincaré quantum group that is the non-commutative algebra of functions generated by Λ^μ_ν and a^μ that leaves the commutators in (2.49) invariant under the following transformation:

$$x^\mu \to x'^\mu = \Lambda^\mu_\nu \otimes x^\nu + a^\mu \otimes 1\,. \tag{2.50}$$

This request is satisfied if Λ^μ_ν and a^μ saitisfy:

$$\begin{aligned} [a^\mu, a^\nu] &= \frac{i}{\kappa}(\delta^\mu_0 a^\nu - \delta^\nu_0 a^\mu), \qquad [\Lambda^\beta_\alpha, \Lambda^\mu_\nu] = 0 \\ [\Lambda^\mu_\nu, a^\rho] &= \frac{i}{\kappa}\left((\Lambda^\mu_0 - \delta^\mu_0)\,\Lambda^\rho_\nu + \left(\Lambda^0_\nu - \delta^0_\nu\right)\eta^{\mu\rho}\right) \end{aligned} \tag{2.51}$$

with the following coalgebra structures:

$$\begin{aligned}
&\Delta a^\mu = a^\nu \otimes \Lambda^\mu_\nu + 1 \otimes a^\mu, \qquad \Delta\Lambda^\mu_\nu = \Lambda^\mu_\rho \otimes \Lambda^\rho_\nu \\
&S(a^\mu) = -a^\nu(\Lambda^{-1})^\mu_\nu, \qquad S(\Lambda^\mu_\nu) = (\Lambda^{-1})^\mu_\nu \\
&\epsilon(a^\mu) = 0, \qquad \epsilon(\Lambda^\mu_\nu) = \delta^\mu_\nu
\end{aligned} \tag{2.52}$$

as can be straightforwardly verified.

The symmetries of timelike κ-Minkowski spacetime can also be described in terms of the dual Hopf Algebra $U_\kappa[iso(3,1)]$ which is the non-commutative deformation of the universal enveloping algebra $U[iso(3,1)]$ of the Poincarè Lie algebra $iso(3,1)$. The standard way to obtain the algebra and the coalgebra sectors of $U_\kappa[iso(3,1)]$ is by applying a finite transformation on non-commutative plane waves, with a given ordering, and extract the action of the generators of the algebra by evaluating the first order of the transformation rules of plane waves [64, 65]. It is well known that such result strongly depends on the ordering chosen for the plane waves. In particular, if we choose the so called time-to-the-right ordering (that we have presented in the previous subsection) we can obtain the famous bicross-product basis introduced for the first time by Majid and Ruegg [11].

In this basis the algebra sector reads:

$$\begin{aligned}
&[P_\mu, P_\nu] = 0, \\
&[P_0, R_j] = 0, \\
&[R_j, P_k] = i\epsilon_{jkl}P_l, \\
&[R_j, N_k] = i\epsilon_{jkl}N_l, \\
&[R_j, R_k] = i\epsilon_{jkl}R_l, , \\
&[N_j, P_0] = iP_j, \\
&[N_j, P_k] = i\kappa\left(\frac{1 - e^{-\frac{2}{\kappa}P_0}}{2} + \frac{\vec{P}^2}{2\kappa^2}\right)\delta_{jk} - \frac{i}{\kappa}P_jP_k, \\
&[N_j, N_k] = -i\epsilon_{jkl}R_l,
\end{aligned} \tag{2.53}$$

where P_μ are the translation generators, R_i the rotations, and N_i the boost generators.

The coproducts read:

$$\begin{aligned}
\Delta P_0 &= P_0 \otimes 1 + 1 \otimes P_0 \,, \\
\Delta P_i &= P_i \otimes 1 + e^{-\frac{P_0}{\kappa}} \otimes P_i \,, \\
\Delta R_i &= R_i \otimes 1 + 1 \otimes R_i \,, \\
\Delta N_i &= N_i \otimes 1 + e^{-\frac{P_0}{\kappa}} \otimes N_i + \frac{i}{\kappa} \epsilon_{ijk} P_j \otimes R_k \,.
\end{aligned} \tag{2.54}$$

Finally, to complete the Hopf algebra description, we provide the antipodes and the counits:

$$\begin{aligned}
S(P_0) &= -P_0 \,, \\
S(P_i) &= -e^{\frac{P_0}{\kappa}} P_i \,, \\
S(R_i) &= -R_i \,, \\
S(N_i) &= -e^{\frac{P_0}{\kappa}} N_i + \frac{i}{\kappa} e^{\frac{P_0}{\kappa}} \epsilon_{ijk} P_j R_k \,, \\
\epsilon(P_\mu) &= \epsilon(N_i) = \epsilon(R_i) = 0 \,.
\end{aligned} \tag{2.55}$$

We can now explicitly verify that commutation relations (2.49) are indeed covariant under the action of the κ-Poincarè algebra. P_μ act on κ-Minkowski space-time by dual action:

$$P_\mu \triangleright x_\nu = -i\eta_{\mu\nu} \tag{2.56}$$

and on products of coordinates as:

$$P_\mu \triangleright x_\alpha x_\beta = (P_{\mu(1)} \triangleright x_\alpha)(P_{\mu(2)} \triangleright x_\beta) \,. \tag{2.57}$$

We can now show that (2.49) is covariant under the action of translation generators:

$$\begin{aligned}
&P_0 \triangleright [x_0, x_i] = 0 = P_0 \triangleright (i x_i) \\
&P_j \triangleright [x_0, x_i] = i(x_0 + \frac{i}{\kappa})\delta_{ji} - i x_0 \delta_{ji} = P_j \triangleright (\frac{i}{k} x_i) \,.
\end{aligned} \tag{2.58}$$

We can now define the action of R_i and N_i on P_μ in the following way:

$$P_\mu \triangleleft R_i = [P_\mu, R_i], \qquad P_\mu \triangleleft N_i = [P_\mu, N_i] \,. \tag{2.59}$$

We can thus derive the action of R_i and N_i on Minkowski spacetime by duality as follows:

$$\begin{aligned}
< P_\mu \triangleleft R_i, x_\nu > &= < P_\mu, R_i \triangleright x_\nu > \\
< P_\mu \triangleleft N_i, x_\nu > &= < P_\mu, N_i \triangleright x_\nu > \ .
\end{aligned} \tag{2.60}$$

From these expressions we obtain:

$$\begin{aligned} R_i \triangleright x_j &= i\epsilon_{ijk}x_k, \qquad & R_i \triangleright x_0 &= 0 \\ N_i \triangleright x_j &= i\delta_{ij}x_0, \qquad & N_i \triangleright x_0 &= ix_i \end{aligned} \tag{2.61}$$

By using(2.61),and the coproducts in (2.54) we obtain:

$$\begin{aligned} R_i \triangleright x_0x_k &= i\epsilon_{ikj}x_0x_j \\ R_i \triangleright x_kx_0 &= i\epsilon_{ikj}x_jx_0 \\ N_i \triangleright x_jx_0 &= i\delta_{ij}x_0^2 + ix_ix_j \\ N_i \triangleright x_0x_j &= i\delta_{ij}x_0^2 + ix_ix_j - \frac{1}{\kappa}\delta_{ij}x_0 \end{aligned} \tag{2.62}$$

from which it is straightforward to show that (2.49) commutation relations are covariant under rotations and boost.
Finally, we can introduce the Casimir operator associated to the algebra (2.53):

$$C = 4\kappa^2 \sinh^2\left(\frac{P_0}{2\kappa}\right) - \vec{P}^2 e^{P_0/\kappa} \tag{2.63}$$

that is the operator that commutes with all the generators of the algebra.

In the next chapter we will discuss the problem of conserved charges in quantum spacetimes. In particular we will focus on particles interacting in quantum spacetimes within a first-quantization hamiltonian framework.

Chapter 3

Conserved charges in quantum spacetimes

In the last decades there has been a strong interest in the fate of relativistic symmetries in quantum spacetimes mainly due to the possibility of attractive opportunities for experimental tests. However, the main focus of this research area has been related to the study of modifications of particle kinematics due to deformations of relativistic transformations rules, while the properties of the associated Noether charges still represent an open issue.

In this chapter we address the problem of conserved charges in quantum spacetimes, a topic much debated recently in literature, because the aspects of non-linearity introduced by the Planck-scale make their definition not straightforward as in the special relativistic case. Furthermore, non-linearities in the addition laws for momenta has been the center of some problems as the much discussed soccer-ball problem [66, 67], according to which small Planck-scale deformations can give rise to drastic macroscopic effects (if one want to analyze the total momentum of a macroscopic body they might have to add up very many of such tiny non-linearities), in contrast with everyday observations. Another conceptual problem is the so-called spectator problem [68] according to which if we consider a system made of a free particle and some interacting particles we cannot disentangle the contribution of the free particle to the conservation laws of the interaction.

Nevertheless, the main objective of this chapter is not to find a solution for these open problems, but we make important steps towards the understanding of how conserved charges has to be sought and defined in quantum spacetimes [69].

Within the special relativity framework symmetries of Minkowski spacetime are described by the Poincarè algebra and the Noether theorem guarantees the existence of conserved charges associated to such symmetry transformations. Furthermore, the linearity of transformation laws inevitably yields charges combining linearly both in the free-particle case and when interactions are introduced. Thus, working within special relativity, we do not appreciate how the form of interaction could affect the conservation laws. In fact, the linearity of relativistic transformations imposes that charges combine linearly, regardless the type of interactions being considered.

However, in quantum spacetimes, things are more complicated due to the non-linearity of the relativistic transformations. Until now, the debate on total charges for quantum spacetimes had not contemplated a possible role for the interactions, and instead relied on some “naturalness arguments" based on the form of the relativistic properties of free particles. However, in this chapter we show that there is a strong

connection between Noether charges and the structure of the laws of interaction among particles [69].

To better understand what these “naturalness arguments" are, let us present the so-called κ-Poincarè momentum-space, that can be constructed by taking inspiration from the κ-Poincarè Hopf algebra structures that we have also presented in section 2.3.3.

3.0.1 κ-Poincarè momentum-space

In this subsection let us consider the most studied κ-Minkowski non-commutativity characterized by spatial coordinates that commute among themselves but do not commute with the time coordinate. For simplicity let us work in 1+1 dimensions where we have the following commutator between the time and the spatial coordinate [11]:

$$[x^0, x^1] = i\ell x^1 \,, \tag{3.1}$$

where for convenience we have called $\ell = \frac{1}{\kappa}$.
It is acknowledged [11,70,71] that the symmetries of 2D κ-Minkowski non-commutativity are described by the 2D κ-Poincaré Hopf algebra (also see section 2.3.3) that in the bicross-product basis, reads:

$$\begin{aligned} &[P_0, P_1] = 0 \\ &[N, P_0] = iP_1 \\ &[N, P_1] = \frac{i}{2\ell}(1 - e^{-2\ell P_0}) - i\frac{\ell P_1^2}{2} \,, \end{aligned} \tag{3.2}$$

where P_0 and P_1 are respectively the time translation and spatial translation generators and N is the generator of boost transformations.
The Casimir operator of this algebra is given by:

$$C = \frac{4}{\ell^2}\sinh^2\left(\frac{\ell P_0}{2}\right) - P_1^2 e^{\ell P_0} \,. \tag{3.3}$$

Finally, the coproducts read:

$$\begin{aligned} \Delta P_0 &= P_0 \otimes 1 + 1 \otimes P_0 \\ \Delta P_1 &= P_1 \otimes 1 + e^{-\ell P_0} \otimes P_1 \\ \Delta N &= N \otimes 1 + e^{-\ell P_0} \otimes N \,. \end{aligned} \tag{3.4}$$

We can now represent the translation generators P_0, P_1 as an algebra of functions over the momentum space [68], such that the two translation generators correspond to the coordinate functions p_0 and p_1:

$$\begin{aligned} P_0 &= p_0 \\ P_1 &= p_1 \,. \end{aligned} \tag{3.5}$$

We can thus provide a physical interpretation of the Hopf algebra structures presented above by establishing a correspondence with the properties of momentum-space. Specifically, a deformed (non-commutative but associative) composition law for momenta is usually read from the coproducts:

$$\begin{aligned} (k \oplus q)_0 &= k_0 + q_0 \\ (k \oplus q)_1 &= k_1 + e^{-\ell k_0} q_1 \,. \end{aligned} \tag{3.6}$$

Finally, one can obtain the mass-shell relation taking inspiration from the Casimir operator of the algebra as usually done in the undeformed case:

$$m^2 = \frac{4}{\ell^2} \sinh^2 \left(\frac{\ell P_0}{2} \right) - P_1^2 e^{\ell P_0} \,. \tag{3.7}$$

The momentum space thus constructed has the geometry of (half of) a de Sitter manifold, with curvature proportional to ℓ^2. This momentum space model has inspired many phenomenological analysis in which it has been taken to describe the kinematics of classical particles [72].

We can now show that the composition law for momenta (3.6) can be obtained by considering the composition of time-to-the-right-ordered non commutative plane-waves in κ-Minkowski spacetime. In this way we will also highlight its connection with the notion of locality in quantum space-times [73]. Let us consider the following Fourier decomposition for a field $\Phi(x)$:

$$\Phi(x) = \int d^2k \tilde{\Phi}(k) e^{ik_1 x^1} e^{ik_0 x^0} \tag{3.8}$$

where

$$\int d^2k e^{ik_1 x^1} e^{ik_0 x^0} = (2\pi)^2 \delta^2(k) \,. \tag{3.9}$$

If we introduce an action that is the product of three fields evaluated at the same "quantum space-time point" we obtain:

$$\begin{aligned} S &= \int d^2x \Phi_1(x)\Phi_2(x)\Phi_3(x) = \\ &= \int d^2x \int d^2k\, d^2p\, d^2q\, (\tilde{\Phi}_1(k)\tilde{\Phi}_2(p)\tilde{\Phi}_3(q) e^{ik_1x^1} e^{ik_0x^0}(p) e^{ip_1x^1} e^{ip_0x^0} e^{iq_1x^1} e^{iq_0x^0}) = \\ &= \int d^2x \int d^2k\, d^2p\, d^2q\, (\tilde{\Phi}_1(k)\tilde{\Phi}_2(p)\tilde{\Phi}_3(q) e^{i(k_1 \oplus p_1 \oplus q_1)x^1} e^{i(k_0 \oplus p_0 \oplus q_0)x^0}) = \\ &= (2\pi)^2 \int d^2k\, d^2p\, d^2q\, (\tilde{\Phi}_1(k)\tilde{\Phi}_2(p)\tilde{\Phi}_3(q)) \delta^2(k \oplus p \oplus q) \end{aligned} \tag{3.10}$$

where

$$(k \oplus q)_0 = k_0 + q_0 \tag{3.11}$$

and

$$(k \oplus q)_1 = k_1 + e^{-\ell k_0} q_1 \, . \tag{3.12}$$

This result, that coincides with (3.6), characterizes how spacetime non-commutativity affects the properties of products of plane-waves.

Through this computation we have also seen how a non-linear law of composition of momenta arises in the characterization of locality. However, as we will show in the following sections, different laws of composition of momenta can be produced by the analysis of translational invariance, and they are these laws of composition of momenta which are relevant for the characterization of the total momentum of a multi-particle system. Indeed total momentum (angular momentum) is the conserved charge for a translational (rotational) invariant system.

In order to explore this, we will work within the so-called 2D spatial κ-Minkowski framework, where spatial coordinates do not commute among themselves and time is just a commutative parameter, so we can work within a first-quantization Hamiltonian framework.

3.0.2 Spatial 2D κ–Minkowski

In the following analysis we focus on a scenario in which the time coordinate is fully commutative and the two spatial coordinates are governed by κ-Minkowski non-commutativity:

$$[x_2, x_1] = i\ell x_1 \, . \tag{3.13}$$

All the results established in a vast literature on the 2D space/time κ-Minkowski of Eq.(3.1) and its Hopf-algebra symmetries can be converted into results for our 2D spatial κ-Minkowski of Eq.(3.13) and its Hopf-algebra symmetries, by applying the following maps:

- replacement of the time coordinate with a spatial one $x^0 \to ix_2$;
- replacement of noncommutativity parameter $\ell \to i\ell$;
- replacement of the time-translator generator with a suitable generator of translations along the x_2 direction $P_0 \to -iP_2$
- the boost generator of 2D space/time κ-Minkowski is replaced by the rotation generator of 2D spatial κ-Minkowski $N \to -iR$.

This leads to a description of the translation and rotation symmetries of 2D spatial κ-Minkowski that close the following algebra:

$$[P_2, P_1] = 0 \qquad [R, P_2] = -iP_1 \qquad [R, P_1] = \frac{i}{2\ell}(1 - e^{-2\ell P_2}) + i\frac{\ell}{2}P_1^2 \tag{3.14}$$

which can be seen as a Planck-scale deformation of the Euclidean algebra in 2 dimensions:

$$[P_2, P_1] = 0 \qquad [R, P_2] = -iP_1 \qquad [R, P_1] = iP_2\,. \tag{3.15}$$

A central element of the deformed algebra (3.14), which will be a fundamental ingredient for the construction of our Hamiltonians, is given by

$$\mathcal{C} = \frac{4}{\ell^2}\sinh^2(\ell P_2/2) + e^{\ell P_2}P_1^2\,. \tag{3.16}$$

This can be thought as a deformation of the Casimir element of the Euclidean algebra, namely $P_1^2 + P_2^2$.

We shall introduce interactions among particles within a Hamiltonian setup and we will be satisfied showing our results to order ℓ^2. In order to satisfy Jacobi identities we also have to deform some commutation relations between coordinates and symmetry generators in the following way:

$$\begin{aligned}
&[x_1, P_1] = i \quad [x_1, P_2] = 0 \quad [x_2, P_1] = -i\ell P_1 \quad [x_2, P_2] = i \\
&[R, x_1] = ix_2 \\
&[R, x_2] = -i\big(x_1 - \ell x_1 P_2 + \frac{\ell}{2}x_2 P_1 + \frac{\ell}{2}P_1 x_2 + \ell^2 x_1 P_2^2 + \frac{\ell^2}{4}(x_1 P_1^2 + P_1^2 x_1)\big)\,.
\end{aligned} \tag{3.17}$$

The non-linearity of the commutators (3.14), typical of Hopf-algebra symmetries, produce the difficulties for the notion of Noether charges which are the main focus of this study. For free particles it has been shown [74, 75] that the charges associated to P_1, P_2 and R are conserved (but of course any non-linear function of a conserved quantity is also conserved). For interacting particles instead it is not clear which combinations of the charges should be conserved in particle reactions. In particular, for a process $A+B \to C+D$ it is clear that $P_1^A + P_1^B = P_1^C + P_1^D$ is not an acceptable conservation law due to the non-linearity of the commutator $[R, P_1]$ (*i.e.* $P_1^A + P_1^B = P_1^C + P_1^D$ would not be covariant). So it is clear that the total momentum of a system composed of particles A and B cannot have the component $P_1^A + P_1^B$, but it is unclear which non-linear combination of the momenta gives the total momentum of the system (and would be therefore conserved in particle reactions). A typical way to guess the momentum-composition formula is based on the so-called "coproduct" argument [76–78], which we have presented in the previous section. For our spatial κ-Minkowski this choice would read:

$$\begin{aligned}(k \oplus_\kappa q)_1 &= k_1 + e^{-\ell k_2} q_1 \\ (k \oplus_\kappa q)_2 &= k_2 + q_2 \,.\end{aligned} \tag{3.18}$$

In order for these quantities to close the single-particle algebra (3.14), also rotation charges should combine non-linearly in the following way:

$$(R_k \oplus_\kappa R_q) = R_k + e^{-\ell k_2} R_q \,. \tag{3.19}$$

Alternative ways for guessing the momentum-composition formula have also been proposed in literature [79, 80]. As an alternative to the "κ-coproduct composition law" of Eqs.(3.18)-(3.19) we shall also consider the "proper-dS composition law",

$$\begin{aligned}\mathcal{P}_1 = (p^A \oplus_{dS} p^B)_1 &= p_1^A + p_1^B - \ell(p_2^A p_1^B + p_1^A p_2^B) + \\ &\quad + \frac{\ell^2}{2}\big[(p_2^A p_1^B + p_1^A p_2^B)(p_2^A + p_2^B) - p_1^A (p_1^B)^2 - (p_1^A)^2 p_1^B\big] \\ \mathcal{P}_2 = (p^A \oplus_{dS} p^B)_2 &= p_2^A + p_2^B + \ell p_1^A p_1^B - \frac{\ell^2}{2}\big[- p_1^B p_1^A (p_2^B + p_2^A) + p_2^A (p_1^B)^2 + (p_1^A)^2 p_2^B\big] \\ \mathcal{R} = (R^A \oplus_{dS} R^B) &= R^A + R^B\end{aligned} \tag{3.20}$$

which is commutative but non-associative and it was motivated using some geometric arguments (one can show that with these choices of composition laws momentum space acquires the geometrical structure of de Sitter space [79]).

3.0.3 Deformed harmonic-oscillator hamiltonians

In this analysis we consider a particular class of Hamiltonians on which we shall focus our search of Noether charges. Their core ingredient is the harmonic oscillator potential in two spatial dimensions and we will consider deformations of the following Hamiltonian

$$H_0^{AB} = \frac{(\vec{p}^A)^2}{2m} + \frac{(\vec{p}^B)^2}{2m} + \frac{1}{2}g(\vec{q}^A - \vec{q}^B)^2 \tag{3.21}$$

where we have called g the coupling constant, the labels A and B refer to the two particles interacting, $\vec{q}^J$ ($J \in \{A, B\}$) are ordinary commutative spatial coordinates, and $\vec{p}^J$ are the corresponding momenta, with standard Heisenberg commutators ($[q_j^J, p_k^K] = i\,\delta^{JK}\delta_{jk}$, with $J, K \in \{A, B\}$ and $j, k = 1, 2$). The total momentum $\vec{P}$ and total angular momentum R_0 defined as

$$\vec{P} = \vec{p}^A + \vec{p}^B \qquad R_0 = R_0^A + R_0^B \tag{3.22}$$

are conserved charges since they commute with the Hamiltonian, $[H_0^{AB}, \vec{P}] = 0$ and $[H_0^{AB}, R_0] = 0$. Both the total generators $\{P_i, R_0\}$ and the single particle generators $\{p_i^I, R_0^I\}$ close the un-deformed Galilean algebra.
Furthermore, we want to test our approach also for interactions among more than two particles, and for that purpose our starting point is the 3-particle Hamiltonian

$$H_0^{ABC} = \frac{(\vec{p}^A)^2}{2m} + \frac{(\vec{p}^B)^2}{2m} + \frac{(\vec{p}^C)^2}{2m} + \frac{1}{2}g(\vec{q}^A - \vec{q}^B)^2 + \frac{1}{2}g(\vec{q}^A - \vec{q}^C)^2 + \frac{1}{2}g(\vec{q}^B - \vec{q}^C)^2\,. \tag{3.23}$$

This is of interest to us particularly because the interacting potential $V_3(\vec{q}^A, \vec{q}^B, \vec{q}^C)$ can be split into the sum $V_2(\vec{q}^A, \vec{q}^B) + V_2(\vec{q}^A, \vec{q}^C) + V_2(\vec{q}^B, \vec{q}^C)$ with V_2 having the same functional form for each pair of particles. However, in the case studies for which we perfomed our Noether-charge analyses this property cannot be maintained in presence of non-commutativity of coordinates as we will show in the following of this chapter.

Clearly, the Hamiltonian (3.23) commutes with the total charges defined as $\vec{P} = \vec{p}^A + \vec{p}^B + \vec{p}^C$ and $R_0 = R_0^A + R_0^B + R_0^C$.

A fundamental ingredient of our deformed Hamiltonians will be of course the kinetic term, for which, inspired from the Casimir element $\mathcal{C}$ of our Eq.(3.14) (to order ℓ^2), we adopt the following expression

$$H_K \equiv \frac{\mathcal{C}}{2m} \approx \frac{p_1^2}{2m} + \frac{p_2^2}{2m} + \ell\frac{p_1^2 p_2}{2m} + \ell^2\frac{p_1^2 p_2^2}{4m} + \ell^2\frac{p_2^4}{24m}\,. \tag{3.24}$$

We will look for suitable interaction potentials by considering the following parameterization:

$$V^{AB} = V(\vec{x}^A, \vec{x}^B) = \frac{1}{2} g(\vec{x}^A - \vec{x}^B)^2 + \ell g \sum \alpha^{IJK}_{ijk} p^I_i x^J_j x^K_k + \ell^2 g \sum \beta^{IJKH}_{ijkh} p^I_i p^J_j x^K_k x^H_h \tag{3.25}$$

where α^{IJK}_{ijk} and β^{IJKH}_{ijkh} are dimensionless coefficients and the sum extends both to spatial indices (lower case letters) and particle indices (upper case letters).

Similarly, for the three-particle case we consider the following parameterization:

$$\begin{aligned} V^{ABC} = V(\vec{x}^A, \vec{x}^B, \vec{x}^C) =& \frac{1}{2} g(\vec{x}^A - \vec{x}^B)^2 + \frac{1}{2} g(\vec{x}^B - \vec{x}^C)^2 + \frac{1}{2} g(\vec{x}^C - \vec{x}^A)^2 + \\ &+ \ell g \sum \tilde{\alpha}^{IJK}_{ijk} p^I_i x^J_j x^K_k + \ell^2 g \sum \tilde{\beta}^{IJKH}_{ijkh} p^I_i p^J_j x^K_k x^H_h \end{aligned} \tag{3.26}$$

where $\tilde{\alpha}^{IJK}_{ijk}$ and $\tilde{\beta}^{IJKH}_{ijkh}$ are other sets of numerical coefficients and the particle indices run over $\{A, B, C\}$.

3.1 Conserved charges with proper-dS composition law

As already stressed before, the debate on the alternative ways to combine charges in a κ-Minkowski setup has mainly relied on naturalness arguments based on the properties of free particles in κ-Minkowski. Our aim is to demonstrate that the concept of "naturalness" is not applicable in this context. The way charges combine is determined by the laws governing the interactions among particles and various composition laws can arise from different descriptions of these interactions. Our argument will be supported by Hamiltonian models within first-quantized quantum mechanics, where all the pertinent issues are particularly evident.

We choose as our first task the one of exhibiting a Hamiltonian (within first-quantized quantum mechanics) which selects uniquely the proper-dS composition law, which we already presented in Eq.(3.20) and we show again here for usefulness:

$$\begin{aligned} \mathcal{P}_1 = (p^A \oplus_{dS} p^B)_1 &= p^A_1 + p^B_1 - \ell(p^A_2 p^B_1 + p^A_1 p^B_2) + \\ &+ \frac{\ell^2}{2}\big[(p^A_2 p^B_1 + p^A_1 p^B_2)(p^A_2 + p^B_2) - p^A_1 (p^B_1)^2 - (p^A_1)^2 p^B_1\big] \\ \mathcal{P}_2 = (p^A \oplus_{dS} p^B)_2 &= p^A_2 + p^B_2 + \ell p^A_1 p^B_1 - \frac{\ell^2}{2}\big[- p^B_1 p^A_1 (p^B_2 + p^A_2) + p^A_2 (p^B_1)^2 + (p^A_1)^2 p^B_2\big] \\ \mathcal{R} = (R^A \oplus_{dS} R^B) &= R^A + R^B \,. \end{aligned} \tag{3.27}$$

One can straightforwardly verify that $\mathcal{P}_1$, $\mathcal{P}_2$, $\mathcal{R}$ close the algebra (3.14) up to order ℓ^2, which we also rewrite here for suitability:

$$[\mathcal{P}_2, \mathcal{P}_1] = 0 \qquad [\mathcal{R}, \mathcal{P}_2] = -i\mathcal{P}_1 \qquad [\mathcal{R}, \mathcal{P}_1] = i(\mathcal{P}_2 - \ell\mathcal{P}_2^2 + \frac{\ell}{2}\mathcal{P}_1^2 + \frac{2\ell^2\mathcal{P}_2^3}{3}) \,. \tag{3.28}$$

We start by showing that for the case of two particles interacting there is a Hamiltonian H_{dS}^{AB}, deformation of the H_0^{AB} of Eq.(3.21), such that $[\vec{\mathcal{P}}, H_{dS}^{AB}] = 0$ and $[\mathcal{R}, H_{dS}^{AB}] = 0$. As anticipated in Subsection 3.0.3, our Hamiltonian H_{dS}^{AB} will be of the form

$$H_{dS}^{AB} = H_K^A + H_K^B + V_{dS}^{AB} \tag{3.29}$$

where H_K is fixed to be the one of Eq.(3.24), while V_{dS}^{AB} must be specified consistently with Eq.(3.25), for some choice of the parameters α_{ijk}^{IJK} and β_{ijkh}^{IJKH} that Eq.(3.25) leaves to be determined.

We partly work by reverse engineering using $[\vec{\mathcal{P}}, H_{dS}^{AB}] = 0$ and $[\mathcal{R}, H_{dS}^{AB}] = 0$ as conditions that must be satisfied by the parameters of Eq.(3.25), and then, once we have such an acceptable V_{dS}^{AB}, we show that the resulting Hamiltonian H_{dS}^{AB} uniquely selects the proper-dS charges (3.27) as its conserved charges.

We find that the following choice of V_{dS}^{AB}:

$$\begin{aligned}
V_{dS}^{AB} =& \frac{g}{2}\Big[(\vec{x}^A - \vec{x}^B)^2 + \\
&+2\ell\Big(- p_2^A (x_1^A)^2 + \frac{1}{2}p_1^A x_1^A x_2^A + \frac{1}{2}x_2^A x_1^A p_1^A + p_2^A x_1^A x_1^B - x_2^A p_1^A x_1^B + (A \leftrightarrow B)\Big) + \\
&+\frac{1}{2}\ell^2\Big((p_1^B)^2(-2(x_2^A)^2 + 6x_2^A x_2^B - 2(x_2^B)^2) + 4p_1^B p_2^B x_1^A x_2^A - p_1^A p_1^B x_2^A x_2^B + p_1^B p_2^A x_1^A x_2^B + \\
&-6p_1^B x_1^A x_2^B p_2^B - 2p_1^B x_1^B (p_2^A x_2^A - x_2^B p_2^B) - 2(p_2^B)^2((x_1^A)^2 - x_1^A x_1^B - (x_1^B)^2) + \\
&+p_2^B p_1^A x_2^A x_1^B - 2p_2^B p_2^A x_1^A x_1^B - 3p_2^B x_2^A x_1^B p_1^B + 2x_1^A p_1^A (p_1^A x_1^A - p_1^A x_1^B + p_2^A x_2^A + \\
&-\frac{3}{2}p_2^A x_2^B + \frac{3}{2}x_2^B p_2^B) + x_2^A p_2^A x_1^B p_1^B + (A \leftrightarrow B)\Big)\Big]
\end{aligned} \tag{3.30}$$

is indeed such that $[\vec{\mathcal{P}}, H_K^A + H_K^B + V_{dS}^{AB}] = 0$ and $[\mathcal{R}, H_K^A + H_K^B + V_{dS}^{AB}] = 0$.

We can notice that our V_{dS}^{AB} is symmetric under exchange of the particles (this is not always the case, see the following sections) reflecting the commutative nature of the composition laws of momenta.

Most importantly, we find that indeed the Hamiltonian $H_K^A + H_K^B + V_{dS}^{AB}$ uniquely selects the proper-dS charges (3.27) as its conserved charges. In order to see this we start from

a general parametrization of the two-particle charges

$$\begin{aligned} P_1^{tot} &= \sum p_1^I + \ell\gamma_{ij}^{IJ} p_i^I p_j^J + \ell^2 \Gamma_{ijk}^{IJK} p_i^I p_j^J p_k^K \\ P_2^{tot} &= \sum p_2^I + \ell\theta_{ij}^{IJ} p_i^I p_j^J + \ell^2 \Theta_{ijk}^{IJK} p_i^I p_j^J p_k^K \\ R^{tot} &= \sum R^I + \ell\phi_i^{IJ} p_i^I R^J + \ell^2 \Phi_{ij}^{IJK} p_i^I p_j^J R^K \end{aligned} \tag{3.31}$$

where $\gamma, \theta, \phi, \Gamma, \Theta, \Phi$ are sets of real coefficients and the sum is intended over particle indices I, J, K (which take values in $\{A, B\}$) and over the spatial indices i, j, k. We also require that no terms with all particle indices equal to each other are present, so that we recover the definition of single particle charge when all the charges of the other particles are equals to zero.

By requiring that these total charges commute with $H_K^A + H_K^B + V_{dS}^{AB}$ the parameters in Eq.(3.31) are fully fixed, giving indeed the proper-dS charges (3.27).

Next we turn to the corresponding three-particle case, for which the proper-dS composition leads to the following formulas for the charges:

$$\begin{aligned} \tilde{\mathcal{P}}_1 = ((p^A \oplus_{dS} p^B) \oplus_{dS} p^C)_1 &= p_1^A + p_1^B + p_1^C - \ell\big(p_2^B(p_1^C + p_1^A) + p_2^C(p_1^B + p_1^A) + \\ &+ p_2^A(p_1^C + p_1^B)\big) + \frac{\ell^2}{2}\big(-2p_1^A p_1^B p_1^C - (p_1^B)^2 p_1^A + 2p_1^A p_2^B p_2^C - p_1^B (p_1^A)^2 - (p_1^C)^2(p_1^B + p_1^A) + \\ &- (p_1^C)(p_1^B + p_1^A)^2 + 2p_2^C p_1^B p_2^A + (p_2^B + p_2^A)(p_2^B p_1^A + p_2^A p_1^B) + \\ &+ (p_2^A + p_2^B + p_2^C)(p_2^C(p_1^B + p_1^A) + p_1^C(p_2^A + p_2^B))\big) \end{aligned}$$

$$\begin{aligned} \tilde{\mathcal{P}}_2 = ((p^A \oplus_{dS} p^B) \oplus_{dS} p^C)_2 &= p_2^A + p_2^B + p_2^C + \ell\big(p_1^B p_1^A + p_1^C p_1^B + p_1^A p_1^C\big) + \\ &- \frac{\ell^2}{2}\big(p_2^C(p_1^A + p_1^B)^2 - p_1^C(p_2^C(p_1^B + p_1^A) + (p_1^B - p_1^A)(p_2^B - p_2^A)) + \\ &+ (p_1^C)^2(p_2^B + p_2^A) + (p_1^B - p_1^A)(-p_2^B p_1^A + p_1^B p_2^A)\big) \end{aligned}$$

$$\tilde{\mathcal{R}} = (R^A \oplus_{dS} R^B) \oplus_{dS} R^C = R^A + R^B + R^C \,. \tag{3.32}$$

Clearly we must find a Hamiltonian H_{dS}^{ABC}, deformation of the H_0^{ABC} of Eq.(3.23), such that $[\vec{\tilde{\mathcal{P}}}, H_{dS}^{ABC}] = 0$ and $[\tilde{\mathcal{R}}, H_{dS}^{ABC}] = 0$. As anticipated in Subsection 3.0.3, our Hamiltonian H_{dS}^{ABC} will be of the form

$$H_{dS}^{ABC} = H_K^A + H_K^B + H_K^C + V_{dS}^{ABC} \tag{3.33}$$

where H_K is again fixed to be the one of Eq.(3.24), while V_{dS}^{ABC} must be specified consistently with Eq.(3.26), for some choice of the parameters that Eq.(3.26) leaves to be determined.

A natural first guess is that the three-particle potential V_{dS}^{ABC} be given (see Eq(3.23)) by a combination of our two-particle potentials given in Eq.(3.30), *i.e.* $V_{dS}^{ABC} = V_{dS}^{AB} + V_{dS}^{BC} + V_{dS}^{AC}$, but one can straightforwardly check that this does not commute with the three-particle proper-dS charges (3.32). What does work is adding an extra term:

$$V_{dS}^{ABC} = V_{dS}^{AB} + V_{dS}^{BC} + V_{dS}^{AC} + V_{dS(\bigstar)}^{ABC} \tag{3.34}$$

with

$$\begin{aligned} V_{dS(\bigstar)}^{ABC} =& \frac{g\ell^2}{2}\Big(p_1^C p_2^B (x_1^C x_2^A - x_2^C x_1^A) - p_1^C p_2^A x_2^C x_1^B - p_2^C p_1^B (x_1^C x_2^A - x_2^C x_1^A) - p_2^C p_1^A x_1^C x_2^B + \\ &+ p_1^B p_1^A x_2^C (2x_2^C - x_2^A - x_2^B) - p_1^B p_2^A x_2^C (2x_1^C - x_1^B) - 2p_2^B p_1^A x_1^C x_2^C + \\ &+ p_2^B p_2^A x_1^C (2x_1^C - x_1^A - x_1^B) + p_1^A x_1^C p_2^B x_2^B + x_1^C p_1^C p_2^A x_2^B + \\ &+ x_2^C p_2^C p_1^A x_1^B + x_1^A p_1^A p_2^B x_2^C + x_2^A p_2^A p_1^B x_1^C \Big) . \end{aligned} \tag{3.35}$$

It is easy to check that the H_{dS}^{ABC} of Eqs.(3.33), (3.34), (3.35) commutes with the proper-dS charges (3.32). Most importantly we find that indeed our Hamiltonian H_{dS}^{ABC} uniquely selects the proper-dS charges (3.32) as its conserved charges. In order to see this we start from a general parametrization of the three-particle charges

$$\begin{aligned} \tilde{P}_1^{\,tot} &= \sum p_1^I + \ell \tilde{\gamma}_{ij}^{IJ} p_i^I p_j^J + \ell^2 \tilde{\Gamma}_{ijk}^{IJK} p_i^I p_j^J p_k^K \\ \tilde{P}_2^{\,tot} &= \sum p_2^I + \ell \tilde{\theta}_{ij}^{IJ} p_i^I p_j^J + \ell^2 \tilde{\Theta}_{ijk}^{IJK} p_i^I p_j^J p_k^K \\ \tilde{R}^{tot} &= \sum R^I + \ell \tilde{\phi}_i^{IJ} p_i^I R^J + \ell^2 \tilde{\Phi}_{ij}^{IJK} p_i^I p_j^J R^K \end{aligned} \tag{3.36}$$

which shares the same properties outlined for the two-particle ansatz (3.31) (the particle indices run over $\{A, B, C\}$ and $\tilde{\gamma}, \tilde{\theta}, \tilde{\phi}, \tilde{\Gamma}, \tilde{\Theta}, \tilde{\Phi}$ are sets of real coefficients).

We find that by requiring that these charges commute with our $H_K^A + H_K^B + V_{dS}^{AB}$ the parameters in Eq.(3.36) get fully fixed, giving indeed the proper-dS charges (3.32).

The meaning of the extra term $V_{dS(\bigstar)}^{ABC}$ is quite non-obvious and maybe future studies shall address the task of exploring it.

Whereas the potential in the original three-particle Hamiltonian H_0^{ABC} of Eq.(3.23) was just a sum of two-particle potentials, we found that the potential in its correct

"proper-dS deformation" H_{dS}^{ABC} must include the extra term $V_{dS(\bigstar)}^{ABC}$ which is cubic in the observables of the three particles and is made of all terms involving simultaneously observables of all the three particles.

It is also noteworthy that for the three-particle case the proper-dS composition gives charges which are not symmetric under particle exchange (this is because of non associativity of proper-dS composition law, see (3.32)) and accordingly our Hamiltonian H_{dS}^{ABC} also is not symmetric under particle-exchange. We do not see any objective issue with this lack of symmetry under particle-exchange, but still it is a bit unsettling. This made us interested in investigating which charges would be conserved if we adopted a particle-exchange symmetrized version of our Hamiltonian H_{dS}^{ABC}

$$H_{dS(sym)}^{ABC} = H_K^A + H_K^B + H_K^C + V_{dS}^{AB} + V_{dS}^{BC} + V_{dS}^{AC} + \frac{1}{6}\sum_{\pi(A,B,C)} V_{dS(\bigstar)}^{\pi(ABC)} \tag{3.37}$$

i.e. the Hamiltonian obtained by summing over all the possible particle permutations, $\pi(ABC)$, of the extra term.
We then ask for which choices of the parameters of our Eq.(3.36) the Hamiltonian $H_{dS(sym)}^{ABC}$ commutes with the charges parametrized in our Eq.(3.36), and we find that

$H^{ABC}_{dS(sym)}$ uniquely selects as its conserved charges the following ones

$$\begin{aligned}
\mathcal{P}_1^{dS(sym)} &= \frac{1}{3}[(p^A \oplus_{dS} p^B) \oplus_{dS} p^C + p^A \oplus_{dS} (p^B \oplus_{dS} p^C) + (p^A \oplus_{dS} p^C) \oplus_{dS} p^B]_1 = \\
&= p_1^A + p_1^B + p_1^C - \ell\big(p_1^A p_2^B + p_1^B p_2^A + p_1^A p_2^C + p_1^C p_2^A + p_1^B p_2^C + p_1^C p_2^B\big) + \\
&+ \frac{\ell^2}{2}\big(p_1^A((p_2^B)^2 + (p_2^C)^2) + (p_1^B + p_1^C)(p_2^A)^2 - p_1^A(p_1^B)^2 - p_1^B(p_1^A)^2 + \\
&- p_1^C(p_1^B)^2 - p_1^B(p_1^C)^2 + p_1^B(p_2^C)^2 + p_1^C(p_2^B)^2 + + p_1^C p_2^C p_2^B + p_1^B p_2^B p_2^C + \\
&- p_1^A(p_1^C)^2 - p_1^C(p_1^A)^2 - 4p_1^A p_1^B p_1^C + \frac{8}{3}(p_1^A p_2^B p_2^C + p_1^B p_2^A p_2^C + p_1^C p_2^B p_2^A) + \\
&+ p_2^A(p_1^C p_2^C + p_1^B p_2^C + p_1^A p_2^C + p_1^A p_2^B)\big)
\end{aligned}$$

$$\begin{aligned}
\mathcal{P}_2^{dS(sym)} &= \frac{1}{3}[(p^A \oplus_{dS} p^B) \oplus_{dS} p^C + p^A \oplus_{dS} (p^B \oplus_{dS} p^C) + (p^A \oplus_{dS} p^C) \oplus_{dS} p^B]_2 = \\
&= p_2^A + p_2^B + p_2^C + \ell(p_1^C(p_1^B + p_1^A) + p_1^B p_1^A) + \\
&- \frac{1}{6}\ell^2(3(p_1^C)^2(p_2^B + p_2^A) - p_1^C(3p_2^C(p_1^B + p_1^A) + 3p_1^B p_2^B - 4p_1^B p_2^A - 4p_2^B p_1^A + 3p_1^A p_2^A) + \\
&+ p_2^C(3(p_1^B)^2 + 4p_1^B p_1^A + 3(p_1^A)^2) + 3(p_1^B - p_1^A)(p_1^B p_2^A - p_2^B p_1^A))
\end{aligned}$$

$$\mathcal{R}^{dS(sym)} = R^A + R^B + R^C \tag{3.38}$$

which are symmetric under particle exchange. Furthermore, these charges $\mathcal{P}_1^{dS(sym)}$, $\mathcal{P}_2^{dS(sym)}$, $\mathcal{R}^{dS(sym)}$ close the algebra (3.14).

3.2 Conserved charges with κ-coproduct composition law

In this section we apply the same strategy of analysis as before to the coproduct composition law of Eqs.(3.18)-(3.19), which we rewrite here at order ℓ^2 for convenience

$$\begin{aligned}
\mathcal{P}_1 &= (p^A \oplus_\kappa p^B)_1 = p_1^A + p_1^B - \ell p_2^A p_1^B + \frac{\ell^2}{2}(p_2^A)^2 p_1^B \\
\mathcal{P}_2 &= (p^A \oplus_\kappa p^B)_2 = p_2^A + p_2^B \\
\mathcal{R} &= R^A \oplus_\kappa R^B = R^A + R^B - \ell p_2^A R^B + \frac{\ell^2}{2}(p_2^A)^2 R^B \,.
\end{aligned} \tag{3.39}$$

As done for the proper-dS case, our first objective is to find a Hamiltonian H_κ^{AB}, that is a deformation of the H_0^{AB} of Eq.(3.21), such that $[\vec{\mathcal{P}}, H_\kappa^{AB}] = 0$ and $[\mathcal{R}, H_\kappa^{AB}] = 0$. Following the same strategy of the previous section, we find that the Hamiltonian $H_\kappa^{AB} = H_K^A + H_K^B + V_\kappa^{AB}$ with

$$\begin{aligned} V_\kappa^{AB} = \frac{g}{2}\Big[&(\vec{x}^A - \vec{x}^B)^2 + \\ &2\ell\left(-p_2^A(x_1^A)^2 + x_1^A p_2^A x_1^B + \frac{1}{2}x_2^A p_1^A x_1^A + \frac{1}{2}x_2^A x_1^A p_1^A - x_2^B p_1^A x_1^A - \frac{1}{2}x_2^B p_1^A x_1^A\right) \\ &2\ell^2\left((p_2^A)^2(x_1^A)^2 + \frac{1}{2}x_1^A(p_1^A)^2 x_1^A - \frac{1}{2}x_1^A(p_2^A)^2 x_1^B\right)\Big] \end{aligned} \tag{3.40}$$

is such that indeed $[\vec{\mathcal{P}}, H_K^A + H_K^B + V_\kappa^{AB}] = 0$ and $[\mathcal{R}, H_K^A + H_K^B + V_\kappa^{AB}] = 0$. And we find that the Hamiltonian $H_K^A + H_K^B + V_\kappa^{AB}$ uniquely selects the κ-coproduct charges (3.39) as its conserved charges. This is easily shown by starting again from the general charge ansatz (3.31) and requiring that they commute with $H_K^A + H_K^B + V_\kappa^{AB}$: this requirement fully fixes all the parameters in Eq.(3.31), giving indeed the κ-coproduct charges (3.39).

It is noteworthy that the κ-coproduct charges (3.39), differently from the proper-dS two particle case, are not symmetric under the exchange of particles A and B, and accordingly also our Hamiltonian H_κ^{AB} is not symmetric (because the potential V_κ^{AB} of (3.40) is not symmetric). We found that the analogous issue of lacking particle-exchange symmetry that we encountered in our analysis of the proper-dS composition law could be "fixed" by resorting to a symmetrized version of the Hamiltonian, but for the κ-coproduct composition law this is not the case: if one considers the symmetrized Hamiltonian

$$H_{\kappa(sym)}^{AB} = \frac{H_\kappa^{AB} + H_\kappa^{BA}}{2} \tag{3.41}$$

then one finds that no choice of the parameters in (3.31) leads to charges that commute with $H_{AB}^{\kappa(sym)}$.

For the three-particle case the κ-coproduct composition law gives

$$\tilde{\mathcal{P}}_1 = (p^A \oplus_\kappa p^B \oplus_\kappa p^C)_1 = p_1^A + p_1^B + p_1^C + \ell\left(-p_1^B p_2^A - p_1^C(p_2^A + p_2^B)\right) + \\ + \ell^2\left(\frac{p_1^B (p_2^A)^2}{2} + \frac{1}{2} p_1^C (p_2^A + p_2^B)^2\right)$$

$$\tilde{\mathcal{P}}_2 = (p^A \oplus_\kappa p^B \oplus_\kappa p^C)_2 = p_2^A + p_2^B + p_2^C \tag{3.42}$$

$$\tilde{\mathcal{R}} = (R^A \oplus_\kappa R^B \oplus_\kappa R^C) = R^A + R^B + R^C + \ell\left(-p_2^A\left(R^B\right) - R^C\left(p_2^A + p_2^B\right)\right) + \\ + \ell^2\left(\frac{1}{2} R^C\left(p_2^A + p_2^B\right)^2 + \frac{1}{2}(p_2^A)^2 R^B\right).$$

Using the same procedure of Section 3.1 one finds that the Hamiltonian

$$H_\kappa^{ABC} = H_K^A + H_K^B + H_K^C + V_\kappa^{AB} + V_\kappa^{BC} + V_\kappa^{AC} + V_{\kappa(\bigstar)}^{ABC}, \tag{3.43}$$

with

$$\begin{aligned} V_{\kappa(\bigstar)}^{ABC} =& g\ell\big(p_1^B(x_1^C x_2^A - x_2^C x_1^A + x_1^A x_2^B - x_1^C x_2^B) + p_2^B x_1^B (x_1^C - x_1^A)\big) + \\ &+ g\frac{\ell^2}{2}\big((p_1^B)^2(x_1^C x_1^A - x_1^B x_1^C + x_1^B x_1^A) - (p_2^B)^2(x_1^C x_1^A - 2x_1^A x_1^B) + p_1^B x_1^C (p_1^A x_1^A - p_2^B x_2^B) + \\ &+ p_1^B p_2^A (x_2^C x_1^A - x_1^A x_2^B) + p_2^B (p_1^B x_1^A x_2^C + p_2^A x_1^A x_1^B)\big), \end{aligned} \tag{3.44}$$

commutes with $\vec{\tilde{\mathcal{P}}}$ and $\tilde{\mathcal{R}}$. It is noteworthy that the κ-coproduct extra term $V_{\kappa(\bigstar)}^{ABC}$, besides involving terms that depend simultaneously on observables of all three particles, also contains terms that depend only on two of the particles (and these additional terms cannot be re-absorbed in a redefinition of the potentials $\tilde{V}_\kappa^{IJ}$ since they are different for different pairs of particles).

Also in this case we find that the Hamiltonian H_κ^{ABC} of our Eq.(3.43) uniquely selects the κ-coproduct charges (3.42) as its conserved charges: by requiring that the parametrized charges of Eq.(3.36) commute with H_κ^{ABC} the parameters in Eq.(3.36) get fully fixed, giving indeed the κ-coproduct charges (3.42).

Finally notice that H_κ^{ABC} is not symmetric under particle exchange and its symmetrized version,

$$H_{\kappa(sym)}^{ABC} = H_K^A + H_K^B + H_K^C + \frac{1}{6}\sum_{\pi(A,B,C)} V_\kappa^{\pi(ABC)}, \tag{3.45}$$

is not a viable alternative since it does not have any associated conserved charges: there is no choice of the parameters in Eq.(3.36) such that the parametrized charges of Eq.(3.36) commute with $H^{ABC}_{\kappa(sym)}$.

3.3 Comments on other quantum spacetimes

In this chapter we have disccused a novel startegy to look for conserved charges in quantum spacetimes.

Until now, the debate on total charges for quantum spacetimes had not considered a possible role for the interactions, relying instead only on some “naturalness arguments" based on the form of the relativistic properties of free particles. However, in this chapter, we have shown that the notion of total momenta in quantum spacetimes cannot be "guessed", but it strongly depends on the kind of interactions that are introduced. Of course our analysis only concerned with the spatial 2D κ-Minkowski toy model, but we are quite confident that the lessons learned within this model apply also to other kind of quantum spacetimes. In particular, we expect that the specific form of spacetime quantization might affect the analysis through the level of complexity of Hamiltonians. Indeed, the Hamiltonians we here exhibited appear to be unpleasantly intricate. It is therefore natural to wonder if some ways to quantize spacetime with deformed relativistic symmetries could produce simpler descriptions of interactions among particles. If such a simplicity aspect was discovered within a specific spacetime quantization framework it might provide encouragement for the studies of other aspects of that quantum spacetime.

Furthermore, it could be interesting to generalize our results also to the 3D case, that is a quite straightforward task, but we essentially expect the same conceptual results we obtained within our bidimensional framework.

Chapter 4

Observers and reference frames in quantum spacetimes

In the previous chapters of this thesis we have presented some examples of quantum spacetimes and we discussed how their deformed symmetries can be described in terms of Hopf algebras structures and quantum groups. These deformations in general lead to modifications of particle kinematics and dynamics. Moreover, it is reasonable to expect that deformations of classical symmetries can also affect in a non-trivial way the properties of the reference frames.
In this chapter we explore the possible role of observers in quantum spacetimes and how the notion of reference frames can be affected by quantum gravity induced effects focusing on a quantum group toy model [81].

In both general relativity and quantum mechanics observers typically assume an "external" position. Specifically, in the former, their influence on spacetime is considered negligible, allowing them to explore it without causing any significant back-reaction. In quantum theory, instead, they are separated from the observed system by the famous Heisenberg cut [82, 83]. The observers are thus described as classical, however, there are mutually-incompatible measurements that they can choose to perform (complementarity). Quantum mechanics introduces therefore an important novelty in the measurement process, namely, the operationally-meaningful properties of the observed systems depend on some choices made by the observer. Observers, in this way, become what we will call “agents", in the sense that their choices have non-trivial consequences for what concerns measurements in quantum mechanics.

In the attempt of combining quantum theory and general relativity into a quantum theory of gravity, we are typically led to consider spacetime as a quantum object. In particular, the most studied possibility in this context is that quantum gravity effects can determine a small-scale discreteness or fuzziness in some geometrical quantities. Such effects have been investigated in the context of several approaches to quantum gravity [84–89] and involve a variety of manifestations.

From this perspective, we are thus led to contemplate the possibility that the agency-dependence of quantum mechanics might challenge the notion of an objective spacetime that all observers agree upon. Specifically, spacetime properties could be affected by some choices the observer (agent) makes. Vice versa, the quantum properties of spacetime could have a non-trivial impact on the spectrum of possible operations available to an agent. Therefore, these observations suggest a picture in which spacetime and the agency of observers affect each other inextricably, so much so that the “externality” idealization that is a good working hypothesis in general relativity and quantum the-

ory, will have to be abandoned in favor of a notion of "internal" observers in quantum gravity [90].

In this chapter, we take first steps toward this largely unexplored aspect of quantum gravity focusing on the relative state of the reference frames of two observers, Alice and Bob, who live in a non-classical spacetime. We will rely on a simplified model, in which we assume that the two observers are exclusively interested in finding out the relative spatial orientations of their frames. In standard quantum mechanics, the rotation matrix connecting the two reference frames can be determined, according to a standard alignment protocol, by exchanging qubits, as discussed in section 4.2. In particular, the two observers can determine the matrix elements with arbitrary precision by a large enough number of exchanges. However, in the case in which Alice and Bob live in a quantum spacetime, reaching an arbitrary precision may be forbidden. In particular, we will show that the non-commutativity aspects introduced by quantum groups establish an intrinsic uncertainty on the entries of the rotation matrix relating two observers, affecting the possibility of determining their relative orientation. Nevertheless, we are still far from developing a deformed version of the standard alignment protocol, but we set the stage for this kind of investigation obtaining many interesting results that we present and discuss in the following of this chapter.

In this analysis, because we are only interested in the relative orientation between reference frames, we can model our non-classical space simply by deforming the rotation group $SO(3)$, or rather its double cover $SU(2)$ which describes the rotations of qubits.

Specifically, we will deal with one of the simplest examples of quantum groups: $SU_q(2)$ [91], which is the (only) quantum-group deformation of the $SU(2)$ group. The lowercase q identifies a dimensionless deformation parameter, such that the case $q = 1$ reproduces the undeformed $SU(2)$ group. One piece of theoretical evidence in favour of quantum/non-classical angles in quantum gravity is the fact that the introduction of a positive cosmological constant in Spin Foams/Loop Quantum Gravity requires changing the internal gauge group of triads from $SU(2)$ to $SU_q(2)$. In these models q is a function of the dimensionless ratio between the Planck length and the Hubble length scale associated to the cosmological constant [27]. It has been argued that this reflects a minimal possible resolution in angular measurements [92]. One could also imagine a physical scenario in which the dimensionless q could acquire a dependence on the characteristic energy scale E of the problem via, for example, the dimensionless ratio E/E_p, with E_p the Planck energy. This feature could arise in field theories in which q is

a parameter appearing in the lagrangian, and thus would run with the energy as other parameters do. To the best of our knowledge, no concrete example with such features has been constructed, so we do not speculate upon this possibility further.

The mathematical details of $SU_q(2)$ have been extensively developed in [91, 93–95]. However, in this analysis we are interested in further exploring the physical features of this quantum group to obtain novel effects that observers would see if, in an effective regime of quantum gravity, rotations of reference frames were described by $SU_q(2)$ transformations.

Before exploring the properties of the $SU_q(2)$ quantum groups, let us briefly review the main aspects of the classical rotation group $SO(3)$ and its double cover $SU(2)$ in the next section.

4.1 $SU(2)$ preliminaries

The $SU(2)$ group is defined as the group of 2×2 unitary matrices with determinant equal to 1. A generic element $U \in SU(2)$ can be parametrized in the following way

$$U = \begin{pmatrix} a & -c^* \\ c & a^* \end{pmatrix} \quad , \tag{4.1}$$

where a and c are two complex numbers satisfying the relation

$$aa^* + cc^* = 1 \quad , \tag{4.2}$$

constraining the degrees of freedom to three real numbers. A typical parametrization for a and c in terms of three real numbers is given by

$$a = e^{i\eta} \cos\frac{\theta}{2} \qquad c = e^{i\delta} \sin\frac{\theta}{2} \quad , \tag{4.3}$$

with $\eta, \delta \in [0, 2\pi)$ and $\theta \in [0, \pi)$. These three angles encode all the information needed to uniquely identify a $SU(2)$ element and are useful in identifying the connection between $SU(2)$ and the rotation group $SO(3)$. Indeed, the canonical homomorphism between the two groups is realized via

$$R_{ij} = \frac{1}{2} \mathrm{Tr}\left\{\sigma_i \, U \, \sigma_j \, U^\dagger\right\} \equiv \frac{1}{2} \mathrm{Tr}\left\{U \, \sigma_j \, U^\dagger \, \sigma_i\right\} \quad , \tag{4.4}$$

where R_{ij} is a rotation matrix, U is parametrized as in (4.1) and σ_i are the Hermitian Pauli matrices that we review here for completeness:

$$\sigma_1 = \begin{pmatrix} 0 & 1 \\ 1 & 0 \end{pmatrix}, \quad \sigma_2 = \begin{pmatrix} 0 & -i \\ i & 0 \end{pmatrix}, \quad \sigma_3 = \begin{pmatrix} 1 & 0 \\ 0 & -1 \end{pmatrix} \tag{4.5}$$

Writing (4.4) explicitly, we obtain

$$R = \begin{pmatrix} \frac{1}{2}(a^2 - c^2 + (a^*)^2 - (c^*)^2) & \frac{i}{2}(-a^2 + c^2 + (a^*)^2 - (c^*)^2) & (a^*c + c^*a) \\ \frac{i}{2}(a^2 + c^2 - (a^*)^2 - (c^*)^2) & \frac{1}{2}(a^2 + c^2 + (a^*)^2 + (c^*)^2) & -i(a^*c - c^*a) \\ -(ac + c^*a^*) & i(ac - c^*a^*) & 1 - 2cc^* \end{pmatrix} . \tag{4.6}$$

Inserting parametrization (4.3) in (4.6) we obtain the rotation matrix in terms of trigonometric functions of the three real angles η, δ and θ. These are simply a re-definition of the well known Euler angles (α, β, γ) in terms of which, a generic rotation matrix is written as $R(\alpha, \beta, \gamma) = R_z(\alpha)R_x(\beta)R_z(\gamma)$, with

$$R_z(\alpha) = \begin{pmatrix} \cos(\alpha) & \sin(\alpha) & 0 \\ -\sin(\alpha) & \cos(\alpha) & 0 \\ 0 & 0 & 1 \end{pmatrix} \qquad R_x(\beta) = \begin{pmatrix} 1 & 0 & 0 \\ 0 & \cos(\beta) & \sin(\beta) \\ 0 & -\sin(\beta) & \cos(\beta) \end{pmatrix} \tag{4.7}$$

where R_z and R_x are rotations around the z-axis and x-axis respectively. Multiplying these out, we obtain

$$R = \begin{pmatrix} \cos(\alpha)\cos(\gamma) - \cos(\beta)\sin(\alpha)\sin(\gamma) & \cos(\beta)\cos(\gamma)\sin(\alpha) + \cos(\alpha)\sin(\gamma) & \sin(\alpha)\sin(\beta) \\ -\cos(\gamma)\sin(\alpha) - \cos(\alpha)\cos(\beta)\sin(\gamma) & \cos(\alpha)\cos(\beta)\cos(\gamma) - \sin(\alpha)\sin(\gamma) & \cos(\alpha)\sin(\beta) \\ \sin(\beta)\sin(\gamma) & -\cos(\gamma)\sin(\beta) & \cos(\beta) \end{pmatrix} \tag{4.8}$$

We can now compare rotation matrices (4.8) and (4.6) by using the definition (4.3) for parameters a, c to find the relation between Euler angles and the parameters of $SU(2)$, which is

$$\theta = \beta \qquad \eta = \frac{\alpha + \gamma}{2} \qquad \delta = \frac{\pi}{2} - \frac{\alpha - \gamma}{2} . \tag{4.9}$$

4.2 Alignment protocol in classical space

Let us illustrate a simple protocol for two observers, who live in a classical Euclidean spatial environment, but do not share a classical reference frame, to synchronize their

spatial orientations by communicating qubits, i.e. SU(2) spinors (see also [96]).

4.2.1 Qubits as $SU(2)$ spinors in standard quantum theory

A single qubit state can be represented as a density matrix ρ that expanded in the basis of the identity $\mathbb{1}$ and Hermitian Pauli matrices σ_i has the following form

$$\rho = \frac{1}{2}(\mathbb{1} + \vec{r}\cdot\vec{\sigma})\,, \tag{4.10}$$

where the expectation values of the spin observables give the components of the Bloch vector:

$$r_i = \langle\sigma_i\rangle = \mathrm{Tr}\,\{\rho\,\sigma_i\}\,. \tag{4.11}$$

The latter relation holds since the Pauli matrices form an orthonormal basis

$$\mathrm{Tr}\,\{\sigma_\mu\,\sigma_\nu\} = 2\,\delta_{\mu\nu}\,, \tag{4.12}$$

where $\sigma_0 := \mathbb{1}$. As such, we can also define a 4-dimensional Bloch vector

$$r_\mu = \mathrm{Tr}\,\{\rho\,\sigma_\mu\} \tag{4.13}$$

whose zero-component

$$r_0 = \mathrm{Tr}\,\rho = 1 \tag{4.14}$$

is simply the normalization of the state.

Consider now an $SU(2)$ transformation of the quantum state. As it turns out, the density matrix (4.10) decomposes into an $SU(2)$-invariant singlet and an $SU(2)$-covariant triplet term, since for any matrix $U \in SU(2)$,

$$\rho \to U\,\rho\,U^\dagger = \frac{1}{2}(\mathbf{1} + \vec{r}\cdot U\,\vec{\sigma}\,U^\dagger) = \frac{1}{2}(\mathbf{1} + \vec{r'}\cdot\vec{\sigma})\,, \tag{4.15}$$

where now the transformed Bloch vector is

$$\vec{r'} = R\cdot\vec{r} \tag{4.16}$$

with

$$R_{ij} = \frac{1}{2}\,\mathrm{Tr}\left\{U\sigma_j\,U^\dagger\,\sigma_i\right\} \tag{4.17}$$

an element of $PSU(2) \simeq SO(3)$. So, if the quantum state is transformed by an $SU(2)$ matrix, the Bloch vector $\vec{r}$ that represents it transforms like a 3-dimensional vector under spatial rotations.

Evidently, the phase of the $SU(2)$ transformations is cancelled and the adjoint action of $SU(2)$ yields a spatial rotation in its fundamental representation. Hence, the normalization r_0 is an $SU(2)$-invariant, while $\vec{r}$ transforms in the adjoint representation of $SU(2)$ and thus under the fundamental representation of $SO(3)$.

In this way, we can associate to every $SU(2)$ transformation of states or spin observables an $SO(3)$ spatial rotation. In particular, we can write the same qubit state relative to different bases of Pauli matrices $U\,\vec{\sigma}\,U^\dagger$ by rotating the corresponding Bloch vector accordingly,

$$\vec{r'}_\rho = \mathrm{Tr}\left\{\rho\, U\,\vec{\sigma}\,U^\dagger\right\} = R^{-1}\cdot\vec{r}_\rho = R^{-1}\cdot\mathrm{Tr}\left\{\rho\,\vec{\sigma}\right\}, \tag{4.18}$$

where $\vec{r'}_\rho$ and $\vec{r}_\rho$ are both Bloch vectors of the same quantum state ρ, however, written relative to different observable bases. Interpreting $U\,\vec{\sigma}\,U^\dagger$ and $\vec{\sigma}$ as being the observables corresponding to differently oriented sets of Stern-Gerlach devices in the lab, this rewriting allows us to express how observers with different spatially oriented reference frames will 'see' the same quantum state of (possibly an ensemble of) a qubit.

4.2.2 Alignment protocol by exchanging qubits

Suppose that two observers, Alice and Bob, do not know the relative orientation between their reference frames. Supposing further that they can communicate classically, they can proceed as follows in order to figure out the relation between their descriptions (see fig. 4.1). Alice prepares three ensembles of qubits, each prepared such that the ensemble state corresponds to a Bloch sphere basis vector. For example, she could prepare three ensembles of N qubits each so that

$$E_{x_A} = \{\vec{r}_{x_A,n} = (1,0,0)\}_{n=1}^N\,, \quad E_{y_A} = \{\vec{r}_{y_A,n} = (0,1,0)\}_{n=1}^N\,, \quad E_{z_A} = \{\vec{r}_{z_A,n} = (0,0,1)\}_{n=1}^N\,, \tag{4.19}$$

i.e., every qubit of the first ensemble is prepared to be in the 'up in x_A-direction' pure state, where x_A is Alice's x-direction, and similarly for the other two ensembles. Alice can then send Bob these three ensembles to perform state tomography on them. Bob could proceed as follows: he divides each ensemble in three subensembles and measures all qubits of the first subensemble with a Stern-Gerlach (SG) device oriented in x_B-direction, of the second in y_B-direction and of the third in z_B-direction. This will tell him how to write Alice's states relative to his basis and, via (4.18), what the relative

SO(3) rotation between their spatial frames is. For example, relative to Alice, the ensemble state of E_{x_A} appears as

$$\rho_{x_A} = \frac{1}{2}(\mathbb{1} + \vec{r}_{x_A} \cdot \vec{\sigma}_A) = \frac{1}{2}(\mathbb{1} + \sigma_{x_A})\,. \tag{4.20}$$

Suppose now that Bob's measurement apparata are in the following relation with Alice's: $\vec{\sigma}_A = U\,\vec{\sigma}_B\,U^\dagger$. Then, using (4.18), we can write the same ensemble state, but now relative to Bob as

$$\rho_{x_A} = \frac{1}{2}\big(\mathbb{1} + \vec{r}_{x_A} \cdot U\,\vec{\sigma_B}\,U^\dagger\big) = \frac{1}{2}(\mathbb{1} + \vec{r}_{x_B} \cdot \vec{\sigma}_B)\,, \tag{4.21}$$

where

$$\vec{r}_{x_B} = R \cdot \vec{r}_{x_A} \tag{4.22}$$

and

$$R_{ij} = \frac{1}{2}\,\mathrm{Tr}\left\{(\sigma_A)_i\,U\,(\sigma_A)_j\,U^\dagger\right\} \equiv \frac{1}{2}\,\mathrm{Tr}\left\{U\,(\sigma_A)_j\,U^\dagger\,(\sigma_A)_i\right\}, \tag{4.23}$$

which is equivalent to (4.17) if we remember that U are unitary matrices. Bob can measure $\vec{r}_{x_B} = \mathrm{Tr}\,\{\rho_{x_A}\vec{\sigma}_B\}$ using tomography on E_{x_A}, which is why he has to split that ensemble into three subensembles to measure its qubits relative to a basis of Stern Gerlach devices.

Proceeding this ways also with E_{y_A}, E_{z_A}, Bob can figure out the Bloch vector basis $\vec{r}_{x_B}, \vec{r}_{y_B}, \vec{r}_{z_B}$ of Alice's ensemble states relative to his frame and if Alice also tells him how she describes the same states, namely as $\vec{r}_{x_A}, \vec{r}_{y_A}, \vec{r}_{z_A}$, then they can simply compute R from the relation of these two sets of bases. In principle, Bob has to perform an infinite number of measurements to determine the rotation matrix connecting his reference frame with Alice's with arbitrary precision. From this, the matrix (4.6) admits a direct, operational interpretation in terms of (4.23): it is the matrix of the asymptotic $N \to \infty$ values of the averages of the spin measurements that Bob performs on the qubit states sent to him by Alice.

4.3 Quantum rotation matrices in $SU_q(2)$

4.3.1 $SU_q(2)$ algebra and homomorphism with $SO_q(3)$

The quantum group $SU_q(2)$ is defined by considering the algebra of complex functions on $SU(2)$, denoted by $C(SU(2))$ and deforming it in a non-commutative way. The

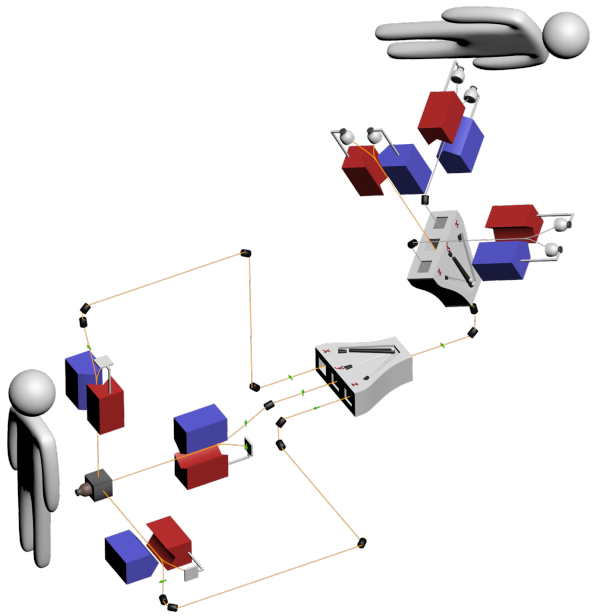

Figure 4.1: Alice (on the left) prepares a set of N qubits (e.g., electron spins) in the spin-up eigenstate of her x-axis (e.g., by passing unpolarized electrons through a x-oriented Stern–Gerlach apparatus, and selecting only the ones that emerge with their spins up). She then sends these electrons to Bob, whose laboratory is rotated by an unknown amount with respect to hers. Bob divides these N qubits in three groups, and sends each group through a machine that measures the spin along one of his three orthogonal axes (e.g., three perpendicular Stern–Gerlach apparata - in the picture, he is passing the electrons through a y-oriented machine). He then counts the number of spin-up and spin-down measurements that each machine reads, and calculates the expectation value of the corresponding observable. Repeating the experiment for a set of N qubits that Alice selected to be polarized along the $y-$axis, and, respectively, $z-$axis allows Bob to build a statistics of the expectation values of the nine observables associated to each pair of choices of axes made by him and Alice. In the large-N limit, these expectation values tend to the nine components of the rotation matrix R that connects Alice's reference frame and Bob's. Notice that, in this illustrative picture the electron beams (in orange) are manipulated with some "mirrors" (the black cylinders) which are assumed not to have any effect on the qubit states.

generators $\{a, c\}$ are regarded as functions on the group, satisfying the following non-

trivial commutation relations:

$$\begin{aligned} &ac = qca \qquad ac^* = qc^*a \qquad cc^* = c^*c \\ &c^*c + a^*a = \mathbb{1} \qquad aa^* - a^*a = (1-q^2)c^*c\,. \end{aligned} \tag{4.24}$$

Here, $\mathbb{1}$ refers to the identity element of the algebra and q is the deformation parameter assumed to be close to 1 and in particular $q \lesssim 1$. Indeed, in the $q \to 1$ limit, we obtain the commutative limit and recover the classical description of $SU(2)$. It is sufficient to consider $q \lesssim 1$ since, if $q > 1$, the mapping $a \mapsto a^*$, $c \mapsto qc^*$ sends the $SU_q(2)$ algebra to the $SU_{q^{-1}}(2)$ one.

The above is an example of a unital *-algebra with generators $\{a, c\}$. This algebra can be enriched with additional structures to form an Hopf algebra. To do this, we present below the coproducts, antipodes and counits acting on the generators:

$$\begin{cases} \Delta(a) = a \otimes a - qc^* \otimes c \\ \Delta(a^*) = a^* \otimes a^* - qc \otimes c^* \\ \Delta(c) = c \otimes a + a^* \otimes c \\ \Delta(c^*) = c^* \otimes a^* + a \otimes c^* \end{cases} \qquad \begin{cases} S(a) = a^* \\ S(a^*) = a \\ S(c) = -q^{-1}c \\ S(c^*) = -qc^* \end{cases} \qquad \begin{cases} \epsilon(a) = 1 \\ \epsilon(a^*) = 1 \\ \epsilon(c) = 0 \\ \epsilon(c^*) = 0 \end{cases} \tag{4.25}$$

To establish a first link with the classical picture, we present the generalization of the spin-1/2 representation (4.1), given by

$$U_q = \begin{pmatrix} a & -qc^* \\ c & a^* \end{pmatrix} \qquad a, c \in C(SU_q(2)) \quad q \in (0,1)\,. \tag{4.26}$$

We will now construct one of the key ingredients of the analysis which is a q-analogue of the homomorphism between $SU(2)$ and $SO(3)$. In order to do so, we promote the classical homomorphism $R_{ij} = \frac{1}{2}\,\mathrm{Tr}\left\{\sigma_j\, U^\dagger\, \sigma_i\, U\right\}$, where σ_i are the Pauli matrices, to its quantum version by replacing U with U_q

$$(R_q)_{ij} = \frac{1}{2}\,\mathrm{Tr}\left\{\sigma_j\, U_q^\dagger\, \sigma_i\, U_q\right\}. \tag{4.27}$$

By computing these elements explicitly, we obtain

$$R_q = \begin{pmatrix} \frac{1}{2}(a^2 - qc^2 + (a^*)^2 - q(c^*)^2) & \frac{i}{2}(-a^2 + qc^2 + (a^*)^2 - q(c^*)^2) & \frac{1}{2}(1+q^2)(a^*c + c^*a) \\ \frac{i}{2}(a^2 + qc^2 - (a^*)^2 - q(c^*)^2) & \frac{1}{2}(a^2 + qc^2 + (a^*)^2 + q(c^*)^2) & -\frac{i}{2}(1+q^2)(a^*c - c^*a) \\ -(ac + c^*a^*) & i(ac - c^*a^*) & 1 - (1+q^2)cc^* \end{pmatrix} \tag{4.28}$$

and one can check that in the commutative limit $q \to 1$ this coincides with the matrix obtained via the classical homomorphism (4.6). This matrix provides a (co)-representation of $SO_q(3)$ related to the (co)-representation found in [95] by a similarity transformation. In this quantization procedure, we have replaced the classical U with the deformed U_q in (4.4), thus replacing the complex numbers a and c with the operators satisfying (4.24), and we do not deform the Pauli matrices. It may be argued that a deformation of the Pauli matrices, such as the one studied in [97], should be considered. However, doing so leads to non-hermitian operators for the entries of the resulting matrix. With our choice instead we get hermitian operators and we also reconstruct a matrix that matches the one obtained in [95] upon doing a change of basis, and this guarantees that we obtain a representation of $SO_q(3)$ as explained shortly.

We also note that in (4.27) the cyclic property of the trace operation does not hold because of the noncommutative nature of a and c. This gives rise to a "quantization ambiguity" which however does not affect our phenomenological results. In particular, we will discuss our results using matrix (4.28) which is obtained quantizing the first ordering in (4.4), but another definition of the quantum rotation matrix is possible. The alternative to (4.28), obtained using the second ordering in (4.4), is

$$P_q = \begin{pmatrix} \frac{1}{2}(a^2 - qc^2 + (a^*)^2 - q(c^*)^2) & \frac{i}{2}(-a^2 + qc^2 + (a^*)^2 - q(c^*)^2) & q(a^*c + c^*a) \\ \frac{i}{2}(a^2 + qc^2 - (a^*)^2 - q(c^*)^2) & \frac{1}{2}(a^2 + qc^2 + (a^*)^2 + q(c^*)^2) & -iq(a^*c - c^*a) \\ -\frac{1+q^2}{2q}(ac + c^*a^*) & i\frac{1+q^2}{2q}(ac - c^*a^*) & 1 - (1+q^2)cc^* \end{pmatrix}. \tag{4.29}$$

It turns out that P_q and R_q are actually similar matrices: $R_q = MP_qM^{-1}$, with

$$M = \begin{pmatrix} 2^{\frac{1}{3}}(\frac{q}{1+q^2})^{\frac{1}{3}} & 0 & 0 \\ 0 & 2^{\frac{1}{3}}(\frac{q}{1+q^2})^{\frac{1}{3}} & 0 \\ 0 & 0 & \frac{(\frac{1}{q}+q)^{\frac{2}{3}}}{2^{\frac{2}{3}}} \end{pmatrix}. \tag{4.30}$$

This matrix (with its inverse) reduces to the identity at first order in $(1-q)$ so that the two matrices are equivalent from a phenomenological point of view. Indeed, since the quantum-gravity expectation is that q is extremely close to 1, the search for experimental manifestations of our q-deformation is not likely to ever go beyond the leading $(1-q)$-order effects [23].

Notice that the two matrices come from an ambiguity of the "quantization procedure", namely the ordering of the matrices in (4.4). This is similar to what happens in stan-

dard quantum mechanics where different orderings in the classical observables give rise to different quantum operators which give the same classical limits.

Let us conclude this discussion clarifying the link between the vector (co)-representation of $SU_q(2)$ is linked to the (co)-representation of the quantum group $SO_q(3)$ via the isomorphism $C(SO_q(3)) \coloneqq C(SU_q(2)/\mathbb{Z}_2)$; the representation reads [95]

$$d_1 = \begin{pmatrix} (a^*)^2 & -(1+q^2)a^*c & -qc^2 \\ c^*a^* & 1-(1+q^2)c^*c & ac \\ -q(c^*)^2 & -(1+q^2)c^*a & a^2 \end{pmatrix} . \tag{4.31}$$

In the commutative limit, this matrix approaches a generic rotation matrix written in the so-called complex basis, and can be rewritten in the Cartesian basis by a similarity transformation, with

$$N = \begin{pmatrix} -1 & -i & 0 \\ 0 & 0 & 1 \\ -1 & i & 0 \end{pmatrix} \tag{4.32}$$

acting as the change of basis. By applying this transformation in the q-deformed case too, one can easily check that $N^{-1}d_1N$ is equal to (4.28). This clarifies the link to the $SO_q(3)$ quantum group. Matrices P_q and R_q are (co)-representations of $SO_q(3)$ since they can be obtained by a similarity transformation from (4.31). Therefore, our ansatz (4.27) realizes the quantum version of the $SU(2)$ to $SO(3)$ homomorphism.

The classical analog of (4.28) describes all possible elements of $SO(3)$ when varying the complex numbers a and c with continuity. Each of these classical matrices describes a possible relative orientation between observers A and B.

In the quantum case (4.28) has no physical meaning when taken alone, but only when paired with a certain state $|\psi\rangle \in \mathcal{H}$, where $\mathcal{H}$ is the Hilbert space on which a and c act. In the classical case, a and c codify information about the alignment of two reference frames, via their angular parametrization. For this reason, when being promoted to operators, we interpret the states on which they act as the ones codifying the relative orientation between the reference frames of observers A and B. The physical information about this orientation can be extracted by computing the expectation values $\langle\psi|(R_q)_{ij}|\psi\rangle$ with their relative uncertainties stemming from the noncommutative nature of these matrix elements, given by

$$(\Delta R_q)_{ij} = \sqrt{\langle\psi|(R_q)^2_{ij}|\psi\rangle - \langle\psi|(R_q)_{ij}|\psi\rangle^2} . \tag{4.33}$$

In this framework, the $(\Delta R_q)_{ij}$ do not vanish simultaneously, in general, for a given state $|\psi\rangle$ introducing a "fuzziness" in the alignment procedure. When this occurs, the latter is affected by an intrinsic uncertainty which cannot be eliminated: A and B are not able to sharply align their reference frames anymore. In light of these arguments, it is crucial to identify $\mathcal{H}$ and study the representations of operators a and c on it.

4.3.2 $SU_q(2)$ representations and quantum Euler angles

The representations of algebra (4.24) have been extensively studied in [95]. The Hilbert space containing the two unique irreducible representations of the $SU_q(2)$ algebra, $q \in (0,1)$, is $\mathcal{H} = \mathcal{H}_\pi \oplus \mathcal{H}_\rho$ where $\mathcal{H}_\pi = \ell^2 \otimes L^2(S^1) \otimes L^2(S^1)$ and $\mathcal{H}_\rho = L^2(S^1)$. If $\chi, \phi \in [0, 2\pi[$ are coordinates on S^1 and $|n\rangle$ is the canonical basis of ℓ^2, the algebra of functions on $SU_q(2)$ is represented as

$$\rho(a)\,|\chi\rangle = e^{i\chi}\,|\chi\rangle \qquad \rho(a^*)\,|\chi\rangle = e^{-i\chi}\,|\chi\rangle \qquad \rho(c)\,|\chi\rangle = \rho(c^*)\,|\chi\rangle = 0 \tag{4.34}$$

$$\begin{aligned} \pi(a)\,|n,\phi,\chi\rangle &= e^{i\chi}\sqrt{1-q^{2n}}\,|n-1,\phi,\chi\rangle \qquad \pi(c)\,|n,\phi,\chi\rangle = e^{i\phi}q^n\,|n,\phi,\chi\rangle \\ \pi(a^*)\,|n,\phi,\chi\rangle &= e^{-i\chi}\sqrt{1-q^{2n+2}}\,|n+1,\phi,\chi\rangle \qquad \pi(c^*)\,|n,\phi,\chi\rangle = e^{-i\phi}q^n\,|n,\phi,\chi\rangle\ . \end{aligned} \tag{4.35}$$

It is not coincidental that quantum number χ is common in both representations. We show in appendix A.2 that representation ρ can be obtained as a limit of representation π, in agreement with the fact that in the classical case we only need three real parameters to specify rotations.

Let us give physical meaning to the quantum numbers appearing in the representations, making a comparison between these relations and the classical parametrization of a and c for $U \in SU(2)$ (4.3) that we report here for convenience:

$$a = e^{i\eta}\cos\frac{\theta}{2} \qquad c = e^{i\delta}\sin\frac{\theta}{2}\,, \tag{4.36}$$

where η, δ and θ are a linear redefinition of Euler angles, as discussed in section 4.1. We note that $\rho(a)$ and $\rho(c)$ act diagonally, therefore we can make the identifications $\chi \equiv \eta$ and $\theta \equiv 0$. For what concerns representation π, c acts diagonally, while a and a^* act as ladder operators. For operator a, we added a phase, that is implicitly set to 0 in the

literature [91], which does not affect the commutation relations (4.24) but is needed in order to have a comparison of (4.35) with (4.3). From this, we identify $\chi \equiv \eta$, $\phi \equiv \delta$ and, exploiting the fact that c acts diagonally, we are led to the significant result

$$q^n = \sin\left(\frac{\theta(n)}{2}\right) \iff \theta(n) = 2\arcsin(q^n)\,. \tag{4.37}$$

The Euler angle θ becomes quantized and this feature is captured in fig. 4.2.

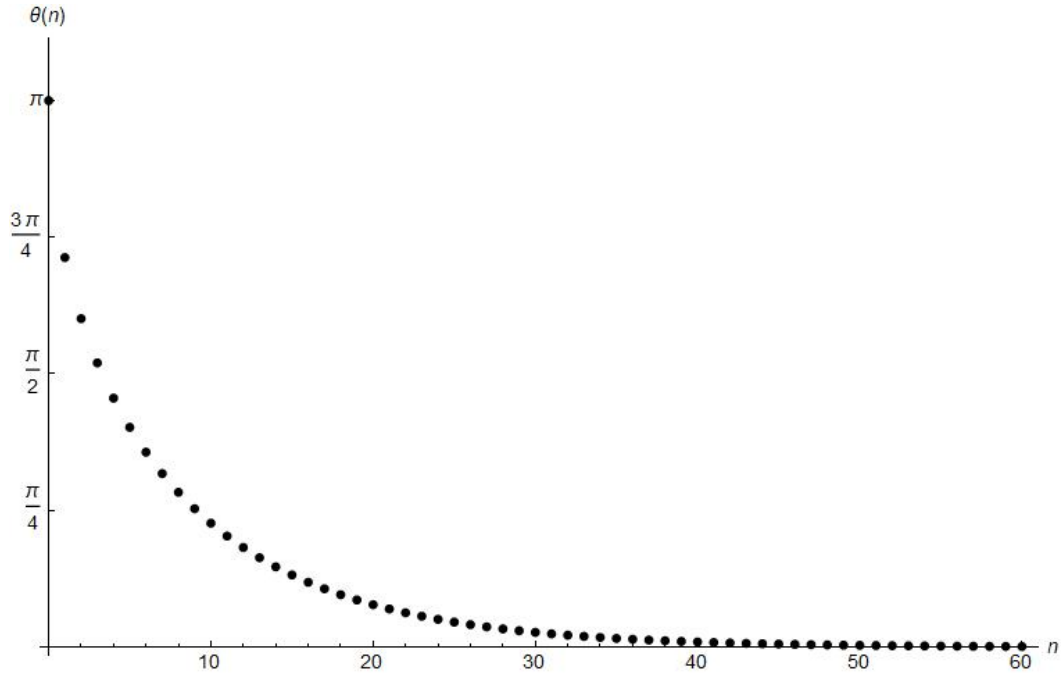

Figure 4.2: Discretized angles (4.37) computed with $q = 0.9$. $\theta(n)$ is decreasing with n starting from π and approaching 0 for large values of n. Interestingly, the step between consecutive angles decreases as n gets very larger, and for very large n we can approximate the angular distribution as being continuous. This can easily be verified analytically by computing $\Delta\theta(n) = \theta(n+1) - \theta(n)$ and taking the limit for $n \to \infty$. Another feature that gives robustness to our proposal is that the angular steps get smaller as q is closer to 1.

We close this section offering some comments on another quantization ambiguity, concerning our definition of the angle $\theta(n)$ in (4.37). We obtained the definition of $\sin\left(\frac{\theta(n)}{2}\right)$ by comparing the eigenvalues of $\pi(c)$ to the classical parametrization of c in (4.3). We

find that this is consistent with the definition of $\cos\left(\frac{\theta(n)}{2}\right)$ in terms of $\pi(a^*a)$, which also acts diagonally. Indeed, on a generic eigenstate $|n,\phi,\chi\rangle$ (cf. (4.35)) one has that

$$\pi(a^*a)\,|n,\phi,\chi\rangle = (1-q^{2n})\,|n,\phi,\chi\rangle = \cos^2\left(\frac{\theta(n)}{2}\right)|n,\phi,\chi\rangle\ . \tag{4.38}$$

Furthermore, this is in agreement with the fact that $a^*a + c^*c = \mathbb{1}$, as can be inferred from (4.24). Nevertheless, it is noteworthy that since a and a^* do not commute (see (4.24)), one could obtain another result for $\theta(n)$ upon defining its cosine in terms of $\pi(aa^*)$, which also acts diagonally (cf. (4.35)), rather than $\pi(a^*a)$. As one can easily check, this would lead to allowed values of θ which are the same as in our $\pi(a^*a)$ case, with the only difference that $\theta = \pi$ would be missing from the spectrum of $\theta(n)$. With this ordering we would have $\sin\left(\frac{\theta(n)}{2}\right) = q^{n+1}$ which is merely a shift of n with respect to the ordering we adopted. Evidently, the main results and the main aspects of physical interpretation of our analysis will be unaffected by this quantization ambiguity.

4.3.3 Semi-classical rotations

To gain further intuition from the classical picture, where the rotation axis and the angle by which the rotation is performed are specified by three Euler angles, we henceforth focus on what we called "semi-classical" rotations, specified by the three quantum numbers $\theta(n), \phi, \chi$, that describe small deformations of classical rotations defined by these angles. More precisely, the states $|\psi(\theta,\phi,\chi)\rangle$ yielding such deformed rotations should satisfy

$$\begin{cases} \langle\psi(\theta,\phi,\chi)|(R_q)_{ij}|\psi(\theta,\phi,\chi)\rangle = R_{ij}(\theta,\phi,\chi) + O(1-q) \\ \\ (\Delta R_q)^2_{ij} = O(1-q) \end{cases} \qquad \forall\ i,j\ , \tag{4.39}$$

where $R_{ij} \in \mathrm{SO}(3)$ and where θ is one of the allowed values in (4.37). This prescription constrains the quantum rotations we can construct to the ones in which the θ Euler angle can only take the allowed values in (4.37), for a fixed q. In order to clarify the meaning of this prescription, we provide some examples.

A first class of states that trivially satisfies requirement (4.39) is the set of eigenstates $|\chi\rangle \in \mathcal{H}_\rho$. It is easy to see that the expectation value of the quantum rotation matrix

(4.28) in such states describes a rotation of angle 2χ around the z-axis, namely:

$$\langle\chi|R_q|\chi\rangle = \begin{pmatrix} \cos(2\chi) & -\sin(2\chi) & 0 \\ \sin(2\chi) & \cos(2\chi) & 0 \\ 0 & 0 & 1 \end{pmatrix} \tag{4.40}$$

with all the $(\Delta R_q)_{ij}$ being zero. Thus, rotations around the z-axis are classical/continuous: two observers, A and B, whose relative orientation is described by $|\chi\rangle \in \mathcal{H}_\rho$, can align themselves sharply.

The relative simplicity of rotations around the z-axis is not representative of the richness of structure of other rotations, and this is mainly due to the fact that for generic basis states of the form $|n, \phi, \chi\rangle$ the first condition in (4.39) is not satisfied, forcing us to consider superpositions of such states. Since ϕ and χ are identified with their classical counterparts, we are led to consider superpositions

$$|\psi\rangle = \sum_{n=0}^{\infty} c_n \, |n, \phi, \chi\rangle \quad , \quad \sum_{n=0}^{\infty} |c_n|^2 = 1 \ . \tag{4.41}$$

Among the states of this form that satisfy (4.39), we need to find those for which the uncertainties are kept under control. The best way to do this is to demand that the coefficients $\{c_n\}$ minimize the functional

$$S\Big[\{c_n\}_{n=0}^{\infty}, \mu\Big] = \sum_{i,j} (\Delta R_q)_{ij}^2 - \mu\big(\langle\psi\rangle - 1\big) \, , \tag{4.42}$$

where μ is a Lagrange multiplier enforcing normalization of $|\psi\rangle$. In general, solving the minimization problem (4.42) is a daunting task computationally. Therefore, in appendix A.1 we invoke physical intuition to construct these states. Fixing a value for q, we build superpositions of states $|n, \phi, \chi\rangle$ centered around a certain $\bar{n} \in \mathbb{N}$. The expectation values and uncertainties relative to such states will reproduce deformations of classical rotation matrices specified by angles $(\theta(\bar{n}), \phi, \chi)$, in the sense of (4.39).

It is worth noticing that there is a special class of such semi-classical rotations for which some simplifications arise. This is the case of rotations with $\theta = \pi$ around axes in the $x - y$ plane. In the classical case $\chi = 0$ and a generic ϕ select a direction in the $x - y$ plane ($\phi = \pi/2$ selects a rotation around the x-axis, while $\phi = 0$ selects one around the y-axis) around which we rotate of an angle θ. As stressed before, since ϕ, χ behave classically, the quantum numbers associated to these angles specify the axis of

rotation also in the quantum case. For the case $\theta(0) = \pi$, building a superposition of basis states is not necessary to satisfy (4.39) and the basis state $|0, \phi, 0\rangle$ is sufficient to describe the corresponding semi-classical rotation around an axis in the $x - y$ plane, specified by ϕ. The expectation value of R_q on such state is

$$\langle 0, \phi, 0|R_q|0, \phi, 0\rangle = \begin{pmatrix} -q\cos(2\phi) & -q\sin(2\phi) & 0 \\ -q\sin(2\phi) & q\cos(2\phi) & 0 \\ 0 & 0 & -1 \end{pmatrix} \tag{4.43}$$

while the Δ_{ij} are non-zero and do not depend on the specific value of ϕ

$$\Delta R_q = \begin{pmatrix} \frac{1}{2}\sqrt{(1-q^2)(1-q^4)} & \frac{1}{2}\sqrt{(1-q^2)(1-q^4)} & \frac{(1+q^2)}{2}\sqrt{(1-q^2)} \\ \frac{1}{2}\sqrt{(1-q^2)(1-q^4)} & \frac{1}{2}\sqrt{(1-q^2)(1-q^4)} & \frac{(1+q^2)}{2}\sqrt{(1-q^2)} \\ \sqrt{q^2-q^4} & \sqrt{q^2-q^4} & 0 \end{pmatrix} \tag{4.44}$$

From the above matrices, it can be verified that the state $|0, \phi, 0\rangle$ satisfy (4.39).

For a generic axis of rotation, the quantum Euler angle θ will play a non-trivial role both in the determination of the axis itself and in the determination of the rotation angle.

4.4 Different skies from the same stars

The results we presented suggest a potential scenario where a new kind of connection between observers and the spacetime they are observing emerges. In this scenario, as we will see shortly, the choices that an observer makes in establishing their reference frame can have a non-trivial impact on the spacetime they observe.

We shall argue this by first advocating Einstein's operational notion of spacetime, whose points have physical meaning only if they label an event there occurring. We use as reference example a network of sources emitting photons ("stars") and each photon emission is a physical point of spacetime. These points of spacetime will be labeled by measured coordinates and uncertainties on those coordinates. The key observation here is that, in our model, these uncertainties are not intrinsic properties of the spacetime points but rather depend on some choices made by the observer (agent). These arguments give rise to a framework in which different skies may originate from the observation of the same stars and we thus don't have an objective notion of the starry sky.

4.4.1 Agency-dependent spacetime

In this subsection we apply the formalism we introduced throughout this chapter to establish the connection between the q-deformation of the $SU(2)$ group and the agency-dependence of space we have anticipated. Before showing this with a concrete numerical example, we will discuss why this property of space is to be expected by presenting a gedanken-experiment.

Consider two observers, Alice and Bob, each equipped with their own set of telescopes, who want to map a starry sky. Each of them chooses their reference frame (in particular their z-axis) in order to assign coordinates to the stars they observe. We assume that their origins coincide (since we are only interested in their relative orientation) but their z-axes do not. Without loss of generality we focus on the (y, z)-plane so that, for each observer, any telescope is mapped onto another by a rotation around the x-axis. In a classical spacetime, Alice and Bob can compare the outcomes of their measurements by rotating their data with a classical rotation matrix. Formally, there exists an element of the $SO(3)$ group that sharply describes the relative orientation between Alice and Bob.

We now investigate how this situation changes in our novel non-commutative framework. We henceforth assume that Alice and Bob can choose the direction along which points can be sharp (the z- axis) independently from one another. For definiteness, we focus on observer Alice first. While mapping the starry sky, she focuses on a specific star, which she observes with one of her telescopes. This instrument is in general not aligned with respect to the z-axis she has chosen. In our framework, this means that there exists a state $|\psi_A\rangle$ connecting the relative orientation between the aforementioned telescope and the z-axis. Following our physical interpretation, $|\psi_A\rangle$ determines a quantum rotation matrix via the expectation value of R_q and an uncertainty matrix defined by (4.33). This means that Alice cannot appreciate the relative orientation between the telescope and her z-axis with arbitrary precision since there will always be some intrinsic uncertainty given by the deformation of the $SU(2)$ group. As a consequence of this, she will not be able to sharply deduce the position of this star in the sky. For that same star, this line of reasoning also applies to Bob but the state $|\psi_B\rangle$ will be in general different from $|\psi_A\rangle$, implying a different degree of fuzziness. This procedure can also be applied to any star in the sky so that Alice and Bob each have their own picture of the celestial sphere, as can be seen in fig. 4.3. The striking result of this

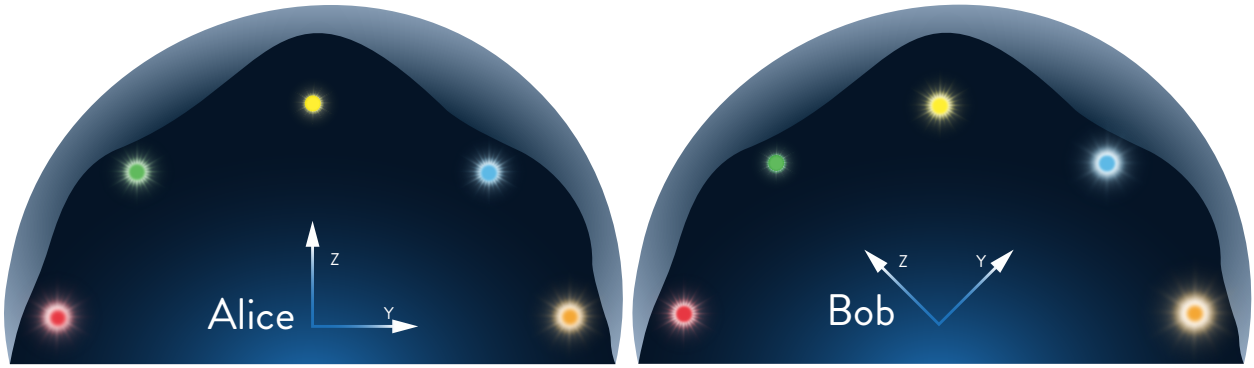

Figure 4.3: A semi-quantitative description of the starry skies observed by Alice and Bob. Alice's z-axis is aligned with the yellow star while Bob's z-axis is aligned with the green star, so that the yellow star is sharp for Alice while the green star is sharp for Bob. For Alice (Bob) the fuzziness increases as the angular deviation from the yellow (green) star increases and the same stars are observed with different fuzziness because of the relative orientation of the z-axes of the two agents.

gedanken-experiment is that the uncertainty associated with each star is not an intrinsic property of spacetime but depends on some choices made by the observers. In particular, different choices of the z-axis give rise to different pictures of the starry sky. The subtle observation is that there is no way for Alice and Bob to define an objective celestial sphere. This means that the definition of space itself cannot be independent of the observer who reconstructs it. In this sense, we say that Alice and Bob are agents, namely we are abandoning the idea of an objective space, replacing it with a notion of observed space from which we cannot subtract the choices of the observer (agent) who infers it.

As mentioned earlier, it is important to understand that, even though the z-axis is a preferred direction for each observer (only its points can be sharp), our framework produces an isotropic description of space. Indeed, spatial rotations are a (q-deformed) symmetry. There is no direction which is preferred *a priori*, and the special role that the z-axis plays in the reference frame of an observer is only the result of the choices made by that observer in setting up their frame. The observer chooses freely their preferred z-direction. This should be contrasted with the case of usual spatial anisotropy, in which different directions have different properties *a priori*, independently of the choices made

by observers, and invariance under spatial rotations is lost.

4.4.2 Some numerical examples

In order to better understand these innovative concepts and comprehend the meaning of fig. 4.3, we now show some numerical examples in support of our claims.

Let us start with Alices's point of view and let her z-axis be aligned with a certain star (α) and consider another star (β) she wants to observe from a telescope, whose relative orientation with respect to the first star is described by the following state:

$$|\psi_A\rangle = |n=0; \phi = \frac{\pi}{2}; \chi = 0\rangle \ . \tag{4.45}$$

This state, already introduced in section section 4.3.3 and which satisfies the "classicality" conditions (4.39), can be seen as a q-deformed rotation of π around the x-axis. The expectation value is obtained by substituting $\phi = \frac{\pi}{2}$ in (4.43) while the variances are the ones in (4.44)

$$\begin{aligned} \langle\psi_A|R_q|\psi_A\rangle &= \begin{pmatrix} q & 0 & 0 \\ 0 & -q & 0 \\ 0 & 0 & -q^2 \end{pmatrix} \\ \Delta R_q &= \begin{pmatrix} \frac{1}{2}\sqrt{(1-q^2)(1-q^4)} & \frac{1}{2}\sqrt{(1-q^2)(1-q^4)} & \frac{(1+q^2)}{2}\sqrt{(1-q^2)} \\ \frac{1}{2}\sqrt{(1-q^2)(1-q^4)} & \frac{1}{2}\sqrt{(1-q^2)(1-q^4)} & \frac{(1+q^2)}{2}\sqrt{(1-q^2)} \\ \sqrt{q^2-q^4} & \sqrt{q^2-q^4} & 0 \end{pmatrix} \end{aligned} \tag{4.46}$$

which at first order in $(1-q)$ give

$$\begin{aligned} \langle\psi_A|R_q|\psi_A\rangle &= \begin{pmatrix} 1-(1-q) & 0 & 0 \\ 0 & -1+(1-q) & 0 \\ 0 & 0 & -1+2(1-q) \end{pmatrix} \\ \Delta R_q &= \begin{pmatrix} \sqrt{2}(1-q) & \sqrt{2}(1-q) & \sqrt{2(1-q)} \\ \sqrt{2}(1-q) & \sqrt{2}(1-q) & \sqrt{2(1-q)} \\ \sqrt{2(1-q)} & \sqrt{2(1-q)} & 0 \end{pmatrix} \end{aligned} \tag{4.47}$$

Identifying Alice's z-axis with the vector $v = (0,0,1)$ and applying these matrices on v, the transformed vector $v' = (v'_1, v'_2, v'_3)$ will lie in the range

$$-\sqrt{2(1-q)} \leq v'_1 \leq \sqrt{2(1-q)} \qquad -\sqrt{2(1-q)} \leq v'_2 \leq \sqrt{2(1-q)} \qquad v'_3 = -1+2(1-q) \tag{4.48}$$

This quantitatively shows what we mean by fuzziness (qualitatively shown in fig. 4.4): the q-rotated vector v' lies in a cone with aperture given by

$$\Delta\alpha \approx 2\sqrt{2(1-q)} \tag{4.49}$$

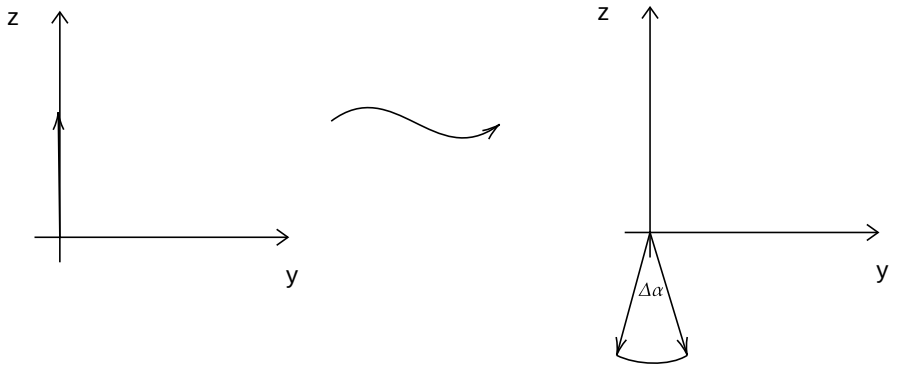

Figure 4.4: A qualitative description of the action a q-deformed rotation of π around the x-axis on the vector $(0, 0, 1)$.

The agency feature of this model can be well understood if we now compare these results with the ones obtained if Alice chose to align her z-axis with star β. In this case she would have seen β sharply and α under a cone with aperture (4.49). This line of reasoning can be extended when considering multiple stars: different states describing the relative orientation of these stars with respect to Alice's z-axis will produce different uncertainties in determining their direction. In turn, this is characterized by different cone apertures under which the stars are seen. In table 4.1 we show some numerical examples expressing this feature.

From this analysis, it is noteworthy that the fuzziness grows as our quantized Euler angle increases, resulting in a starry sky inferred by Alice, similar to what is depicted in fig. 4.3. Of course, the analysis can also be repeated for Bob, who chooses a different z-axis, in principle, and observes the same stars as Alice. The states describing the relative orientation between these stars and his z-axis will be different from the ones characterizing Alice's frame. The degree of fuzziness he observes for a particular star

$\theta(n)$	Aperture
$0°$	0
$\pm 45.275°$	0.210
$\pm 90.560°$	0.284
$\pm 137.518°$	0.402
$\pm 180°$	0.442

Table 4.1: Dependence of the aperture on the observation angle $\theta(n)$ using $q = 0.99$. The aperture is monotonically increasing as the angles grow in absolute value. The states used to obtain these results are constructed numerically in appendix A.1. For consistency, the aperture for $180°$ is not truncated at first order in $(1-q)$ as in (4.49), but is computed numerically with eq. (4.46) with $q = 0.99$.

will be different from the one assigned to it by Alice, resulting in a different inference of the starry sky, as shown in fig. 4.3.

4.5 Towards a quantum alignment protocol for $\mathrm{SU_q(2)}$

In this chapter we have achieved important progress about the physical interpretation of the $SU_q(2)$ quantum group. In particular, by exploring the properties of its representations we derived a framework in which one of the Euler angles becomes quantized and reference frames exhibit fuzziness properties. This is not the first time that quantum properties associated to reference frames are found in literature. Another example of non-classical reference frames is given by the quantum reference frames research program [98–106]. However, the nature of the fuzziness we obtained is distinct from the one usually associated with quantum references frames (QRFs). In fact, that kind of fuzziness arises when the frame itself is described as an ordinary quantum system. The key difference is the source of the frame fuzziness, indeed for QRFs it is governed by the Planck's constant $\hbar$ and follows from the standard laws of quantum mechanics, while in our scenario it is the deformation of spatial rotations, governed by the parameter q, that produces the fuzziness. Accordingly, the states encoding the fuzziness are associated with physical systems (including the frame) in the context of QRFs, while here they describe the relation between two frames. QRFs can be in relative superposition,

however, the transformations between them act on the states of the physical systems directly, without being described by a quantum state of their own.

Furthermore, one of our main result is the agency-dependence of spacetime we discussed in the previous section. For instance, if we consider a starry sky, classically all observers can objectively reconstruct it. However, in our framework, observers become agents in the sense that they reconstruct their own version of the sky based on their choices of the z-axis and there is no operational procedure they can use to reconstruct it objectively. In fact, even if they were to exchange their data, they would need to q-rotate it in their coordinates, inevitably introducing the intrinsic uncertainty predicted by our $SU_q(2)$ model.

The next step in this research program would be to develop a fully relativistic and relational picture. To do so, we should first consider the case in which more observers are involved, understanding which states can describe the composition of deformed rotations. Then the framework should be extended also to the translations and boosts sectors.

Moreover, the full quantum regime should also be investigated since in order to derive some novel qualitative properties we only focused on a semi-classical regime, in which the expectation values and the variances of the q-deformed rotation matrix act on classical vectors. This will be a crucial step toward a description of a q-deformed version of the alignment procedure described in section 4.2. Nevertheless, to go further, we need a more developed characterization of physical objects like spinors/qubits and Stern-Gerlach apparata, as well as a consistent interpretational framework for such "quantum mechanics on a quantum spacetime". In particular, we would need a description of qubits in a world in which rotations are described by $SU_q(2)$, and this would require facing some open questions such as:

- Can we assume that the standard 1-qubit Hilbert space describes the spins that Alice sends to Bob? Or does consistency require generalizing the notion of spinors to some non-commutative objects (e.g., see [97])?

- How does the measurement procedure affect the state of the system? For instance, is the relative orientation of Alice's and Bob's laboratories changed by their gaining information about each other while exchanging spins?

Besides their conceptual interest, investigating these possibilities might open a path

[22, 23] towards much-needed experimental tests, which in turn could guide further theoretical development of quantum gravity.

Chapter 5

Phenomenology of in-vacuo dispersion

In this chapter we delve into the possibility of a quantum gravity phenomenology. As already discussed in the introductory chapter of this thesis, the primary focus of this research area revolves around investigating the fate of Lorentz symmetry at the Planck-scale looking for potential new effects that might become discernible at energies accessible to us, significantly below the Planck-scale. Among these effects that have favored the birth and the development of quantum gravity phenomenology, the possibility of in-vacuo dispersion in particle propagation has certainly played a prominent role. This focus is driven by both the theoretical findings in quantum-spacetime research where the possibility of modified dispersion relations emerges from many approaches to the quantum gravity problem and the availability of interesting opportunities for analyzing experimental data mainly coming from the astrophysical sector. Indeed the large cosmological distances, generally characterizing the propagation of particles in astrophysical observations, can provide a source of amplification of the possible tiny Planckian effects, such that they can be within the reach of the present experimental sensitivity. In this perspective Gamma Ray Bursts represent of course the main source to test these kind of effects due to their wide energy spectrum of emission and their quite large redshift distances.

In this chapter we concern with the possibility of testing the fate of relativistic symmetries in quantum gravity through time of flight measurements. Specifically, throughout this chapter, we will discuss both LIV scenarios in which relativistic invariance is broken [25, 47, 48], giving rise to a preferred reference frame, and DSR scenarios in which relativistic invariance is merely deformed [49–51], preserving the equivalence of reference frames (also see section 1.3.1).

We will start our discussion focusing on Minkowski spacetime where effects due to spacetime curvature are neglected. Then, we will extend our analysis first to the de Sitter scenario and finally to expanding spacetime of Friedman-Lemaitre-Robertson-Walker (FLRW) type [107].

5.1 Covariant mechanics in maximally symmetric spacetimes

In this section we review the covariant Hamiltonian formalism [108, 109] that allows us to describe the motion of classical particles in (deformed) maximally symmetric

spacetimes.

The starting point is to consider the Casimir $\mathcal{C}$ of the algebra of (deformed) relativistic symmetries that allows us to introduce the following Hamiltonian $H = \mathcal{C} - m^2$, with m the mass of the particle. It can be taken to describe the particles on-shell relation by imposing $H = 0$, and then it can be used as Hamiltonian constraint, in the spirit of a "covariant formulation" of classical mechanics, providing equations of motion in terms of an auxiliary affine parameter, that we denote by τ, such that $\{H, f\} = \frac{df}{d\tau}$.
In this way we can derive the velocity of particles from the Hamiltonian constraint:

$$v = \frac{dx}{dt} = \frac{\{H, x\}}{\{H, t\}}\bigg|_{H=0}, \tag{5.1}$$

from which, in general, the (deformed) expression for the worldlines can be obtained by integration:

$$x(t) = x(t_0) + \int_{t_0}^{t} v\, dt\,. \tag{5.2}$$

In the next sections we discuss time delay analyses starting from flat spacetimes and then we will consider curverd/expanding spacetimes.

5.2 Time delay analysis in flat spacetime

When we analyze time of flights in flat spacetime we cannot distinguish between the implications of the broken-symmetry and the deformed-symmetry scenarios. In particular, in both cases one gets the same leading correction Δt to the special-relativistic time of flight which reads

$$\Delta t = \eta \frac{E}{E_p} T\,, \tag{5.3}$$

where T is the time distance of the source, η is a phenomenological dimensionless parameter, E_p is the Planck energy and E is the energy of the particle. Notice that even if the ratio E/E_p is very tiny for the particles we have currently access, T can be a huge amplifier for this effect when cosmological distances are considered, making Δt measurable by our present experimental apparata.

5.2.1 Time delay in DSR-deformed Minkowski spacetime

In this subsection we review how to construct DSR models (in 1+1D), when spacetime curvature is neglected, in order to study Planck-scale deformations of particle kinemat-

ics. The starting point of this kind of analysis is the special relativistic Casimir $\mathcal{C}$ of the Poincarè algebra :

$$\mathcal{C} = E^2 - p^2 \,, \tag{5.4}$$

where E, p are respectively the time translation and spatial translation generators. The Casimir generator is invariant under the action of the Poincarè algebra that can be realized in terms of Poisson brackets in the following way:

$$\begin{aligned} \{E, p\} &= 0, \\ \{N, E\} &= p, \\ \{N, p\} &= E \,, \end{aligned} \tag{5.5}$$

where N, E, p are respectively the boost generator, the time translation and the spatial translation generators.

Our analysis takes off from an investigation of the most general Planck-scale deformation of the Poincarè algebra. In the following, as usual, we denote by ℓ the deformation parameter, assumed to be of the order of the Planck-scale, and we will work at leading order in ℓ that is sufficient for phenomenological purposes.

The most general deformation of the Casimir element at leading order in ℓ is given by:

$$\mathcal{C} = E^2 - p^2 + \ell(\alpha E^3 + \beta E p^2) \,, \tag{5.6}$$

where α, β are free dimensionless parameters. In this analysis we required that deformations are analytic and the vectorial properties of the generators are accounted for, so that the generalization to higher spatial dimensions does not affect space-rotational invariance.

The most general deformation of the Poincarè algebra that leaves invariant the Casimir element (5.6) can be described in terms of the following set of Poisson brackets between the symmetry generators/charges:

$$\begin{aligned} \{E, p\} &= 0, \\ \{N, E\} &= p - \ell E(\alpha + \beta - \sigma) p, \\ \{N, p\} &= E + \frac{\ell}{2} \left[(\alpha + 2\sigma) E^2 + \beta p^2 \right] . \end{aligned} \tag{5.7}$$

Notice that, in addition to the parameters characterizing deformations of the Casimir, the algebra admits an additional numerical parameter σ.

In the time delay analysis, that relies on the Hamiltonian formalism introduced in the previous section, it is fundamental to keep safe from possible relativistic artifacts due to the relativity of locality [109–113] which is in general present in these deformed-relativistic scenarios. For this purpose we rely on two observers, one local to the emission event and the other one local to the detection event. Since we are interested in physical predictions made by the observer at detector we have to perform a finite translation that allows us to express the coordinates of this observer (t^B, x^B) in terms of the coordinates of the observer at the source (t^A, x^A), defined by the following prescription

$$(t^B, x^B) = e^{-\xi p} \triangleright e^{-\zeta E} \triangleright (t^A, x^A), \tag{5.8}$$

where $\triangleright$ stands for the action by Poisson bracket of the corresponding generators[1] and ξ and ζ are respectively the space and time translation parameters.

Two photons, emitted simultaneously according to an observer local to the source, with energy difference ΔE at the detector, will thus reach the detector with a time difference [108–110]

$$\Delta t = \ell \Delta E T(\alpha + \beta), \tag{5.9}$$

where T is the time distance between the source and the detector.
The same result is also obtained in a LIV scenario assuming the same deformation for the mass-shell relation but undeformed algebra of symmetry.

5.3 Time delay analysis in curved/expanding spacetime

In this section we extend the time delay analysis to scenarios in which spacetime curvature is not neglected, in order to obtain results suitable for comparison with the experimental data coming from the astrophysics sector.
The differences between the broken-symmetry and the deformed-symmetry scenario become tangible if one takes into account the expansion of spacetime. The interplay between quantum-gravity effects and curvature of spacetime can indeed produce several alternative forms of redshift dependence of the effect. In the LIV scenario one has no

[1] For a generator G with parameter a, the finite action on a coordinate x is $e^{aG} \triangleright x \equiv \sum_{n=0}^{\infty} \frac{a^n}{n!} \{G, x\}_n$, where $\{G, x\}_n = \{G, \{G, x\}_{n-1}\}$, $\{G, x\}_0 = x$. In this formalism, the composed action of a spatial translation followed by a time translation is given by $e^{-\xi p} \triangleright e^{-\zeta E} \triangleright x$.

constraints from symmetries and in principle any arbitrary form of redshift dependence could be allowed (see for instance [114,115]); however, LIV-based data analyses all rely on a particular form of redshift dependence introduced in Ref. [116] (also see Ref. [117]) which gives the following redshift dependence:

$$\Delta t = \eta \frac{\Delta E}{E_p} \int_0^z \frac{1+\bar{z}}{H(\bar{z})} d\bar{z}\,, \tag{5.10}$$

where z is the redshift distance of the source, related to the scale factor $a(t)$ by the relation $z(t) = 1/a(t) - 1$, $H(z)$ is the Hubble parameter, that for the ΛCDM model is [2] $H(z) = H_0\sqrt{\Omega_\Lambda + (1+z)^3\Omega_m}$.
The main assumptions underlying this result are that redshift of momenta works as in general relativity and the two photons travel the same comoving distance.
In the DSR deformed-symmetry scenario the possibilities for the interplay between quantum-gravity effects and curvature of spacetime are instead significantly limited by the requirement that the final picture has to be compatible with deformed relativistic invariance. In [108] two examples of DSR-compatible forms of redshift dependence were already identified and here we present what is the most general form of redshift dependence allowed by the requirement of DSR compatibility. In particular, we find that, in addition to the two forms of redshift dependence already previously identified [108], only a third possible form of redshift dependence is allowed and of course, also linear combinations of these three possible forms of redshift dependence are allowed. Our analysis will start from considering the case of propagation in the maximally symmetric de Sitter spacetime, where the possible DSR-relativistic scenarios can be characterized fully in terms of deformations of the relativistic symmetries, which are described, in 3+1D, by an algebra of 10 generators (spacetime translations, rotations and boosts) [119,120], and finally we extend our results to expanding spacetimes of FLRW type.

5.3.1 Most general deformation of the de Sitter algebra of symmetries

As announced before, our analysis starts from an investigation of the most general Planck-scale deformation of the de Sitter algebra. In the following we denote by H

[2] Ω_Λ, H_0 and Ω_m denote, respectively, the cosmological constant, the Hubble constant and the matter fraction, for which we take the values given in Ref. [118].

the curvature parameter of the de Sitter algebra and, as before, we denote by ℓ the deformation parameter and we will be satisfied working at leading order in ℓ.

Working in 1+1 spacetime dimensions, we start by characterizing the most general deformation of the mass Casimir asking that the limits for vanishing curvature and vanishing deformation, namely $H \to 0$ and $\ell \to 0$ respectively, are well-defined and in particular that the latter leaves us with the standard de Sitter Casimir which reads:

$$\mathcal{C} = E^2 - p^2 - 2HNp \tag{5.11}$$

Moreover, as for the flat case, we require that the vectorial properties of the generators are accounted for, so that the generalization to higher spatial dimensions does not affect space-rotational invariance. The most general deformation of the de Sitter Casimir which satisfies these requirements is:

$$\mathcal{C} = E^2 - p^2 - 2HNp + \ell\left(\alpha E^3 + \beta E p^2 + 2\gamma HNEp + 4\mu H^2 N^2 E\right). \tag{5.12}$$

Here $\alpha, \beta, \gamma, \mu$ are dimensionless parameters. The Casimir (5.12) is general and does not come from a specific quantum gravity model, but we can interpret the terms proportional to ℓH in the framework of a "quantum group" q-deformation of the Poincaré algebra, where the deformation is triggered by a combination of the curvature scale and the "quantum gravity" scale encoded in the parameter q (see e.g. [121, 122]).
The most general algebra of symmetry generators/charges that leaves the Casimir (5.12) invariant can be described by the following set of Poisson brackets:

$$\begin{aligned}
\{E, p\} &= Hp - \ell HE\left[(\alpha + \gamma - \sigma)\, p + 4\mu HN\right], \\
\{N, E\} &= p + HN - \ell E\left[(\alpha + \beta - \sigma)\, p + HN\,(\alpha + \gamma - \sigma)\right], \\
\{N, p\} &= E + \frac{\ell}{2}\left[(\alpha + 2\sigma)\, E^2 + \beta p^2 + 2\gamma HNp + 4\mu H^2 N^2\right].
\end{aligned} \tag{5.13}$$

These expressions define our deformation of the standard de Sitter algebra. Notice that in addition to the parameters characterizing deformations of the Casimir, the algebra admits the additional numerical parameter σ.
Therefore, at kinematical level, five independent parameters characterize departures from the standard relativistic symmetries. Apart from the deformation of the mass Casimir and the algebra of relativistic symmetry generators, another important ingredient of DSR models concerns the conservation law of energy-momenta for processes involving multiple particles. In order for the conservation law to be invariant under the

deformed symmetries, it must be accordingly deformed [49, 53].
In order to study the possible deformations of the energy-momenta conservation law for the deformed de Sitter scenario, we consider the total energy and momentum charges resulting from the composition law in the two-particle case. We keep the description as general as possible considering all the possible terms that can be added to the standard (linear) special relativistic addition law of energy-momenta at leading order in the deformation parameter ℓ and asking that no deformation terms which involve only one particle charge are present, so that we recover the definition of single particle charge when the charges of the second particle are zero [69, 79]. Moreover, we also require the same conditions of analyticity, dimensional consistency, and "vectorial properties" adopted for the algebra deformation. The most general composition laws complying with these requirements is given by the following:

$$\begin{aligned} E_{tot} &= E_1 + E_2 + \ell(A_1 P_1 P_2 + A_2 H N_1 P_2 + A_3 P_1 N_2 \\ &\quad + A_4 E_1 E_2 + A_5 H^2 N_1 N_2) \\ P_{tot} &= P_1 + P_2 + \ell\,(B_1 E_1 P_2 + B_2 E_2 P_1 + B_3 H N_1 E_2 + B_4 H E_1 N_2) \\ N_{tot} &= N_1 + N_2 + \ell\,(C_1 E_1 N_2 + C_2 E_2 N_1)\ . \end{aligned} \tag{5.14}$$

Where A_i, B_i, C_i are dimensionless parameters.
By requiring that the total charges close the same algebra (5.13) as the single particle energy and momenta in order to guarantee the relativistic properties of the composition law we obtain:

$$\begin{aligned} E_{tot} &= E_1 + E_2 + \ell((2\sigma - \beta - a - b) P_1 P_2 + (c - \gamma + \sigma) H (N_1 P_2 + P_1 N_2) \\ &\quad - \alpha E_1 E_2 + 2(c - 2\mu) H^2 N_1 N_2) \\ P_{tot} &= P_1 + P_2 + \ell\,((\sigma - b) E_1 P_2 + (\sigma - a) E_2 P_1 + c H (N_1 E_2 + E_1 N_2)) \\ N_{tot} &= N_1 + N_2 + \ell\,(a E_1 N_2 + b E_2 N_1)\ . \end{aligned} \tag{5.15}$$

Notice that three additional parameters (a, b, c), that didn't appear in (5.13), are allowed.

5.3.2 Time delays for deformed de Sitter spacetimes

In this section we present the most general result for the time delay in a deformed de Sitter spacetime. In the time delay analysis, that relies on the Hamiltonian formalism

introduced before, we recall that we must keep safe from possible relativistic artifacts due to the relativity of locality [109–113] and, as already described in section 5.2.1, we accomplish that by relying on two observers (Alice and Bob), one local to the emission event (A) and the other one local to the detection event (B) whose coordinates are related by a finite spatial translation followed by a finite time translation:

$$(t^B, x^B) = e^{-\xi p} \triangleright e^{-\zeta E} \triangleright (t^A, x^A), \tag{5.16}$$

where ξ and ζ are respectively the space and time translation parameters. These parameters are chosen such that Bob's origin coincides with the event of detection of a soft photon for which we neglect Planck-scale effects, namely $\zeta = T$, $\xi = \frac{1-e^{-HT}}{H}$, where T is the comoving (time) distance between the source and the detector. Moreover, in future studies, it will be appropriate to investigate the possible dependence on the sequence of spatial and time translations.

We then find that two photons with energy difference ΔE at the detector, emitted simultaneously by a distant source, reach the detector with a time difference

$$\Delta t = \ell \Delta E \left((\beta - \gamma + \sigma + \mu) \frac{e^{2HT} - 1}{2H} + (\alpha + \gamma - \sigma - 2\mu)\, T + \mu \frac{1 - e^{-2HT}}{2H} \right), \tag{5.17}$$

We can rewrite this result in terms of the redshift of the source $z = e^{HT} - 1$, obtaining:

$$\Delta t = \frac{\ell \Delta E}{H} \left((\beta - \gamma + \sigma + \mu) \left(z + \frac{z^2}{2} \right) + (\alpha + \gamma - \sigma - 2\mu) \ln(1+z) + \mu \left(\frac{z + z^2/2}{1 + 2z + z^2} \right) \right). \tag{5.18}$$

As announced, we find that the five numerical parameters that characterize the deformation of the kinematics in Eqs. (5.12)-(5.13) combine in such a way to produce only three different terms characterizing the functional dependence of the time delay on the redshift.

5.3.3 Time delay in FLRW spacetime

In the previous sections we showed that in-vacuo dispersion in (DSR-)relativistic quantum de Sitter spacetimes can only be characterized by linear combinations of three independent forms of redshift dependence just assuming the quantum de Sitter invariance. However, for what concerns the phenomenology of in-vacuo dispersion, we cannot

rely on the constant curvature assumption that applies to de Sitter spacetime but we need to generalize our results to a FLRW expanding spacetime. However, a DSR relativistic FLRW quantum geometry has still not been developed. We would need some generalization of Einstein's equation applicable to quantum geometries, but that looks still like a distant goal for quantum spacetime research.

We shall thus rely on a semi-heuristic approach, which makes the reasonable assumption that the relationship between travel times in quantum de Sitter and FLRW spacetimes should preserve at least some aspects of the structure of the corresponding relationship between travel times in classical de Sitter and FLRW spacetimes.

Our strategy of analysis can be better appreciated by taking as reference the successful semi-heuristic approach of Refs. [114, 116] which led to the identification of the Jacob-Piran redshift dependence, which is the standard of reference for LIV quantum spacetime phenomenology. Starting from the results on in-vacuo dispersion in LIV flat quantum spacetimes, as already stressed in the previous sections, one can in principle contemplate any arbitrary form of redshift dependence in a LIV FLRW quantum spacetime, since the LIV case provides no relativistic symmetry constraints. Indeed, in Ref. [114], some alternative forms of redshift dependence were considered. The Jacob-Piran redshift dependence was singled out through the assumption [114, 116] that, in LIV quantum spacetimes, momenta should be affected by redshift as that they do in classical general-relativistic spacetime. However, it is turning out that this assumption is valid only in a subgroup of quantum spacetime models since the interplay between spacetime expansion and quantum properties of spacetime often modifies the effect of redshift on momenta (see, e.g., [115, 123]).

To see how the strategy of analysis that we propose is connected to the Jacob-Piran approach we observe that in the ordinary general-relativistic case travel times in FLRW can be equivalently obtained from travel times in de Sitter assuming that momenta redshift general-relativistically and assuming that the travel time in FLRW is obtained by "de Sitter slicing", *i.e.* describing propagation in FLRW, with its time-dependent expansion rate $H(t) = \dot{a}(t)/a(t)$, as a sequence of infinitesimal steps of propagation in de Sitter spacetime with scale factor $a(t) = \exp(Ht)$.

5.3.4 The slicing technique

In this subsection we present the so-called slicing technique according to which we will describe propagation of signals in a modified (LIV or DSR) FLRW spacetime by defining a sequence of intermediate observers along the particle's trajectory, such that each observer is local to the particle at a given spacetime point. Propagation of signal between two such nearby observers is described by using the modified de Sitter kinematics. The full trajectory (and the corresponding total time delay) in the modified FLRW spacetime is reconstructed by appropriately matching [120] the observations made by subsequent observers and considering a limiting procedure in which the number of intermediate observers is sent to infinity, while decreasing their distance to zero [120]. We consider an observer Alice local to the event of emission (Alice's frame origin coincides with the emitter), and an observer Bob local to the detector (Bob's frame origin coincides with the detector), and we assume that the soft photon has been emitted at the (comoving) Bob time $-T$. In order to reconstruct the trajectories of the photons we divide the time interval between the event of emission and the event of detection in N time intervals of equal temporal size T/N, such that in each slice spacetime is described, to good approximation, by a constant expansion rate $H_n = H(t_n)$, where t_n is the initial time of the n-th slice, and $n = 1, \ldots, N$. We now consider a set of intermediate observers Bob_n such that the soft photon crosses the origin of their reference frame at the time t_n, so that $\text{Bob}_N = \text{Bob}$ (and Bob_0=Alice). Each observer Bob_n, in the corresponding n-th slice, which goes from t_{n-1} to t_n, will describe the motion of particles in terms of a constant expansion rate H_n, and will describe the photons to travel with a speed $v_n^{B_n}$.

To obtain the time-delay at the detector, we are interested in the trajectory that Bob_N assigns to the hard photon in the final N-th slice (the soft photon arrives by assumption in Bob_N's spatial and temporal origin), which is given by

$$x^{B_N}\left(t^{B_N}\right)_N = x_{O_A}^{B_N} + \sum_{n=1}^{N-1} \int_{t_{O_{n-1}}^{B_N}}^{t_{O_n}^{B_N}} v_n^{B_N} dt^{B_N} + \int_{t_{O_{N-1}}^{B_N}}^{t^{B_N}} v_N^{B_N} dt^{B_N} \ , \tag{5.19}$$

with $v_n^{B_N}$ the velocity that Bob_N assigns to the photon in the nth slice, and $(x_{O_n}^{B_N}, t_{O_n}^{B_N})$ the coordinates that Bob_N assigns to the photon when it crosses the (time) origin of observer Bob_n's frame.

In order to compute these quantities, it is crucial to establish the relations between the observers coordinates. We describe each Bob_n as the observer connected to Alice

by a set of n spatial translations followed by a set of n time translations, with each k-th translation characterized by the relative constant expansion rate H_k and finite translation parameters ζ_k, ξ_k, i.e.

$$(t,x)^{B_n} = e^{-\sum_{k=1}^{n}\xi_k p} \triangleright e^{-\sum_{k=1}^{n}\zeta_k E_{H_k}} \triangleright (t,x)^{A} \ . \tag{5.20}$$

Before presenting the results for the DSR scenario, our strategy of analysis can be better appreciated by taking as reference the successful semi-heuristic approach of Refs. [114, 116] which led to the identification of the Jacob-Piran redshift dependence.

5.3.5 de Sitter slicing for the LIV Jacob-Piran scenario

We here focus on showing that applications of the de Sitter slicing to the LIV Jacob-Piran scenario produce results that are equivalent to those found redshifting the relevant momenta with the standard general relativistic scale factor.

We work with comoving-time coordinates and we start by considering the folowing LIV-modified relationship between energy and momentum for a massless particle in (1+1D) de Sitter spacetime

$$E^2 = e^{-2Ht}p^2 - \lambda e^{-2Ht}Ep^2 \ , \tag{5.21}$$

where λ is the LIV scale, and this formula reproduces the Jacob-Piran redshift dependence [116] in the de Sitter limit for which the FLRW scale factor is $a(t) \to e^{Ht}$, with constant H.

The speed of a massless particle can be easily obtained from (5.21) to be (working again at first order in λ)

$$v(t) = \frac{\partial E}{\partial p} \simeq e^{-Ht}\left(1 - \lambda e^{-Ht}p\right) \ . \tag{5.22}$$

We want to determine the difference in arrival times between a hard photon (a high-energy photon, tangibly affected by LIV) and a soft photon (a low energy photon, for which the LIV effects can be neglected), emitted simultaneously by a distant source, traveling through a LIV-modified FLRW spacetime corresponding to (5.21). As described in the previous subsection, we consider an observer Alice local to the event of emission (Alice's frame origin coincides with the emitter), and an observer Bob local at the detector (Bob's frame origin coincides with the detector), and we assume that the

soft photon has been emitted at the (comoving) Bob time $-T$. Since in the LIV case the relativistic transformations are not deformed, one easily finds the following relation between Bob_n's and Alice's coordinates

$$\begin{aligned} t^{B_n}\left(t^A, x^A\right) &= t^A - \sum_{k=1}^{n} \zeta_k, \\ x^{B_n}\left(t^A, x^A\right) &= e^{\sum_{k=1}^{n} H_k \zeta_k} \left(x^A - \sum_{k=1}^{n} \xi_k \right). \end{aligned} \tag{5.23}$$

The requirement for each observer Bob_n to be along the soft photon trajectories at the time t_n, is then ensured by imposing that the translation parameters satisfy the conditions

$$\zeta_n = \zeta = T/N, \qquad \xi_n = e^{-\sum_{k=1}^{n} H_k \zeta_n} \frac{e^{H_n \zeta_n} - 1}{H_n}, \tag{5.24}$$

and Alice describes each n-th slice to be of temporal size ζ and spatial size ξ_n.

The computation of $v_n^{B_N}$ requires the use of these formulas and a suitable matching of the scale factors $a_n(t) = \exp(H_n t)$ at the junction of each slice, after which one obtains

$$v_n^{B_N} = \frac{1}{a_n^{B_N}\left(t^{B_N}\right)} \left(1 - \lambda \frac{p^{B_N}}{a_n^{B_N}\left(t^{B_N}\right)} \right) , \tag{5.25}$$

where

$$a_n^{B_N}\left(t^{B_N}\right) = e^{-\sum_{k=n+1}^{N} H_k \zeta} e^{(N-n) H_n \zeta} e^{H_n t^{B_N}} . \tag{5.26}$$

The velocity (5.25) can be easily integrated in each slice in (5.19), where we take

$$t_{O_n}^{B_N} = t^{B_N}\left(t^{B_n} = 0\right) = -(N-n)\,\zeta , \tag{5.27}$$

and considering that, combining (5.23) and (5.24), one has that

$$x_{O_A}^{B_N} = x^{B_N}\left(x^A = 0, t^A = 0\right) = -\sum_{k=1}^{N} e^{\sum_{s=k}^{N} H_s \zeta} \frac{1 - e^{-H_k \zeta}}{H_k} , \tag{5.28}$$

the trajectory in the N-th slice is given by

$$x^{B_N}\left(t^{B_N}\right) = \frac{1 - e^{-H_N t^{B_N}}}{H_N} - \lambda p^{B_N} \left(\sum_{n=1}^{N} e^{2\sum_{k=n}^{N} H_k \zeta} \frac{1 - e^{-2H_n \zeta}}{2H_n} + \frac{1 - e^{-2H_N t^{B_N}}}{2H_N} \right) . \tag{5.29}$$

From the trajectory we obtain the hard-photon time delay (at first order in λ) by solving for $t^{B_N}\left(x^{B_N}=0\right)$,

$$\Delta t^{B_N} = \lambda p^{B_N} \sum_{n=1}^{N} e^{2\sum_{k=n}^{N} H_k \zeta} \frac{1-e^{-2H_n\zeta}}{2H_n} \ . \tag{5.30}$$

We take now the limit $N \to \infty$, in which the slices are infinitesimally small. Using the formulas ($\zeta = T/N$)

$$\sum_{k=n_i+1}^{n_f} \zeta \to \int_{t_{n_i}}^{t_{n_f}} dt \ , \tag{5.31}$$

and, noticing that, since $H(t)=\dot{a}(t)/a(t)$, $a\left(t_f\right)/a\left(t_i\right) = \exp\left(\int_{t_i}^{t_f} dt\ H\left(t\right)\right)$, and

$$e^{\sum_{s=k+1}^{n} H_s \zeta} \to \frac{a\left(t_n\right)}{a\left(t_k\right)} \ , \tag{5.32}$$

we obtain

$$\Delta t \to \lambda p_h \int_{-T}^{0} \frac{dt}{a^2\left(t\right)} \ , \tag{5.33}$$

where we denoted by p_h the momentum of the hard particle observed at the detector, we considered that for $N \to \infty$ one has that $\frac{e^{2H_k\zeta}-1}{2H_k} \to \zeta$, that $t_0 = -T$, $t_N = 0$, and that $a\left(t_N\right) = a\left(0\right) = 1$. Finally, we can rewrite the time delay in terms of the redshift of the source $z \equiv z(-T)$, noticing that, for $\bar{z} \equiv z(t)$, $a\left(t\right) = 1/(1+\bar{z})$ and $dt = -d\bar{z}/(H(\bar{z})(1+\bar{z}))$, so that

$$\Delta t = \lambda p_h \int_{0}^{z} \frac{d\bar{z}\left(1+\bar{z}\right)}{H\left(\bar{z}\right)} \ , \tag{5.34}$$

which coincides with the formula obtained by Jacob and Piran in [116].

5.3.6 DSR-FLRW time delays

In our opinion, in relativistic quantum spacetimes, the status of “de Sitter slicing" is much safer than that of the effect of redshift of momenta, and we shall therefore rely on de Sitter slicing.

Following the same strategy presented in the previous subsection we can find that

from our Eq.(5.18) the time delay in the DSR-deformed FLRW case reads:

$$\Delta t = \frac{\Delta E}{E_p}\int_0^z \frac{d\overline{z}\,(1+\overline{z})}{H\,(\overline{z})}\left[\eta_1 + \eta_2\left(1-\left(1-\frac{H\,(\overline{z})}{1+\overline{z}}\int_0^{\overline{z}}\frac{d\overline{z}'}{H\,(\overline{z}')}\right)^2\right) + \eta_3\left(1-\left(1-\frac{H\,(\overline{z})}{1+\overline{z}}\int_0^{\overline{z}}\frac{d\overline{z}'}{H\,(\overline{z}')}\right)^4\right)\right]. \tag{5.35}$$

It describes the most general form of redshift dependence for time delays in FLRW compatible with the DSR requirements. As we anticipated, the time delay depends on only three numerical parameters η_1, η_2, and η_3 that are to be determined by experiments. Their relation with the parameters of the deformed algebra introduced in Sec. 5.3.1 is given by

$$\eta_1 = \ell E_p(\alpha+\beta)\,, \quad \eta_2 = \ell E_p(-\alpha-\gamma+\sigma+2\mu)\,, \quad \eta_3 = -\ell E_p \mu\,.$$

Of course, for the case in which the $H(z)$ is actually redshift independent the FLRW picture turns into a de Sitter picture and our result (5.35) reproduces the one obtained in (5.18).

In Figure 5.1 we plot the redshift dependence of the three terms in (5.35).

Any linear combination of the three redshift-dependent terms in (5.35) is a good candidate for a DSR-FLRW time-delay formula but we find that the parametrization in terms of η_1, η_2, and η_3 turns out to be convenient for the comparison of some specific phenomenological scenarios that we are going to discuss in the next section. In particular, when $\eta_2 = \eta_3 = 0$, we are left with the term parametrized by η_1 which gives the same time delay that was obtained in the LIV scenario by Jacob and Piran in [116]. On the other hand, scenarios with vanishing η_1 or η_2 characterize, respectively, two noteworthy cases that we shall discuss in the following: when η_1 vanishes one obtains curvature-induced scenarios (see Subsec. 5.4.1), while vanishing η_2 relates to theoretical models where energies add up trivially (see Subsec. 5.4.2).

5.4 Some noteworthy special cases of DSR-FLRW time delay

We have shown that only linear combinations of 3 independent forms of redshift dependence are compatible with the DSR requirements, strongly limiting the possible

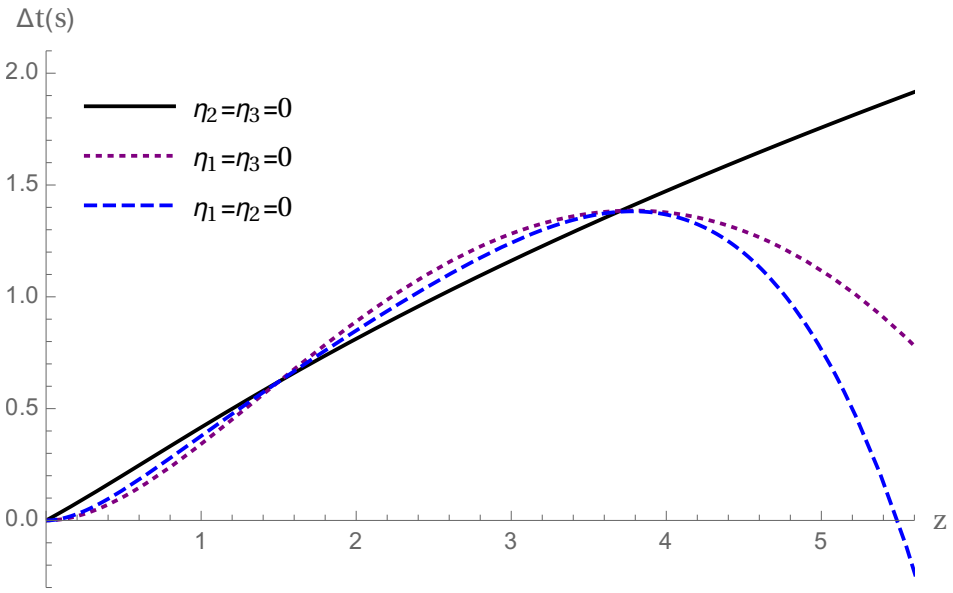

Figure 5.1: The redshift dependence of the three terms contributing to the time delay in Eq. (5.35). Each curve corresponds to the time delay (5.35) when only one of the three parameters η_1, η_2 and η_3 is different from zero. The continuous black line assumes that $\eta_1 = 1$ (while $\eta_2 = \eta_3 = 0$) and $\Delta E = 10$ GeV. The dotted purple and dashed blue lines still assume $\Delta E = 10$ GeV, and they are obtained by fixing, respectively, η_2 and η_3 so that the time delay matches the one of the black continuous curve at $z = 1.5$.

scenarios for our time-delay phenomenology with respect to the LIV case where in principle any form of redshift dependence is allowed since relativistic invariance imposes no constraints when it is broken. Still, even just a 3-parameter formula is a rather wide "hunting field" for the phenomenology of time delays in astrophysics, where data are scarce and often of low quality. In this section we attempt to motivate from a theoretical perspective some specific choices of the parameters η_1, η_2, and η_3 in (5.35) which might deserve being the "first targets" for the phenomenology.

5.4.1 Curvature-induced scenarios

A first scenario that we want to discuss is the curvature induced one, namely a scenario where the quantum gravity effects are triggered by spacetime curvature. Specifically, this is a scenario where the interplay between curvature effects and Planck-scale effects

produces results that are quite distant from what one would guess based on analysing Planck-scale effects in the flat-spacetime approximation. Indeed, in this scenario in-vacuo dispersion occurs only in combination with spacetime curvature/expansion so that when curvature is negligible there is no expected time delay. This scenario so far received little attention in the literature, but it could have interesting phenomenological implications as already highlighted in [124], that is the first study of these "curvature-induced" scenarios and it relies on a toy model where relativistic symmetries are broken (LIV). The preliminary results reported in [124], confronting the slow onset of the quantum gravity effects in the FLRW time-delays, that are typically expected in curvature-induced scenarios, with data relative to gamma-ray-burst observations, showed how these features might have interesting implications for experimental studies.

Theoretically, these scenarios find motivation in some studies based on a Hopf-algebra description of the symmetries of quantum spacetime [121, 125], as well as in some considerations arising from loop-quantum-gravity research [126]. Specifically, the main idea of Ref. [126] is that some non-trivial physical effects can be switched on by a dimensionless combination of the Planck length and the Hubble length associated to the cosmological constant. For instance, in a Lorentzian world with a horizon at distance $\frac{1}{H}$ a sphere of radius r cannot be seen under an angle smaller than rH. Suppose that no object with size smaller than $l_{min} = \ell$ exists in the universe, then a minimum angular resolution shows up (see fig. 5.2):

$$\phi_{min} = \ell H \tag{5.36}$$

This result is clearly a manifestation of the interplay between Planck-scale and spacetime curvature effects.

Here we want to show that there is a choice of parameters that produces a curvature-induced time-delay also in the DSR-FLRW framework we constructed in the previous sections. As explained in [124], the requirement for having only curvature-induced terms in the time-delay formula amounts to asking that the coefficient of the first-order term in an expansion around $z = 0$ of the expression (5.35) vanishes. Indeed, expanding the redshift formula $z(t) = 1/a(t) - 1$ for small distances (i.e. small (negative) times $t = -T$), one gets $z(-T) \simeq H_0 T$, where the Hubble constant is defined as $H_0 = \frac{1}{a}\frac{da}{dt}|_{t=0}$. It follows that terms linear in z in the expansion of Δt will be proportional to $\frac{\Delta E}{E_p}\frac{z}{H_0} \simeq \frac{\Delta E}{E_p} T$, and will survive even in the absence of spacetime curvature. Thus,

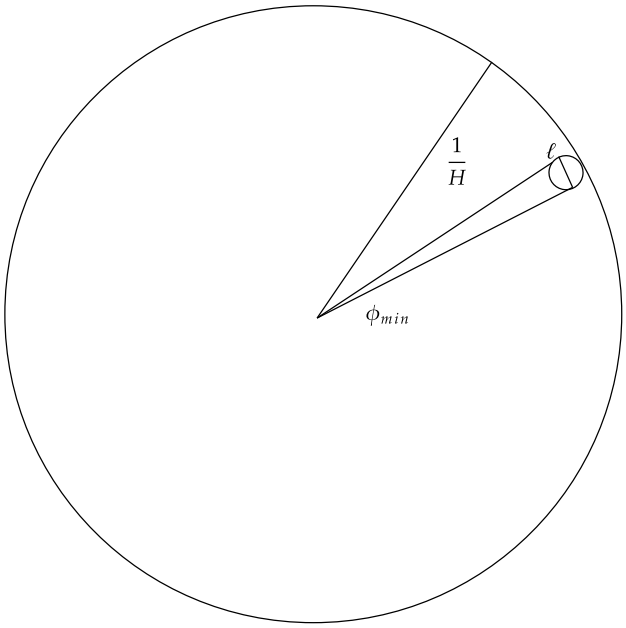

Figure 5.2: A sphere of radius ℓ at distance $1/H$ from an observer cannot be resolved under an angle smaller than $\phi_{min} = \ell H$.

only terms involving powers of z higher than 1 contribute to curvature-induced time-delay effects.

The leading order expansion in terms of the redshift of Eq. (5.35) gives

$$\Delta t \simeq \frac{\Delta E}{E_p H_0} \left(\eta_1 z + O(z^2)\right). \tag{5.37}$$

Setting to zero the first order term corresponds to imposing the constraint $\eta_1 = 0$ (i.e. $\alpha = -\beta$ in terms of the kinematical parameters). Notice also that the same condition is obtained in the DSR-de Sitter case of Subsec. 5.3.2 if one asks that the time delay of Eqs. (5.17) and (5.18) vanishes in the limit of vanishing spacetime curvature H. Indeed, considering the limit $H \to 0$ in (5.17) (or in (5.18), noticing that $z \simeq HT + O(H^2T^2)$, we obtain

$$\Delta t = \ell \frac{\Delta E}{H} \left((\alpha + \beta) z + O(z^2)\right) = \ell \Delta E \left((\alpha + \beta) T + O(HT^2)\right), \tag{5.38}$$

which gives again the condition $\alpha = -\beta$, i.e. $\eta_1 = 0$.

By imposing the condition $\eta_1 = 0$ in (5.35) the time delay expression reduces to

$$\Delta t = \frac{\Delta E}{E_p}\int_0^z \frac{d\overline{z}\,(1+\overline{z})}{H\,(\overline{z})}\left[\,\eta_2\left(1-\left(1-\frac{H\,(\overline{z})}{1+\overline{z}}\int_0^{\overline{z}}\frac{d\overline{z}'}{H\,(\overline{z}')}\right)^2\right) + \eta_3\left(1-\left(1-\frac{H\,(\overline{z})}{1+\overline{z}}\int_0^{\overline{z}}\frac{d\overline{z}'}{H\,(\overline{z}')}\right)^4\right)\right]. \tag{5.39}$$

This formula, in which only two independent parameters appear, describes the most general curvature-induced in-vacuo dispersion scenario arising from the deformation of symmetries under the assumptions of Subsecs. 5.3.1 and 5.3.3.

5.4.2 Scenarios with undeformed addition of energy

In this subsection we discuss possible choices of the parameters analyzing the possible forms of the composition law of momenta discussed in section 5.3.1. While all possibilities contemplated by our Eq. (5.15) deserve being investigated, we think that priority should be given to scenarios in which the addition law of particle energies remains undeformed. This is suggested by experience [53, 79] with the implications of these modified addition laws in which one finds that preserving the linearity of addition of energies is advantageous from the point of view of the interpretation of the results. Moreover this requirement finds further motivation in scenarios where the DSR framework can be associated with a quantum group deformation of de Sitter symmetries, where the summation law of the charges/generators corresponds to a “coproduct rule" of the Hopf-algebra generators. In that case an undeformed summation law of energies would correspond to a “primitive coproduct" for energy/time-translation generators, that is necessary for having a “time-like" q-deformation of de Sitter symmetries [127–130].

The requirement for the composition of energy to be undeformed imposes the following constraints between the kinematical parameters:

$$\alpha = 0 \qquad \gamma - \sigma = 2\mu\ , \tag{5.40}$$

amounting to $\eta_2 = 0$ in (5.35). The expression for time delay in the deformed FLRW scenario then becomes

$$\Delta t = \frac{\Delta E}{E_p}\int_0^z \frac{d\overline{z}\,(1+\overline{z})}{H\,(\overline{z})}\left[\eta_1 + \eta_3\left(1-\left(1-\frac{H\,(\overline{z})}{1+\overline{z}}\int_0^{\overline{z}}\frac{d\overline{z}'}{H\,(\overline{z}')}\right)^4\right)\right]\ , \tag{5.41}$$

in which, again, only two independent parameters appear.

5.4.3 A one-parameter scenario: curvature-induced and undeformed addition of energy

In this subsection we obtain a one-parameter scenario combining the requirements of Subsecs. 5.4.1 and 5.4.2. Specifically we obtain a scenario that has only one free numerical parameter to be determined by experiments, η_3, and is characterized by undeformed composition law of energies and a curvature-induced time delay effect.

The resulting formula for the time delay is

$$\Delta t = \eta_3 \frac{\Delta E}{E_p} \int_0^z \frac{d\overline{z}\,(1+\overline{z})}{H\,(\overline{z})} \left[1 - \left(1 - \frac{H\,(\overline{z})}{1+\overline{z}} \int_0^{\overline{z}} \frac{d\overline{z}'}{H\,(\overline{z}')}\right)^4\right]. \tag{5.42}$$

In Figure 5.3 we compare the redshift dependence described by this formula to the one of the Jacob-Piran case (5.10).

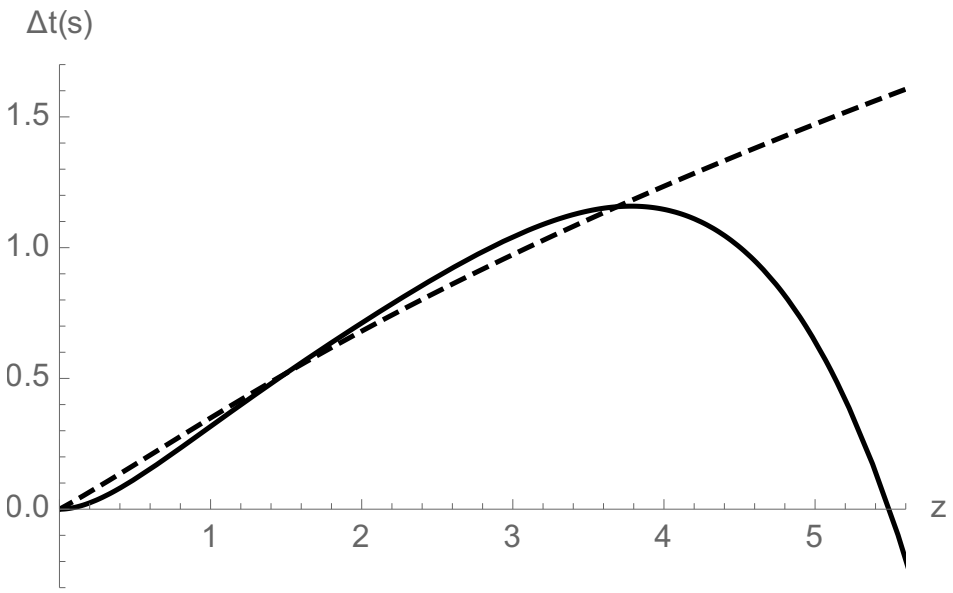

Figure 5.3: The continuous line corresponds to the one-parameter scenario described by (5.42), with $\Delta E = 10$ GeV and $\eta_3 = 1$. The dashed line represents the expected time delay for the Jacob-Piran case (5.10), corresponding to setting $\eta_2 = \eta_3 = 0$ in (5.35); the remaining free parameter in (5.35), η_1, is fixed by asking that the two lines cross at $z = 1.5$. Also for the dashed line we use $\Delta E = 10$ GeV.

5.4.4 Alternative picture with the time delay changing sign

It is rather noteworthy that in our one-parameter scenario which is curvature induced and is compatible with undeformed addition of energy the time delay changes sign at high redshift. So far all the scenarios motivated in the literature gave rise to monotonic dependence of the time delay on redshift, and it is interesting that our one-parameter scenario, with its appealing theoretical qualities, is not monotonic. This led us also to investigate how frequently in our 3-dimensional parameter space such changes of the sign of the time delay occur and what sort of functional dependence on redshift are then found in such cases. We found that cases in which the time delay changes sign are not at all exceptional, and a variety of forms of dependence on redshift can be found.

As an illustrative example we focused on the case of effects which are curvature induced ($\eta_1 = 0$) and with $\eta_2 = 4, \eta_3 = -3$. With this choice, Eq. (5.35) becomes

$$\Delta t = \frac{\Delta E}{E_p}\int_0^z \frac{d\overline{z}\,(1+\overline{z})}{H\,(\overline{z})}\left[4\left(1-\left(1-\frac{H\,(\overline{z})}{1+\overline{z}}\int_0^{\overline{z}}\frac{d\overline{z}'}{H\,(\overline{z}')}\right)^2\right) - 3\left(1-\left(1-\frac{H\,(\overline{z})}{1+\overline{z}}\int_0^{\overline{z}}\frac{d\overline{z}'}{H\,(\overline{z}')}\right)^4\right)\right]. \tag{5.43}$$

As shown in Figure 5.4, in this scenario the redshift dependence starts off at small redshifts with opposite sign with respect to the Jacob-Piran case, but then for redshift greater than 1 (up to redshift of about 4.5) approximates reasonably well (oscillating around it) the Jacob-Piran case. It would therefore be a valuable aspect of maturity of this phenomenology when the quality of data at high redshift will prove to be sufficient for discriminating between this scenario and the Jacob-Piran case.

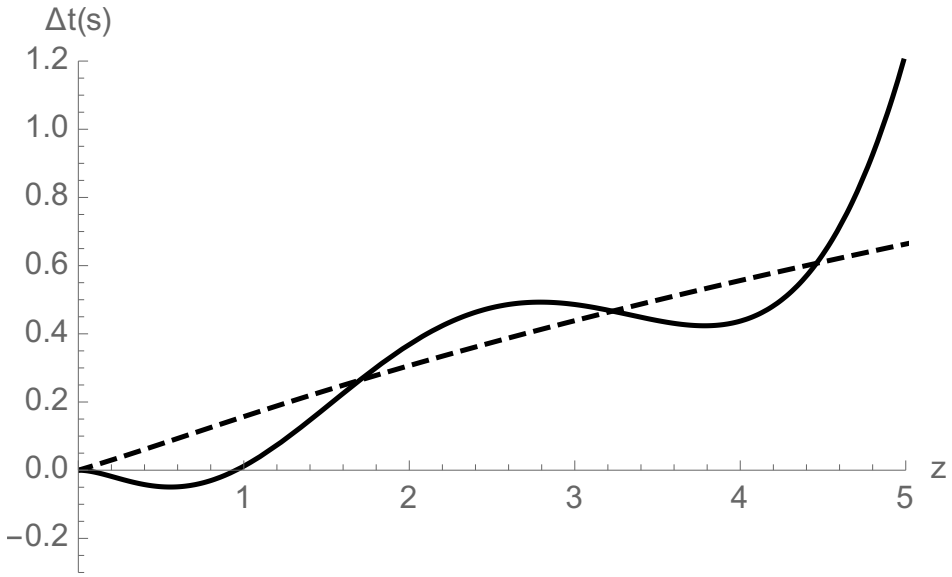

Figure 5.4: The continuous line corresponds to the "curvature-induced" scenario described by (5.39) with $\eta_2 = 4$ and $\eta_3 = -3$, see Eq. (5.43). The dashed line represents the expected time delay for the Jacob-Piran case (5.10), corresponding to setting $\eta_2 = \eta_3 = 0$ in (5.35); the remaining free parameter in (5.35), η_1, is fixed by asking that the two lines cross at $z = 1.7$ (which allows for a particularly interesting comparison). As for Figure 5.3, we set $\Delta E = 10$ GeV for both lines.

5.4.5 Another one parameter scenario: curvature-induced and monotonicity

In the previous subsections we described some noteworthy curvature-induced scenarios where the redshift dependence of the time delay is not monotonic. We do not see any robust argument against the lack of monotonicity, the lack of monotonicity produces no "pathology". Still, one might simply wonder whether monotonicity is at all possible in the curvature-induced scenario. For this scope we must check if it is possible for the derivative of the time delay with respect to the redshift parameter z to never change sign. We find that this condition is satisfied only when $\eta_2 = -2\eta_3$ (see appendix B.1). Therefore, the two conditions of monotonicity and curvature-induced effects lead to

another one-parameter model. With this constraint, Eq. (5.35) reads

$$\Delta t = \eta_3 \frac{\Delta E}{E_p} \int_0^z \frac{d\overline{z}\,(1+\overline{z})}{H\,(\overline{z})} \Bigg[-2\left(1-\left(1-\frac{H\,(\overline{z})}{1+\overline{z}}\int_0^{\overline{z}} \frac{d\overline{z}'}{H\,(\overline{z}')}\right)^2\right) + \left(1-\left(1-\frac{H\,(\overline{z})}{1+\overline{z}}\int_0^{\overline{z}} \frac{d\overline{z}'}{H\,(\overline{z}')}\right)^4\right)\Bigg]. \tag{5.44}$$

We show the behaviour of this time delay in Figure 5.5. Interestingly, in this scenario there is a range of redshifts, between ~ 3 and ~ 4.5, where the time delay is approximately constant (in particular it has a stationary point at $z \sim 3.8$). This range does not depend on the value of the model parameter.

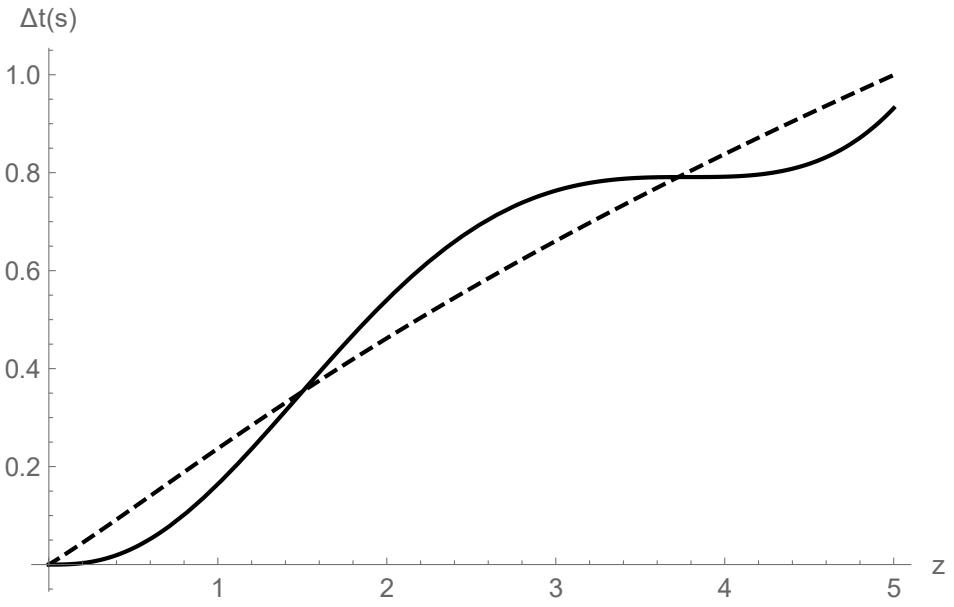

Figure 5.5: The continuous line corresponds to the "curvature-induced" monotonic scenario described by (5.44) with $\eta_3 = -1$. The dashed line represents the expected time delay for the Jacob-Piran case (5.10), corresponding to setting $\eta_2 = \eta_3 = 0$ in (5.35); the remaining free parameter in (5.35), η_1, is fixed by asking that the two lines cross at $z = 1.5$. As for Figure 5.3, we set $\Delta E = 10$ GeV for both lines.

5.4.6 Monotonicity for $\eta_1 \neq 0$

In the previous subsection we have found an interesting (at least unique) scenario by requesting monotonicity in the curvature-induced case ($\eta_1 = 0$), thus we find appropriate to also explore monotonicity for the most general case ($\eta_1 \neq 0$). When $\eta_1 \neq 0$ the requirement of monotonicity of the time delay can be expressed by identifying a region of the parameter space $\{\eta_2/\eta_1,\, \eta_3/\eta_1\}$ where monotonicity holds. We illustrate this in Figure 5.6 by fixing $\eta_1 = 1$ and considering the range $\eta_2, \eta_3 \in [-20, 20]$. The blue area identifies the values of η_2, η_3 such that $\frac{d\Delta t}{dz} \geq 0$ for every value of the redshift.

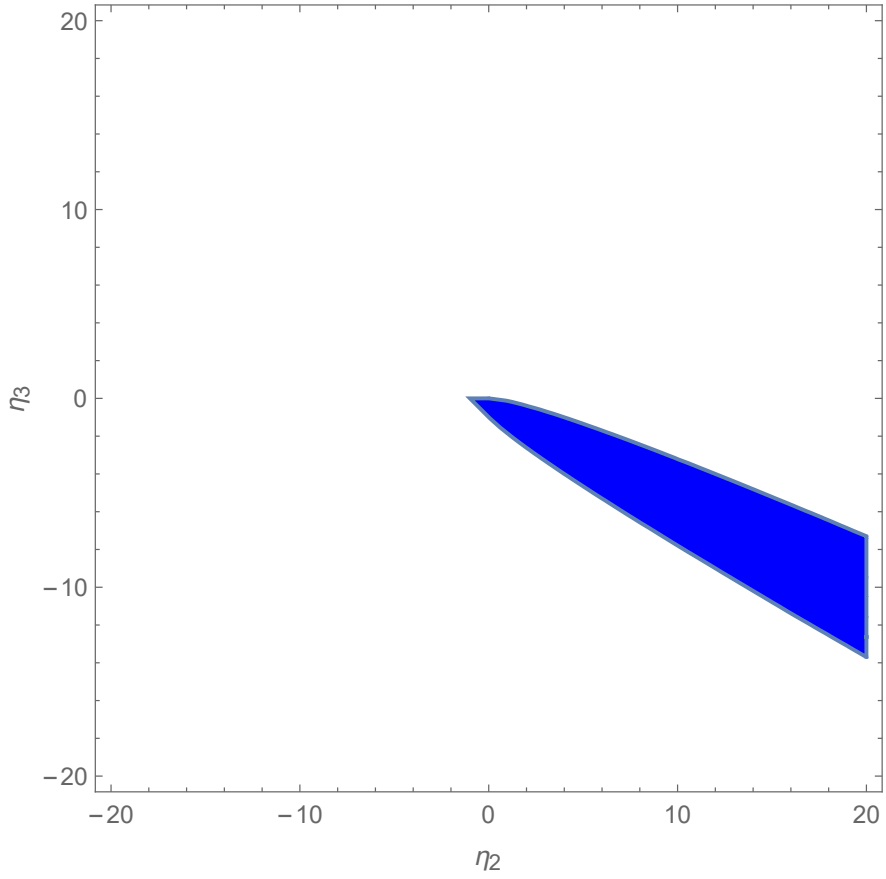

Figure 5.6: The blue region identifies the range of parameters η_2, η_3 such that the time delay of Eq. (5.35) depends monotonically on redshift when $\eta_1 = 1$.

We conclude this subsection showing just an example of a monotonic time delay behaviour (when $\eta_1 = 1$) that does not coincide with the Jacob and Piran result. A possible choice of parameters is the following:

$$\eta_1 = 1 \qquad \eta_2 = 2 \qquad \eta_3 = -2 \tag{5.45}$$

With this choice of parameters we obtain the plot in Figure 5.7.

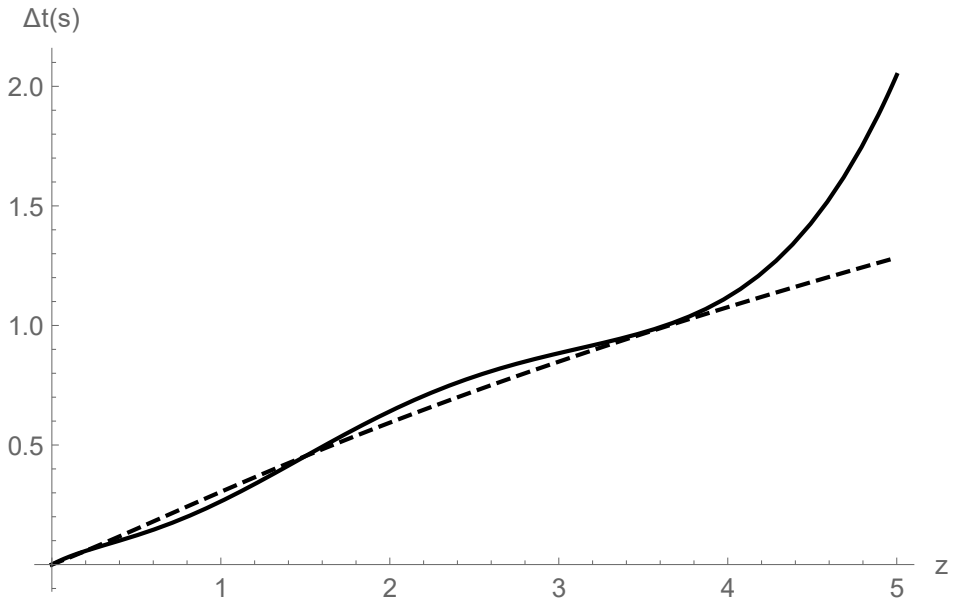

Figure 5.7: The continuous line corresponds to a monotonic scenario described by $\eta_1 = 1$, $\eta_2 = 2$, $\eta_3 = -2$. The dashed line represents the expected time delay for the Jacob-Piran case (5.10), corresponding to setting $\eta_2 = \eta_3 = 0$ in (5.35); the remaining free parameter in (5.35), η_1, is fixed by asking that the two lines cross at $z = 1.5$. As for Figure 5.3, we set $\Delta E = 10$ GeV for both lines.

5.5 Concluding remarks

In this chapter we have presented the most general formula that describes the leading order time delays (assuming linear dependence on the particle energy) for ultra-relativistic particles propagating in an FLRW expanding spacetime with deformed (DSR) relativistic symmetries. In particular, we found that the requirement of relativistic consistency of the DSR scenario allows for only three possible independent forms of redshift dependence. This result is completely different from the LIV scenario, where relativistic symmetries are broken and the lack of relativistic constraints allows in principle any possible form of redshift dependence in the time-delay formula.
In this chapter we have thus made important steps forward from a theoretical perspective, but considering the quite poor quality of presently obtainable data, even the exploration of the small three-parameter space we obtained is a big challenge for phenomenological studies. For this reason we also present some choices of the parameters corresponding to scenarios that according to us might deserve priority from the quantum-gravity perspective. Nevertheless, we expect that in the (near) future an increasing quantity of astrophysical data will be available allowing us to test this three parameter space of parameters.

In the next chapter we will explore the possibility of testing in-vacuo dispersion through gamma ray bursts data. In particular, we present a novel analysis that provides intriguing preliminary results that encourage further investigation of our novel scenarios in which the possibility of a non-monotonic dependence of time delay with redshift emerges.

Chapter 6

Testing in-vacuo dispersion through Gamma Ray Bursts

In this chapter we concern with the possibility of testing in-vacuo dispersion through gamma ray bursts (GRBs) data. Gamma ray bursts are indeed the main sources to test this effect due to their wide energy spectrum of emission (from keV to hundreds of GeV) and their large redshift distances (up to $z \sim 8$) (see [22] and references therein).

In the last decades various works exposed rather strong statistical evidence about the possibility of having in-vacuo dispersion analyzing data coming from GRBs [22,131–135]. These results thus motivate and encourage further investigation in this research direction.

The core of this chapter will be a novel analysis on in vacuo dispersion-like spectral lags in gamma ray bursts that also includes data coming from the recently observed GRB221009A. It was the brightest gamma ray burst ever detected and although being over 2 billion light-years away, it was powerful enough to affect Earth's atmosphere, having the strongest effect ever recorded by a gamma-ray burst on our planet [136].
In this analysis we will follow a quite novel strategy inspired by the one in [137]. Precisely, we will focus on the delay of detection between all the pairs of photons that are selected according to some selection criteria, described in detail below, coming from the GRBs reported in table 6.4. We will thus look for a linear correlation between time of observation and energy of GRB particles testing the in-vacuo dispersion hypothesis. Specifically, we will rely on the much tested formula for the time delay proposed by Jacob and Piran that we have extensively illustrated in the previous chapter.

Nevertheless, we are well conscious that the correlation between time of arrival and energy we are looking for, may be not the consequence of in-vacuo dispersion but rather the result of some other physical mechanisms related to, so far unknown astrophysical properties of the sources. It will be indeed not surprising that correlations between energy and time of arrival of photons are not connected to quantum gravity effects, but they are consequence of astrophysical spectral lags connected to the pulse evolution. This hypothesis is indeed the most probable and conservative one and only when more data will be available and a better understanding of GRBs mechanisms is achieved we can truly trust on these results.

Before focusing on our novel analysis let us briefly review the main properties of GRBs and summarize the main aspects of some previous analyses on in-vacuo dispersion conducted to date.

6.1 Gamma Ray Bursts

Gamma ray bursts are intense and short pulses of gamma rays observed in distant galaxies, that can last from fractions of second to several hundred seconds [138]. Then, they are followed by an afterglow, namely a lower-energy, long-lasting emission [22, 139, 140]. Afterglow radiation in GRBs that extends from the radio band to GeV energies, is produced as a result of the interaction between the relativistic jet and the ambient medium [141].
The first GRB was detected in 1967 by the Vela satellites and many others have been observed so far. Their origin is not very clear, but the intense radiation of most observed GRBs is thought to be released during a supernova or superluminous supernova as a high-mass star implodes to form a neutron star or a black hole, whereas a subclass of GRBs appears to originate from the merger of binary neutron stars.
Various observations suggested the existence of two classes of GRBs, short and long, based on the duration of the prompt phase, with a boundary around 2 s. Short GRBs account for just about 30% of the observed gamma-ray bursts while the majority of the observed events ($\sim 70\%$) have a duration of greater than two seconds and are thus classified as long gamma-ray bursts. Because these events constitute the majority of the population, they have been observed in greater detail than their short counterparts.

6.2 Preliminaries for the analysis

In this section we introduce some preliminary elements needed to test the in-vacuo dispersion hypothesis through astrophysical data coming from gamma ray bursts. In particular, in this chapter, we will focus on the class of scenarios which predict a linear dependence of corrections to the special relativistic time of flight Δt on the energy E of the particle that can be in general described in terms of the following formula [28, 132, 133, 142, 143]:

$$\Delta t = \eta_X \frac{E}{E_p} D(z) \pm \delta_X \frac{E}{E_p} D(z)\,, \tag{6.1}$$

where $D(z)$ carries information about the redshift distance of the source and the values of the parameters η_X and δ_X characterize the specific model we want to investigate.
In principle different kind of particles can be affected by quantum gravity effects in a

different way and we account for this by allowing for both η_X and δ_X to take different values for different particles and the label X specifies the particle of our interest. Notice that in (6.1) the notation $\pm\delta_X$ reflects the fact that it parametrizes the size of quantum-uncertainty (fuzziness) effects. On the contrary, the parameter η_X characterizes systematic effects. For instance, in our conventions for positive η_X and $\delta_X = 0$ a high-energy particle is systematically detected after a low-energy one if the two particles are emitted simultaneously.
In the following we will focus on a particular choice of $D(z)$ characterizing the Jacob and Piran formula:

$$D(z) = \int_0^z \frac{1+\bar{z}}{H_0\sqrt{\Omega_\Lambda + (1+\bar{z})^3\Omega_m}} d\bar{z}\,, \tag{6.2}$$

but we will gain interesting insights on alternative choices of $D(z)$ connected to the analysis presented in the previous chapter 5 that motivate and encourage further explorations.

The main limitation for this kind of analyses comes from the fact that an intrinsic time delay due to quite unknown emission mechanisms of the source can contribute to the observed time delay. Therefore, in order to solve this problem, a better understanding of GRBs mechanisms is required and in this direction recent studies of emission and acceleration models in order to constrain intrinsic delays in astrophysical sources have been carried out, but a lot of progress is still needed. However, to alleviate this issue, some strategies have been developed during these years. In particular, one of these is based on the introduction of a "distance-rescaled energy" E^* [131, 144] defined as:

$$E^* = E\frac{D(z)}{D(1)} \tag{6.3}$$

that allows us to rewrite (6.1) as:

$$\Delta t = \eta_X D(1)\frac{E^*}{E_p} \pm \delta_X D(1)\frac{E^*}{E_p}\,. \tag{6.4}$$

This reformulation of (6.1) allows us to describe the relevant quantum-spacetime effects, which in general depend both on redshift and energy, as effects that depend exclusively on energy. In general, as stressed before, we have to take into account the time offset t_{off} at the source that would imply that Δt is not exactly proportional to E^*. Taking into account the redshift effects on t_{off} we obtain the following expression:

$$\frac{\Delta t}{1+z} = t_{off} + \frac{\eta_X}{E_p}D(1)\frac{E^*}{1+z} \pm \frac{\delta_X}{E_p}D(1)\frac{E^*}{1+z}\,. \tag{6.5}$$

Notice that with this parametrization we can look for a relationship between $\frac{\Delta t}{1+z}$ and $\frac{E^*}{1+z}$ such that t_{off} is just a constant contribution.
In the following we will neglect a possible contribution due to δ_X and we focus only on the parameter η_X which characterizes possible systematic effects.

6.3 Some previous analyses with GRBs photons and neutrino candidates

In the previous section, we emphasized the current challenge in comprehending the intrinsic temporal dependencies of the GRBs spectrum, making it difficult to separate them from possible effects induced by quantum gravity. Despite this obstacle, the past 15 years have witnessed significant interest in exploring the possibility of quantum gravity induced in-vacuo dispersion and numerous analyses have delved into possible correlations between time of arrival of cosmological particles and their energies. Indeed, the fact that any given time of arrival difference among two particles can in principle always be attributed to emission mechanisms can be compensated by suitable techniques of statistical analysis.

When focusing on analyses involving photons, a common strategy implemented during these year to conduct these investigations is based on the time difference of arrival between the highest-energy photons observed in gamma-ray bursts and the first observed low-energy peak of the GRB [131, 132, 144]. The main assumption underlying these analyses is that the most energetic photons coincide with the first peak. Moreover, these analyses do not typically rely on all the photons coming from a GRB, but some selection criteria are adopted. For this purpose, in general, many reasonable criteria can be introduced and these can vary from an analysis to another.

In [131, 144], for instance, Ma and collaborators only considered photons with energy greater than 10 GeV observed within 90 seconds of the first peak.

In [132] instead slightly different selection criteria are introduced. Amelino-Camelia and collaborators specify the time window by mainly exploiting the fact that, as already observed in [131], an high percentage of the photons selected by the criteria of Ma and collaborators are quite consistent with the same value of the time offset at the source. In particular, it is thus required that selected photons to have emission times consistent with an offset of up to 20 seconds compared to the time of emission of the first GRB

peak and also possible effects due to in-vacuo dispersion are taken into account giving the following requirement:

$$|\Delta t| \leq 10^{-16} D(z) + 20s(1+z)\,. \tag{6.6}$$

In addition to this temporal criteria an energy cut of 40 GeV at the source is introduced, namely $E \geq 40\,\mathrm{Gev}/(1+z)$.

For more than a decade the in-vacuo dispersion analyses through data coming from GRBs were conducted limiting considerations only to photons. However, recently, Amelino-Camelia and collaborators have extended in-vacuo dispersion analyses also to neutrinos [132–134].

The IceCube neutrino telescope, to date, has not identified any evidence of gamma-ray burst neutrinos assuming equal travel times for neutrinos and photons from source to telescope. However, accounting for in-vacuo dispersion effects on both photons and neutrinos could yield intriguing outcomes in the research of GRB-neutrinos as firstly outlined in [134]. Moreover, the very high energy of observed neutrinos (typically between TeV and PeV) strongly diminishes the impact of the intrinsic time delay on these analyses. In fact, we expect delays of the order of days if we assume the quantum gravity scale to be around the Planck-scale. However, even if the intrinsic time delay does not represent a significant obstacle for these analyses, other non-trivial complications are still present. Specifically, it is not straightforward to get associations between GRBs and neutrinos. Consequently, it is very important the role played by the criteria used for selecting GRB-neutrino candidates that is not at all an easy task. Such criteria for selecting GRB-neutrino candidates shall involve a temporal window and some criteria of angular selection to establish whether or not it is reasonable that the direction of the GRB and the one of the neutrino are compatible.

In [132, 133] the following selection criteria are adopted:

- A temporal window of 3 days is contemplated, and only IceCube events with energy between 60 TeV and 500 TeV are considered;

- the angular distance between the direction of the neutrino and the direction of the GRB is within a $n\sigma$ region, with $\sigma = \sqrt{\sigma_\nu^2 + \sigma_{GRB}^2}$, with $n = 2$ in [132] and $n = 3$ in [133] (where σ_ν is the directional uncertainty of the neutrino and σ_{GRB} is the one of the GRB).

Moreover, it is important to stress that even if the main prediction related to in-vacuo dispersion is a correlation between time of arrival of particles and their energies, in these analyses an estimate of this correlation alone is not truly significant. In fact, in order to estimate the truly significance of the outcomes of these analyses, together with the computation of the correlations between energy and time of arrival of particles it is also necessary to characterize quantitatively how rare it would be for such features to arise accidentally, as a result of unknown aspects of the mechanisms that produce photons at source or as a result of background neutrinos accidentally fitting the profile of a GRB neutrino affected by in-vacuo dispersion [132, 133].

From many analyses conducted so far, mainly based on these strategies we have just presented, preliminary evidence of quantum gravity-induced effects on the propagation of both photons and neutrinos has emerged and the results obtained to date of course motivate and encourage further investigation. However, only when additional data will be available, we may truly ascertain the reliability of these observed quantum gravity effects.

In the following section we present a novel analysis in which we focus only on time of flights of photons, relying on a quite novel strategy inspired by the one in [137].

6.4 In vacuo dispersion-like spectral lags in gamma ray bursts

In this section, inspired by the analysis in [137], we will investigate the possibility of having in vacuo dispersion-like spectral lags. Our strategy, differently from those discussed in the previous section, does not involve the time delay between the most energetic photons and the first low-energy peak. Instead, for each GRB considered, we will focus on the time delay between all the pairs of photons that are selected according to some selection criteria described in detail below.

The sample of GRBs on which our analysis relies is the one considered in [137], but also includes the recently observed GRB221009A. For completeness we report in table 6.4 the full list of GRBs that we consider together with their redshift distance z.

Some novel aspects of this analysis are motivated by various results we obtained in chapter 5. In particular, in the previous chapter, we have shown that in many scenarios

GRBs	
GRB	z
GRB080916C	4.35
GRB090510	0.90
GRB090902B	1.82
GRB090926A	2.11
GRB100414A	1.37
GRB130427A	0.34
GRB160509A	1.17
GRB221009A	0.15

Table 6.1: List of all the GRBs considered in this analysis togheter with their redshift distance z.

the sign of time delay can depend on the redshift distance of the source when it is not a monotonic function of z. Nevertheless, in this analysis, we will rely on the much tested Jacob and Piran formula for the time delay expression, but the results we obtain encourage further analyses involving alternative expressions for the function $D(z)$ as we will show in the following.

Therefore, inspired by this possibility of having a possible dependence of the sign of quantum gravity effects on the redshift distance of the source z, we thus organize our sample of GRBs into three groups according to their redshift distance. Specifically, we consider a first class of GRBs including the ones with redshift quite smaller than one. Then, we consider a second class of GRBs including that with redshift $z \sim 1$ and finally we consider the "distant" GRBs which redshift distance is greater than one. In particular, in the following sections, we will conduct three distinct analyses, one for each of these three classes of GRBs adopting for the photons the following selection criteria regarding their energies and their angular compatibility with the source:

- we consider only photons with energy at emission greater than 3 GeV:

$$E(1+z) \geq 3\text{Gev}\,, \tag{6.7}$$

- the angular direction of the photon must be compatible with the direction of the GRB within 3°.

The main idea of this analysis is to consider a Δt_{pair}, which gives for each pair of photons (belonging to the same GRB) in our sample their difference of time of observation. Thus, for each pair of photons, we can estimate the value of η_γ:

$$\eta_\gamma^{pair} = \frac{E_p \Delta t_{pair}}{D(1)\Delta E^*_{pair}}\,, \tag{6.8}$$

where ΔE^*_{pair} is the difference in values of E^* for the two photons considered.
Of course, many of the pairs considered in this analysis will be bogus in the sense that the two photons are not emitted nearly simultaneously and will be noise for the analysis. However, we also expect that various pairs of photons in our sample were emitted nearly simultaneously, and for those pairs the Δt_{pair} could really estimate η_{pair} [137].

We consider bins of width equals to eight for the values of η_γ^{pair} and each pair of photons typically contributes to more than one of our bins, considering the fact that the energies of the photons are not known very precisely and we assume that the energy uncertainty is 10%. The contribution of a given pair to each bin is thus computed generating a gaussian distribution with mean value η_γ^{pair} and standard deviation σ_γ^{pair} obtained via error propagation. Then, we compute the area of this distribution falling within each bin, in order to evaluate the value to assign to a given bin. This enable us to realize histograms for η_γ^{pair} that we restrict to the range $\eta_\gamma^{pair} \in [-80, 80]$ and we normalize it in such a way that the sum of the frequencies of the values of η_γ^{pair} within this range is equal to one.

Furthermore, following the same strategy of analysis as in [137] we estimate how frequently η^γ_{pair} should occur within each bin in absence of correlation between Δt_{pair} and ΔE^* by producing 10^5 sets of simulated data, each obtained by reshuffling randomly the times of observation of the photons. In this way any eventual correlation between energy and time of arrival is of course destroyed and we can estimate the probability of having values of η^γ_{pair} falling within each bin.

We start our analysis by considering the class of GRBs with redshift smaller than one that is the subject of the next subsection.

6.4.1 Analysis with "close" GRBs

The first class of GRBs of our interest (GRBs with redshift z smaller than one) includes GRB130427A with redshift $z = 0.34$ and GRB221009A with $z = 0.15$. As anticipated previously, for each GRB in this group we consider all the possible pairs of photons,

selected according to the selection criteria presented in section 6.4, from which we estimate the values for η_{pair}. Then, we combine the results obtained from the two GRBs of our interest into a unique normalized histogram (see the histogram in blue in fig. 6.1).

From this plot, by comparing the histogram in blue which corresponds to the one

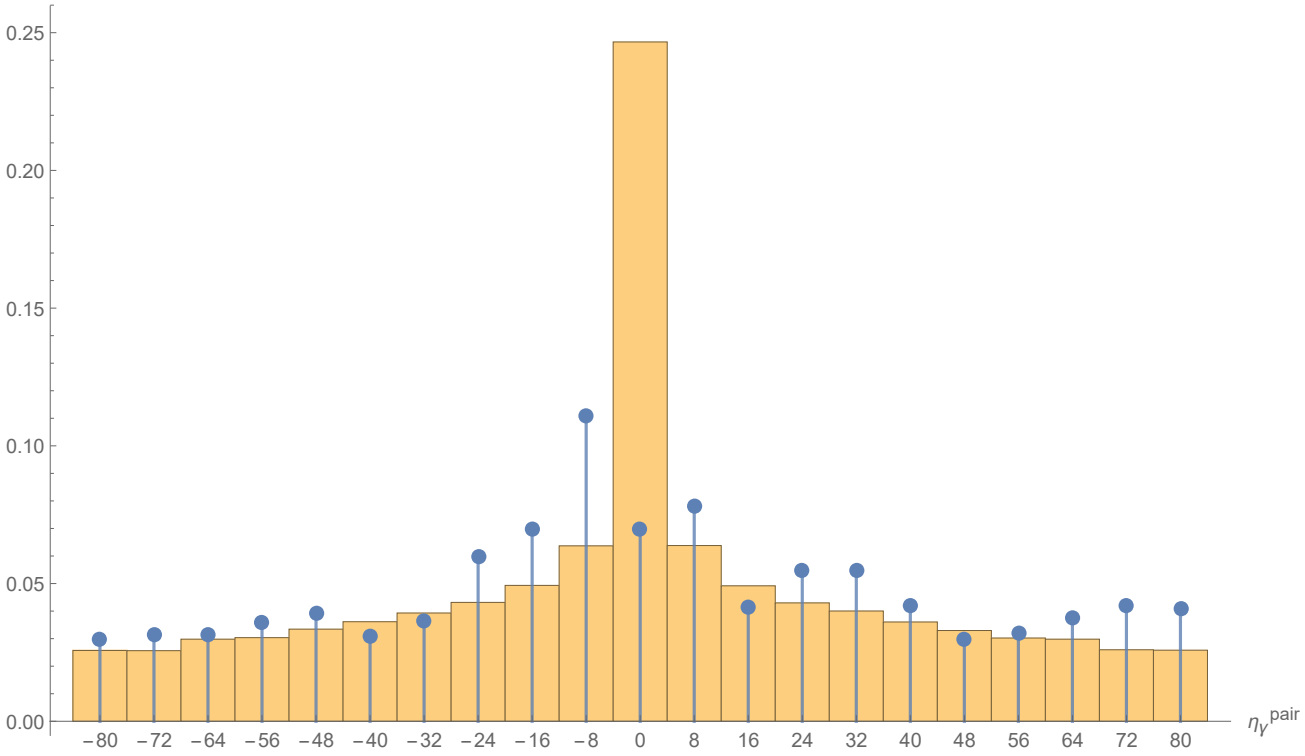

Figure 6.1: Normalized distribution for η_γ^{pair}. The histogram in blue is the one obtained analyzing photons coming from GRB130427A and GRB221009A. In orange we have the histogram obtained producing 10^5 sets of simulated data, each obtained by reshuffling randomly the times of observation of the photons in our sample.

obtained analyzing the true data and the histogram in orange that is obtained considering the data that are simulated as explained in the previous section, we can notice an excess of negative values for η_{pair}. In particular, the values which occur most frequently with respect to the expected ones in absence of correlation are those that fall within the first negative bin, namely within the range [-4,-12].

This result thus suggests the possibility of a quantum gravity parameter $\eta_\gamma \leq 0$, implying quantum gravity induced effects that speed up more energetic photons when

the redshift distance of the source is smaller than one. Thus, in this case, high-energy photons are detected systematically before low-energy ones if they are emitted simultaneously.

6.4.2 Analysis with GRBs with $z \sim 1$

In this subsection we focus on our second class of GRBs that includes those which redshift distance is close to one. Specifically, we included in this analysis GRB090510 that has a redshift $z = 0.90$, GRB160509A with a redshift $z = 1.17$ and GRB100414A with $z = 1.37$. Perhaps including GRB100414A in this class can be a little questionable since its redshift distance is close to one but not much. However, this GRB contributes to this analysis with a tiny number of photons with respect to the other GRBs in this class, therefore its contribute does not change significantly the outcome of the following analysis.

Following the same strategy as before, we obtain the histogram 6.2, where again the histogram in blue is the one obtained analyzing the true data and in orange we have the histogram obtained by producing 10^5 sets of simulated data, each obtained by reshuffling randomly the times of observation of the photons in order to destroy any eventual correlation between energy and time of arrival.

We can notice that for this second sample of GRBs the distribution of η^{γ}_{pair} is quite symmetric and piqued around zero. The histogram in blue practically follows the profile of the orange one, showing a slight excess of values of η^{γ} in the first negative bin and in the first positive one. This result thus suggests the possibility that eventual quantum gravity effects related to in-vacuo dispersion could be negligible when the redshift distance of the source is $z \sim 1$.

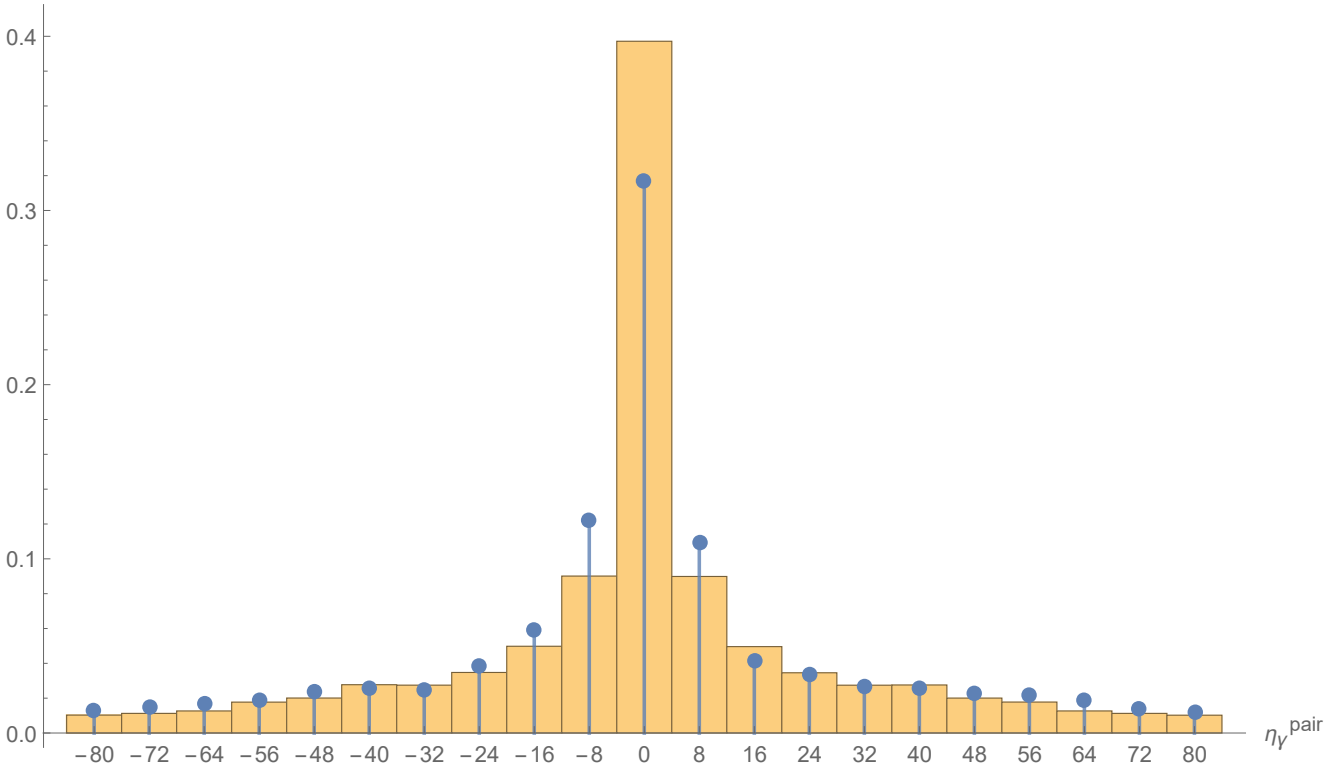

Figure 6.2: Normalized distribution for η_γ^{pair}. The histogram in blue is the one obtained analyzing photons coming from GRB090510, GRB160509A and GRB100414A. In orange we have the histogram obtained producing 10^5 sets of simulated data, each obtained by reshuffling randomly the times of observation of the photons.

6.4.3 Analysis with "distant" GRBs

Finally, in this subsection, we consider the last class of GRBs of our interest, the "distant" GRBs, namely the ones with redshift distance quite greater than one. These class include GRB080916C with redshift $z = 4.35$, GRB090902B with $z = 1.82$ and GRB090926A with $z = 2.11$.

By repeating the same analysis as done for the two previous classes of GRBs, we obtain the histogram in fig. 6.3.

As before, in blue we present the normalized distribution for η_{pair}^{γ} in the range $[-80, 80]$ and we estimate how frequently η_{pair}^{γ} should occur within each bin (orange histogram) in absence of correlation between Δt_{pair} and ΔE^* by producing 10^5 sets of

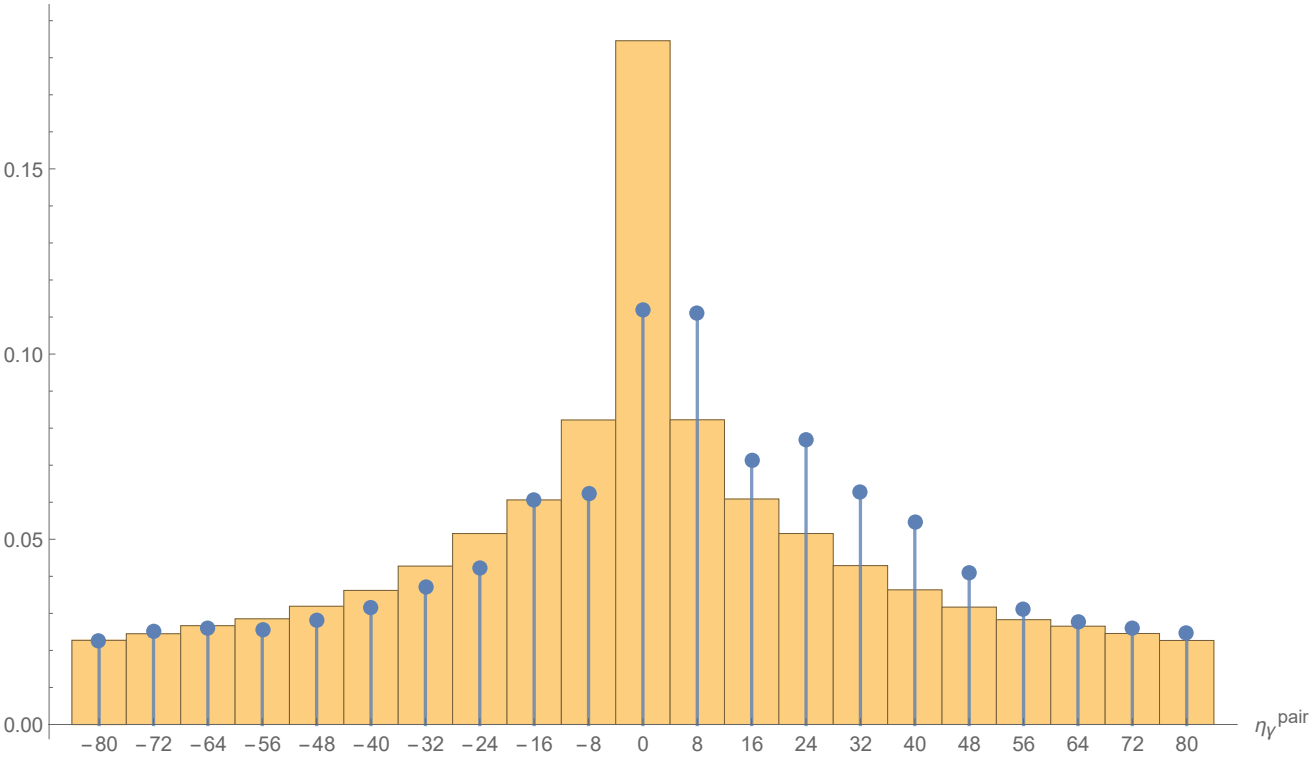

Figure 6.3: Normalized distribution for η_γ^{pair}. In blue there is the histogram obtained analyzing photons of GRB080916C, GRB090902B and GRB090926A. In orange we have the histogram obtained producing 10^5 sets of simulated data, each obtained by reshuffling randomly the times of observation of the photons.

simulated data, each obtained by reshuffling randomly the times of observation of the photons.

From this plot we can observe that, differently from the "close" GRBs class, an excess of positive values for η_{pair}^{γ} is now obtained.
This preliminary result, thus highlights the possibility of quantum gravity induced effects that slow down more energetic photons when the redshift distance of the source is greater than one. Thus, high-energy photons are detected systematically after low-energy photons when they are emitted simultaneously.

6.5 Concluding remarks and future directions

In this analysis of in-vacuo dispersion we relied on the much tested formula for the time delay proposed by Jacob and Piran. We found results that are not in good agreement with such formula since for the three different classes of GRBs we obtain outcomes that are not compatible among themselves. This result instead suggests the intriguing possibility of having a changing sign time delay with the redshift distance of the source z. In particular from this analysis the following preliminary picture has emerged:

- quantum gravity effects could speed up more energetic particles when the redshift distance of the source is smaller than one;
- quantum gravity effects on the propagation of particles emitted by sources with $z \sim 1$ could be negligible;
- quantum gravity effects could slow down more energetic particles when the redshift distance of the source is greater than one.

Until now, the possibility of having a redshift dependent sign of the quantum gravity induced time delay has never been contemplated in literature. People indeed have always considered the hypothesis that quantum gravity effects should accumulate with increasing distance, expecting a monotonic behaviour for Δt as a function of z, keeping fixed the other parameters.

The preliminary results obtained in this analysis instead encourage future studies in which the possibility of having a non-monotonic behaviour for the time delay is considered. In particular, it will be interesting to compare to data also some of the alternatives formulas derived in the previous chapter and I plan to conduct these novel analyses in the next months expecting that those in which time delay is not monotonic as in eq. (5.43) could have a good agreement to data.

Nevertheless, as already stressed at the beginning of this chapter, our findings may be not the consequence of in-vacuo dispersion but rather the result of some other physical mechanism related to, so far unknown, astrophysical properties of the sources. It will be indeed not surprising that such findings are not connected to quantum gravity effects but they are just astrophysical spectral lags, consequence of pulse evolution. For this reason, only when a better understanding of GRBs mechanisms is achieved and more data will be available we shall truly trust on these results.

Chapter 7

Conclusions

We conclude this dissertation providing a summary of the structure of this work and the main results we obtained.

- In chapter 1 we have introduced the quantum gravity problem and we discussed how in the last decades the possibility of a quantum gravity phenomenology is increasing realistic. The primary objective of this research program is to explore physical effects that are expected to be low-energy remnants of the Planck-scale physics and to identify amplifiers capable of magnifying these tiny effects expected from quantum gravity such that we can test them with our present experimental apparata. The most active area in this research program concerns the investigation of phenomenological opportunities coming from departures from Lorentz invariance at Planck-scale both in the context of LIV and DSR scenarios.

- In chapter 2 we reviewed the main mathematical structures, namely Hopf algebras and quantum groups, needed to describe the symmetries of quantum spacetimes. In particular, we present the θ Moyal-Weyl non-commutativity and finally we introduce the famous κ-Minkowski spacetime and discuss its deformed symmetries.

- In chapter 3 we address the much debated problem of conserved charges in quantum spacetimes. We tackle this problem focusing on first-quantized particles described within a Hamiltonian framework, using as toy model the so-called "spatial kappa-Minkowski non-commutative spacetime". Within this framework we derived all the Noether charges and we revealed a strong connection between their properties and the structure of the laws of interaction among particles.

- In chapter 4 we explored the possible role of observers and the notion of reference frames in quantum spacetimes by focusing on a quantum group toy model. In particular, we focused on the case in which two observers are exclusively interested in finding out the relative spatial orientations of their respective frames. For this scope we invoked the quantum group $SU_q(2)$ as a description of deformed spatial rotations. We have interpreted states of a representation of its algebra as describing the relative orientation between two reference frames and this led to a quantization of one of the Euler angles and to the new paradigm of agency-dependence. Specifically, in this framework, space is reconstructed as a collection of fuzzy points, exclusive to each agent, which depends on their choice of reference frame. Every agent is limited to selecting a single direction in which points can

exhibit sharpness. Simultaneously, points in all other directions become fuzzy in a way that depends on the direction chosen. Consequently, when two agents make disparate choices, they will perceive the same points with different degrees of fuzziness. These intriguing results pave the way for further understanding the connection between quantum gravity and quantum information/quantum foundations, opening the way for new studies to better comprehend the role of observers and reference frames in quantum gravity.

- In chapter 5 we concerned with the possibility of testing the fate of relativistic symmetries in quantum gravity through time of flight measurements. Studies of in-vacuo dispersion are indeed the most active area of quantum-gravity phenomenology. We derived the most general formula for the leading order redshift-dependent correction to the time of flight for the scenario in which relativistic symmetries are deformed at the Planck-scale (DSR). We did this first for the constant-curvature case and then we also derived a generalization of our results to the FLRW scenario. We found that, contrary to the broken symmetries scenario (LIV), where in principle any arbitrary form of redshift dependence could be allowed, for the DSR scenario only linear combinations of three possible forms of redshift dependence are allowed. Finally, we discussed some specific combinations of the three forms of redshift dependence whose investigation might deserve priority from the quantum-gravity perspective. These noteworthy special cases can be motivated by theoretical arguments based on the possible requirement that the quantum gravity effects are "curvature induced", so that the time-delay vanishes when the spacetime curvature/expansion is negligible, the possible requirement that the total energy of a multi-particle system should be obtained with a standard linear law of addition of particle energies and the requirement of monotonicity of time delay as a function of the redshift distance of the source.

- In the last chapter 6 we discussed the possibility of testing in-vacuo dispersion through gamma ray bursts data. In particular, after reviewing the strategy of some of the main analyses conducted to date, we discussed a novel analysis that also includes data coming from the recently observed GRB221009A. In this analysis we focused on the delay of detection between all the pairs of photons, that are selected according to some selection criteria, coming from various GRBs. Of course, many of these pairs considered in the analysis will be spurious in the sense

that the two photons are not emitted nearly simultaneously and will be noise for the analysis. However, we also expect that various pairs of photons in our sample were emitted nearly simultaneously, and for those pairs we obtain a reasonable estimate of the quantum gravity parameter. We found results that are not in good agreement with the much tested formula proposed by Jacob and Piran, but instead suggest the interesting possibility of having a changing sign time delay with the redshift distance of the source. These results, thus encourages future analyses to compare to data also some of the alternatives formulas we derived in chapter 5 and it is plausible that those in which time delay is not monotonic shall have a good agreement to data.

Bibliography

[1] I. Antoniadis, "A possible new dimension at a few tev," *Physics Letters B*, vol. 246, no. 3, pp. 377–384, 1990.

[2] G. Veneziano, "A stringy nature needs just two constants," *Europhysics Letters*, vol. 2, p. 199, aug 1986.

[3] E. Witten, "Strong coupling expansion of Calabi-Yau compactification," *Nucl. Phys. B*, vol. 471, pp. 135–158, 1996, hep-th/9602070.

[4] C. Csaki, "TASI lectures on extra dimensions and branes," in *Theoretical Advanced Study Institute in Elementary Particle Physics (TASI 2002): Particle Physics and Cosmology: The Quest for Physics Beyond the Standard Model(s)*, pp. 605–698, 4 2004, hep-ph/0404096.

[5] C. Rovelli, "Loop quantum gravity," *Living Rev. Rel.*, vol. 1, p. 1, 1998, gr-qc/9710008.

[6] A. Ashtekar and J. Lewandowski, "Background independent quantum gravity: A Status report," *Class. Quant. Grav.*, vol. 21, p. R53, 2004, gr-qc/0404018.

[7] L. Smolin, "How far are we from the quantum theory of gravity?," 3 2003, hep-th/0303185.

[8] T. Thiemann, "Lectures on loop quantum gravity," *Lect. Notes Phys.*, vol. 631, pp. 41–135, 2003, gr-qc/0210094.

[9] H. S. Snyder, "Quantized space-time," *Phys. Rev.*, vol. 71, pp. 38–41, 1947.

[10] S. Doplicher, K. Fredenhagen, and J. E. Roberts, "Space-time quantization induced by classical gravity," *Phys. Lett. B*, vol. 331, pp. 39–44, 1994.

[11] S. Majid and H. Ruegg, "Bicrossproduct structure of kappa Poincare group and noncommutative geometry," *Phys. Lett. B*, vol. 334, pp. 348–354, 1994, hep-th/9405107.

[12] J. Lukierski, H. Ruegg, and W. J. Zakrzewski, "Classical quantum mechanics of free kappa relativistic systems," *Annals Phys.*, vol. 243, pp. 90–116, 1995, hep-th/9312153.

[13] R. Loll, "Quantum Gravity from Causal Dynamical Triangulations: A Review," *Class. Quant. Grav.*, vol. 37, no. 1, p. 013002, 2020, 1905.08669.

[14] E. Manrique, S. Rechenberger, and F. Saueressig, "Asymptotically Safe Lorentzian Gravity," *Phys. Rev. Lett.*, vol. 106, p. 251302, 2011, 1102.5012.

[15] T. Krajewski, "Group field theories," *PoS*, vol. QGQGS2011, p. 005, 2011, 1210.6257.

[16] D. Oriti, "Group Field Theory and Loop Quantum Gravity," 8 2014, 1408.7112.

[17] E. Bianchi, C. Rovelli, and F. Vidotto, "Towards spinfoam cosmology," *Phys. Rev. D*, vol. 82, p. 084035, Oct 2010.

[18] T. Biswas, E. Gerwick, T. Koivisto, and A. Mazumdar, "Towards singularity and ghost free theories of gravity," *Phys. Rev. Lett.*, vol. 108, p. 031101, 2012, 1110.5249.

[19] A. Kempf and G. Mangano, "Minimal length uncertainty relation and ultraviolet regularization," *Phys. Rev. D*, vol. 55, pp. 7909–7920, 1997, hep-th/9612084.

[20] J. Ambjorn, A. Gorlich, J. Jurkiewicz, R. Loll, J. Gizbert-Studnicki, and T. Trzesniewski, "The Semiclassical Limit of Causal Dynamical Triangulations," *Nucl. Phys. B*, vol. 849, pp. 144–165, 2011, 1102.3929.

[21] R. Loll, G. Fabiano, D. Frattulillo, and F. Wagner, "Quantum Gravity in 30 Questions," *PoS*, vol. CORFU2021, p. 316, 2022, 2206.06762.

[22] A. Addazi *et al.*, "Quantum gravity phenomenology at the dawn of the multi-messenger era—A review," *Prog. Part. Nucl. Phys.*, vol. 125, p. 103948, 2022, 2111.05659.

[23] G. Amelino-Camelia, "Quantum-Spacetime Phenomenology," *Living Rev. Rel.*, vol. 16, p. 5, 2013, 0806.0339.

[24] R. Alves Batista *et al.*, "White Paper and Roadmap for Quantum Gravity Phenomenology in the Multi-Messenger Era," 12 2023, 2312.00409.

[25] J. Alfaro, H. A. Morales-Tecotl, and L. F. Urrutia, "Quantum gravity corrections to neutrino propagation," *Phys. Rev. Lett.*, vol. 84, pp. 2318–2321, 2000, gr-qc/9909079.

[26] G. Amelino-Camelia, L. Smolin, and A. Starodubtsev, "Quantum symmetry, the cosmological constant and Planck scale phenomenology," *Class. Quant. Grav.*, vol. 21, pp. 3095–3110, 2004, hep-th/0306134.

[27] L. Smolin, "Quantum gravity with a positive cosmological constant," 2002, hep-th/0209079.

[28] G. Amelino-Camelia and S. Majid, "Waves on noncommutative space-time and gamma-ray bursts," *Int. J. Mod. Phys. A*, vol. 15, pp. 4301–4324, 2000, hep-th/9907110.

[29] G. Amelino-Camelia, J. R. Ellis, N. E. Mavromatos, D. V. Nanopoulos, and S. Sarkar, "Tests of quantum gravity from observations of gamma-ray bursts," *Nature*, vol. 393, pp. 763–765, 1998, astro-ph/9712103.

[30] D. Mattingly, T. Jacobson, and S. Liberati, "Threshold configurations in the presence of Lorentz violating dispersion relations," *Phys. Rev. D*, vol. 67, p. 124012, 2003, hep-ph/0211466.

[31] J. M. Carmona, J. L. Cortés, L. Pereira, and J. J. Relancio, "Bounds on Relativistic Deformed Kinematics from the Physics of the Universe Transparency," *Symmetry*, vol. 12, no. 8, p. 1298, 2020, 2008.10251.

[32] H. Li and B.-Q. Ma, "Searching Lorentz invariance violation from cosmic photon attenuation," *Eur. Phys. J. C*, vol. 83, no. 3, p. 192, 2023, 2210.05563.

[33] C. Li and B.-Q. Ma, "Ultrahigh-energy photons from LHAASO as probes of Lorentz symmetry violations," *Phys. Rev. D*, vol. 104, no. 6, p. 063012, 2021, 2105.07967.

[34] J. M. Carmona, J. L. Cortés, J. J. Relancio, M. A. Reyes, and A. Vincueria, "Modification of the mean free path of very high-energy photons due to a relativistic deformed kinematics," *Eur. Phys. J. Plus*, vol. 137, no. 7, p. 768, 2022, 2109.08402.

[35] G. Amelino-Camelia, G. Mandanici, and K. Yoshida, "On the IR / UV mixing and experimental limits on the parameters of canonical noncommutative space-times," *JHEP*, vol. 01, p. 037, 2004, hep-th/0209254.

[36] R. J. Szabo, "Quantum field theory on noncommutative spaces," *Phys. Rept.*, vol. 378, pp. 207–299, 2003, hep-th/0109162.

[37] G. Amelino-Camelia, C. Laemmerzahl, F. Mercati, and G. M. Tino, "Constraining the Energy-Momentum Dispersion Relation with Planck-Scale Sensitivity Using Cold Atoms," *Phys. Rev. Lett.*, vol. 103, p. 171302, 2009, 0911.1020.

[38] F. Mercati, D. Mazon, G. Amelino-Camelia, J. M. Carmona, J. L. Cortes, J. Indurain, C. Laemmerzahl, and G. M. Tino, "Probing the quantum-gravity realm with slow atoms," *Class. Quant. Grav.*, vol. 27, p. 215003, 2010, 1004.0847.

[39] M. Arzano, J. Kowalski-Glikman, and A. Walkus, "A Bound on Planck-scale modifications of the energy-momentum composition rule from atomic interferometry," *EPL*, vol. 90, no. 3, p. 30006, 2010, 0912.2712.

[40] S. Majid, "Algebraic approach to quantum gravity: relative realism," May 2007.

[41] S. Doplicher, K. Fredenhagen, and J. E. Roberts, "The Quantum structure of space-time at the Planck scale and quantum fields," *Commun. Math. Phys.*, vol. 172, pp. 187–220, 1995, hep-th/0303037.

[42] J. Lukierski, H. Ruegg, A. Nowicki, and V. N. Tolstoy, "q-deformation of poincaré algebra," *Physics Letters B*, vol. 264, no. 3, pp. 331–338, 1991.

[43] J. Lukierski, A. Nowicki, and H. Ruegg, "New quantum poincaré algebra and -deformed field theory," *Physics Letters B*, vol. 293, no. 3, pp. 344–352, 1992.

[44] F. Lizzi, M. Manfredonia, and F. Mercati, "The momentum spaces of κ-Minkowski noncommutative spacetime," *Nucl. Phys. B*, vol. 958, p. 115117, 2020, 2001.08756.

[45] M. Arzano and T. Trzesniewski, "Diffusion on κ-Minkowski space," *Phys. Rev. D*, vol. 89, no. 12, p. 124024, 2014, 1404.4762.

[46] A. Blaut, M. Daszkiewicz, and J. Kowalski-Glikman, "Doubly special relativity with light cone deformation," *Mod. Phys. Lett. A*, vol. 18, p. 1711, 2003, hep-th/0302157.

[47] G. Amelino-Camelia, J. R. Ellis, N. E. Mavromatos, D. V. Nanopoulos, and S. Sarkar, "Tests of quantum gravity from observations of gamma-ray bursts," *Nature*, vol. 393, pp. 763–765, 1998, astro-ph/9712103.

[48] R. Gambini and J. Pullin, "Nonstandard optics from quantum space-time," *Phys. Rev. D*, vol. 59, p. 124021, 1999, gr-qc/9809038.

[49] G. Amelino-Camelia, "Relativity in space-times with short distance structure governed by an observer independent (Planckian) length scale," *Int. J. Mod. Phys. D*, vol. 11, pp. 35–60, 2002, gr-qc/0012051.

[50] J. Magueijo and L. Smolin, "Generalized Lorentz invariance with an invariant energy scale," *Phys. Rev. D*, vol. 67, p. 044017, 2003, gr-qc/0207085.

[51] J. Kowalski-Glikman and S. Nowak, "Doubly special relativity theories as different bases of kappa Poincare algebra," *Phys. Lett. B*, vol. 539, pp. 126–132, 2002, hep-th/0203040.

[52] N. R. Bruno, G. Amelino-Camelia, and J. Kowalski-Glikman, "Deformed boost transformations that saturate at the Planck scale," *Phys. Lett. B*, vol. 522, pp. 133–138, 2001, hep-th/0107039.

[53] G. Amelino-Camelia, "On the fate of Lorentz symmetry in relative-locality momentum spaces," *Phys. Rev. D*, vol. 85, p. 084034, 2012, 1110.5081.

[54] J. M. Carmona, J. L. Cortes, and F. Mercati, "Relativistic kinematics beyond Special Relativity," *Phys. Rev. D*, vol. 86, p. 084032, 2012, 1206.5961.

[55] G. Amelino-Camelia, L. Freidel, J. Kowalski-Glikman, and L. Smolin, "The principle of relative locality," *Phys. Rev. D*, vol. 84, p. 084010, 2011, 1101.0931.

[56] G. Amelino-Camelia, L. Freidel, J. Kowalski-Glikman, and L. Smolin, "Relative locality: A deepening of the relativity principle," *Gen. Rel. Grav.*, vol. 43, pp. 2547–2553, 2011, 1106.0313.

[57] M. Born, "A suggestion for unifying quantum theory and relativity," *Proc. Roy. Soc. Lond. A*, vol. 165, no. 921, pp. 291–303, 1938.

[58] J. Kowalski-Glikman and G. Rosati, "Relative Locality in Curved Space-time," *Mod. Phys. Lett. A*, vol. 28, p. 1350101, 2013, 1303.7216.

[59] F. Cianfrani, J. Kowalski-Glikman, and G. Rosati, "Generally covariant formulation of Relative Locality in curved spacetime," *Phys. Rev. D*, vol. 89, no. 4, p. 044039, 2014, 1401.2057.

[60] F. Mercati and J. J. Relancio, "Relative Locality in curved spacetimes and event horizons," 6 2023, 2306.11451.

[61] S. Majid, *Foundations of Quantum Group Theory*. Cambridge University Press, 1995.

[62] A. Agostini, G. Amelino-Camelia, and F. D'Andrea, "Hopf algebra description of noncommutative space-time symmetries," *Int. J. Mod. Phys. A*, vol. 19, pp. 5187–5220, 2004, hep-th/0306013.

[63] N. Seiberg and E. Witten, "String theory and noncommutative geometry," *JHEP*, vol. 09, p. 032, 1999, hep-th/9908142.

[64] F. Lizzi and F. Mercati, "κ-Poincaré-comodules, Braided Tensor Products and Noncommutative Quantum Field Theory," *Phys. Rev. D*, vol. 103, p. 126009, 2021, 2101.09683.

[65] G. Fabiano and F. Mercati, "Multiparticle states in braided lightlike κ-Minkowski noncommutative QFT," 10 2023, 2310.15063.

[66] G. Amelino-Camelia, L. Freidel, J. Kowalski-Glikman, and L. Smolin, "Relative locality and the soccer ball problem," *Phys. Rev. D*, vol. 84, p. 087702, Oct 2011.

[67] S. Hossenfelder, "Multiparticle states in deformed special relativity," *Phys. Rev. D*, vol. 75, p. 105005, May 2007.

[68] G. Gubitosi and S. Heefer, "Relativistic compatibility of the interacting κ-poincaré model and implications for the relative locality framework," *Phys. Rev. D*, vol. 99, p. 086019, Apr 2019.

[69] G. Amelino-Camelia, G. Fabiano, and D. Frattulillo, "Total momentum and other Noether charges for particles interacting in a quantum spacetime," 2 2023, 2302.08569.

[70] M. Arzano and J. Kowalski-Glikman, *Deformations of Spacetime Symmetries: Gravity, Group-Valued Momenta, and Non-Commutative Fields*, vol. 986 of *Lecture Notes in Physics*. 6 2021.

[71] J. Lukierski, A. Nowicki, and H. Ruegg, "New quantum Poincare algebra and k deformed field theory," *Phys. Lett. B*, vol. 293, pp. 344–352, 1992.

[72] G. Amelino-Camelia, L. Barcaroli, G. Gubitosi, and N. Loret, "Dual redshift on Planck-scale-curved momentum spaces," *Class. Quant. Grav.*, vol. 30, p. 235002, 2013, 1305.5062.

[73] G. Amelino-Camelia, "Planck-scale soccer-ball problem: a case of mistaken identity," *Entropy*, vol. 19, no. 8, p. 400, 2017, 1407.7891.

[74] G. Amelino-Camelia, G. Gubitosi, A. Marciano, P. Martinetti, and F. Mercati, "A No-pure-boost uncertainty principle from spacetime noncommutativity," *Phys. Lett. B*, vol. 671, pp. 298–302, 2009, 0707.1863.

[75] G. Amelino-Camelia, F. Briscese, G. Gubitosi, A. Marciano, P. Martinetti, and F. Mercati, "Noether analysis of the twisted Hopf symmetries of canonical noncommutative spacetimes," *Phys. Rev. D*, vol. 78, p. 025005, 2008, 0709.4600.

[76] A. Agostini, F. Lizzi, and A. Zampini, "Generalized Weyl systems and kappa Minkowski space," *Mod. Phys. Lett. A*, vol. 17, pp. 2105–2126, 2002, hep-th/0209174.

[77] P. Kosinski, J. Lukierski, and P. Maslanka, "Local field theory on kappa Minkowski space, star products and noncommutative translations," *Czech. J. Phys.*, vol. 50, pp. 1283–1290, 2000, hep-th/0009120.

[78] S. Majid, "Meaning of noncommutative geometry and the Planck scale quantum group," *Lect. Notes Phys.*, vol. 541, pp. 227–276, 2000, hep-th/0006166.

[79] G. Amelino-Camelia, G. Gubitosi, and G. Palmisano, "Pathways to relativistic curved momentum spaces: de Sitter case study," *Int. J. Mod. Phys. D*, vol. 25, no. 02, p. 1650027, 2016, 1307.7988.

[80] J. M. Carmona, J. L. Cortés, and J. J. Relancio, "Relativistic deformed kinematics from momentum space geometry," *Phys. Rev. D*, vol. 100, no. 10, p. 104031, 2019, 1907.12298.

[81] G. Amelino-Camelia, V. D'Esposito, G. Fabiano, D. Frattulillo, P. A. Höhn, and F. Mercati, "Quantum euler angles and agency-dependent spacetime," *Progress of Theoretical and Experimental Physics*, p. ptae015, 01 2024.

[82] W. Heisenberg, *The physical principles of the quantum theory*. Courier Corporation, 1949.

[83] H. M. Wiseman and G. J. Milburn, *Quantum measurement and control*. Cambridge university press, 2009.

[84] D. J. Gross and P. F. Mende, "String Theory Beyond the Planck Scale," *Nucl. Phys. B*, vol. 303, pp. 407–454, 1988.

[85] D. Amati, M. Ciafaloni, and G. Veneziano, "Classical and Quantum Gravity Effects from Planckian Energy Superstring Collisions," *Int. J. Mod. Phys. A*, vol. 3, pp. 1615–1661, 1988.

[86] R. J. Adler and D. I. Santiago, "On gravity and the uncertainty principle," *Mod. Phys. Lett. A*, vol. 14, p. 1371, 1999, gr-qc/9904026.

[87] C. Rovelli and L. Smolin, "Discreteness of area and volume in quantum gravity," *Nucl. Phys. B*, vol. 442, pp. 593–622, 1995, gr-qc/9411005. [Erratum: Nucl.Phys.B 456, 753–754 (1995)].

[88] A. Ashtekar and J. Lewandowski, "Quantum theory of geometry. 1: Area operators," *Class. Quant. Grav.*, vol. 14, pp. A55–A82, 1997, gr-qc/9602046.

[89] A. Ashtekar and J. Lewandowski, "Quantum theory of geometry. 2. Volume operators," *Adv. Theor. Math. Phys.*, vol. 1, pp. 388–429, 1998, gr-qc/9711031.

[90] P. A. Höhn, "Reflections on the information paradigm in quantum and gravitational physics," *J. Phys. Conf. Ser.*, vol. 880, no. 1, p. 012014, 2017, 1706.06882.

[91] S. Woronowicz, "Twisted su (2) group. an example of a non commutative differential calculus," *Publications of the Research Institute for Mathematical Sciences*, vol. 23, 03 1987.

[92] E. Bianchi and C. Rovelli, "A Note on the geometrical interpretation of quantum groups and non-commutative spaces in gravity," *Phys. Rev. D*, vol. 84, p. 027502, 2011, 1105.1898.

[93] L. L. Vaksman and Y. S. Soibel'man, "Algebra of functions on the quantum group su(2)," *Functional Analysis and Its Applications*, vol. 22, pp. 170–181, 1988.

[94] T. Masuda, K. Mimachi, Y. Nakagami, M. Noumi, and K. Ueno, "Representations of the quantum group suq(2) and the little q-jacobi polynomials," *Journal of Functional Analysis*, vol. 99, pp. 357–386, Aug 1991.

[95] P. Podlés, "Symmetries of quantum spaces. subgroups and quotient spaces of quantum su(2) and so(3) groups," *Communications in Mathematical Physics*, vol. 170, pp. 1–20, May 1995.

[96] S. D. Bartlett, T. Rudolph, and R. W. Spekkens, "Reference frames, superselection rules, and quantum information," *Rev. Mod. Phys.*, vol. 79, pp. 555–609, 2007, quant-ph/0610030.

[97] X.-C. Song, "Spinor analysis for quantum group $SU_q(2)$," *Journal of Physics A: Mathematical and General*, vol. 25, no. 10, pp. 2929–2944, 1992.

[98] R. M. Angelo, N. Brunner, S. Popescu, A. J. Short, and P. Skrzypczyk, "Physics within a quantum reference frame," *Journal of Physics A: Mathematical and Theoretical*, vol. 44, no. 14, p. 145304, 2011.

[99] F. Giacomini, E. Castro-Ruiz, and C. Brukner, "Quantum mechanics and the covariance of physical laws in quantum reference frames," *Nature Commun.*, vol. 10, no. 1, p. 494, 2019, 1712.07207.

[100] A. Vanrietvelde, P. A. Höhn, F. Giacomini, and E. Castro-Ruiz, "A change of perspective: switching quantum reference frames via a perspective-neutral framework," *Quantum*, vol. 4, p. 225, 2020, 1809.00556.

[101] S. Ahmad Ali, T. D. Galley, P. A. Höhn, M. P. E. Lock, and A. R. H. Smith, "Quantum Relativity of Subsystems," *Phys. Rev. Lett.*, vol. 128, no. 17, p. 170401, 2022, 2103.01232.

[102] A.-C. de la Hamette and T. D. Galley, "Quantum reference frames for general symmetry groups," *Quantum*, vol. 4, p. 367, 2020, 2004.14292.

[103] A.-C. de la Hamette, T. D. Galley, P. A. Höhn, L. Loveridge, and M. P. Müller, "Perspective-neutral approach to quantum frame covariance for general symmetry groups," 10 2021, 2110.13824.

[104] E. Castro-Ruiz, F. Giacomini, A. Belenchia, and C. Brukner, "Quantum clocks and the temporal localisability of events in the presence of gravitating quantum systems," *Nature Commun.*, vol. 11, no. 1, p. 2672, 2020, 1908.10165.

[105] P. A. Höhn, A. R. H. Smith, and M. P. E. Lock, "Trinity of relational quantum dynamics," *Phys. Rev. D*, vol. 104, no. 6, p. 066001, 2021, 1912.00033.

[106] F. Lizzi, M. Manfredonia, F. Mercati, and T. Poulain, "Localization and Reference Frames in κ-Minkowski Spacetime," *Phys. Rev. D*, vol. 99, no. 8, p. 085003, 2019, 1811.08409.

[107] G. Amelino-Camelia, D. Frattulillo, G. Gubitosi, G. Rosati, and S. Bedić, "Phenomenology of DSR-relativistic in-vacuo dispersion in FLRW spacetime," 7 2023, 2307.05428.

[108] G. Rosati, G. Amelino-Camelia, A. Marciano, and M. Matassa, "Planck-scale-modified dispersion relations in FRW spacetime," *Phys. Rev. D*, vol. 92, no. 12, p. 124042, 2015, 1507.02056.

[109] G. Amelino-Camelia, A. Marciano, M. Matassa, and G. Rosati, "Deformed Lorentz symmetry and relative locality in a curved/expanding spacetime," *Phys. Rev. D*, vol. 86, p. 124035, 2012, 1206.5315.

[110] G. Amelino-Camelia, M. Matassa, F. Mercati, and G. Rosati, "Taming Nonlocality in Theories with Planck-Scale Deformed Lorentz Symmetry," *Phys. Rev. Lett.*, vol. 106, p. 071301, 2011, 1006.2126.

[111] G. Amelino-Camelia, L. Freidel, J. Kowalski-Glikman, and L. Smolin, "The principle of relative locality," *Phys. Rev. D*, vol. 84, p. 084010, 2011, 1101.0931.

[112] G. Amelino-Camelia, N. Loret, and G. Rosati, "Speed of particles and a relativity of locality in κ-Minkowski quantum spacetime," *Phys. Lett. B*, vol. 700, pp. 150–156, 2011, 1102.4637.

[113] S. Mignemi and G. Rosati, "Physical velocity of particles in relativistic curved momentum space," *Mod. Phys. Lett. A*, vol. 35, no. 22, p. 2050180, 2020, 1909.09173.

[114] M. Rodriguez Martinez and T. Piran, "Constraining Lorentz violations with gamma-ray bursts," *JCAP*, vol. 04, p. 006, 2006, astro-ph/0601219.

[115] C. Pfeifer, "Redshift and lateshift from homogeneous and isotropic modified dispersion relations," *Phys. Lett. B*, vol. 780, pp. 246–250, 2018, 1802.00058.

[116] U. Jacob and T. Piran, "Lorentz-violation-induced arrival delays of cosmological particles," *JCAP*, vol. 01, p. 031, 2008, 0712.2170.

[117] J. R. Ellis, N. E. Mavromatos, D. V. Nanopoulos, and A. S. Sakharov, "Quantum-gravity analysis of gamma-ray bursts using wavelets," *Astron. Astrophys.*, vol. 402, pp. 409–424, 2003, astro-ph/0210124.

[118] N. Aghanim *et al.*, "Planck 2018 results. VI. Cosmological parameters," *Astron. Astrophys.*, vol. 641, p. A6, 2020, 1807.06209. [Erratum: Astron.Astrophys. 652, C4 (2021)].

[119] A. Marciano, G. Amelino-Camelia, N. R. Bruno, G. Gubitosi, G. Mandanici, and A. Melchiorri, "Interplay between curvature and Planck-scale effects in astrophysics and cosmology," *JCAP*, vol. 06, p. 030, 2010, 1004.1110.

[120] G. Amelino-Camelia, A. Marciano, M. Matassa, and G. Rosati, "Deformed Lorentz symmetry and relative locality in a curved/expanding spacetime," *Phys. Rev. D*, vol. 86, p. 124035, 2012, 1206.5315.

[121] G. Amelino-Camelia, L. Smolin, and A. Starodubtsev, "Quantum symmetry, the cosmological constant and Planck scale phenomenology," *Class. Quant. Grav.*, vol. 21, pp. 3095–3110, 2004, hep-th/0306134.

[122] L. Barcaroli and G. Gubitosi, "Kinematics of particles with quantum-de Sitter-inspired symmetries," *Phys. Rev. D*, vol. 93, no. 12, p. 124063, 2016, 1512.03462.

[123] I. P. Lobo, N. Loret, and F. Nettel, "Investigation of Finsler geometry as a generalization to curved spacetime of Planck-scale-deformed relativity in the de Sitter case," *Phys. Rev. D*, vol. 95, no. 4, p. 046015, 2017, 1611.04995.

[124] G. Amelino-Camelia, G. Rosati, and S. Bedić, "Phenomenology of curvature-induced quantum-gravity effects," *Phys. Lett. B*, vol. 820, p. 136595, 2021, 2012.07790.

[125] P. Aschieri, A. Borowiec, and A. Pacho, "Dispersion relations in κ-noncommutative cosmology," *JCAP*, vol. 04, p. 025, 2021, 2009.01051.

[126] E. Bianchi and C. Rovelli, "A Note on the geometrical interpretation of quantum groups and non-commutative spaces in gravity," *Phys. Rev. D*, vol. 84, p. 027502, 2011, 1105.1898.

[127] A. Ballesteros, F. Herranz, M. Olmo, and M. Santander, "Quantum (2 + 1) kinematical algebras: A global approach," *Journal of Physics A Mathematical and General*, vol. 27, pp. 1283–1297, 02 1994.

[128] A. Ballesteros, F. J. Herranz, C. Meusburger, and P. Naranjo, "Twisted (2+1) κ-AdS Algebra, Drinfel'd Doubles and Non-Commutative Spacetimes," *SIGMA*, vol. 10, p. 052, 2014, 1403.4773.

[129] A. Ballesteros, G. Gubitosi, I. Gutiérrez-Sagredo, and F. J. Herranz, "Curved momentum spaces from quantum (anti–)de Sitter groups in (3+1) dimensions," *Phys. Rev. D*, vol. 97, no. 10, p. 106024, 2018, 1711.05050.

[130] G. Rosati, "κ–de Sitter and κ-Poincaré symmetries emerging from Chern-Simons (2+1)D gravity with a cosmological constant," *Phys. Rev. D*, vol. 96, no. 6, p. 066027, 2017, 1706.02868.

[131] H. Xu and B.-Q. Ma, "Light speed variation from gamma ray burst GRB 160509A," *Phys. Lett. B*, vol. 760, pp. 602–604, 2016, 1607.08043.

[132] G. Amelino-Camelia, G. D'Amico, G. Rosati, and N. Loret, "In-vacuo-dispersion features for GRB neutrinos and photons," *Nature Astron.*, vol. 1, p. 0139, 2017, 1612.02765.

[133] G. Amelino-Camelia, M. G. Di Luca, G. Gubitosi, G. Rosati, and G. D'Amico, "Could quantum gravity slow down neutrinos?," *Nature Astron.*, vol. 7, no. 8, pp. 996–1001, 2023, 2209.13726.

[134] G. Amelino-Camelia, D. Guetta, and T. Piran, "Icecube Neutrinos and Lorentz Invariance Violation," *Astrophys. J.*, vol. 806, no. 2, p. 269, 2015.

[135] H.-N. Lin, X. Li, and Z. Chang, "Gamma-ray burst polarization reduction induced by the Lorentz invariance violation," *Mon. Not. Roy. Astron. Soc.*, vol. 463, no. 1, pp. 375–381, 2016, 1609.00193.

[136] M. Piersanti, P. Ubertini, R. Battiston, A. Bazzano, G. D'Angelo, J. G. Rodi, P. Diego, Z. Zeren, R. Ammendola, D. Badoni, *et al.*, "Evidence of an upper ionospheric electric field perturbation correlated with a gamma ray burst," *nature communications*, vol. 14, no. 1, p. 7013, 2023.

[137] G. Amelino-Camelia, G. D'Amico, F. Fiore, S. Puccetti, and M. Ronco, "In Vacuo Dispersion-Like Spectral Lags in Gamma-Ray Bursts," *Symmetry*, vol. 13, no. 4, p. 541, 2021, 1707.02413.

[138] P. D'Avanzo, "Short gamma-ray bursts: A review," *Journal of High Energy Astrophysics*, vol. 7, pp. 73–80, 2015. Swift 10 Years of Discovery, a novel approach to Time Domain Astronomy.

[139] T. Piran, "The physics of gamma-ray bursts," *Rev. Mod. Phys.*, vol. 76, pp. 1143–1210, 2004, astro-ph/0405503.

[140] V. A. Acciari *et al.*, "Observation of inverse Compton emission from a long γ-ray burst," *Nature*, vol. 575, no. 7783, pp. 459–463, 2019, 2006.07251.

[141] D. Miceli and L. Nava, "Gamma-Ray Bursts Afterglow Physics and the VHE Domain," *Galaxies*, vol. 10, no. 3, p. 66, 2022, 2205.12146.

[142] U. Jacob and T. Piran, "Neutrinos from gamma-ray bursts as a tool to explore quantum-gravity-induced Lorentz violation," *Nature Phys.*, vol. 3, pp. 87–90, 2007, hep-ph/0607145.

[143] R. C. Myers and M. Pospelov, "Ultraviolet modifications of dispersion relations in effective field theory," *Phys. Rev. Lett.*, vol. 90, p. 211601, 2003, hep-ph/0301124.

[144] H. Xu and B.-Q. Ma, "Light speed variation from gamma-ray bursts," *Astropart. Phys.*, vol. 82, pp. 72–76, 2016, 1607.03203.

Appendix A

A.1 Numerical construction of semi-classical states

In this appendix we discuss the construction of semi-classical states discussed in chapter 4. In order to construct such states, we have resorted to numerical computations, focusing on the case $q = 0.99$ as illustrative example. However, by increasing the value of q, we have checked that the below states satisfy the condition (4.39), thus approximating classical rotations with increasing precision.

We will focus on the (y, z)-plane setting $\chi = 0$, $\phi = \frac{\pi}{2}$, as can be seen from (4.9). We want to construct states that semi-classically describe a deformed rotation of a certain angle in this plane. Since n defines the only angle left, θ, we choose to build superpositions (4.41) centered on particular values of n, dubbed $\bar{n}$, with coefficients c_n multiplying the states $|n, \phi, \chi\rangle$ rapidly decreasing as $\theta(n)$ deviates from $\theta(\bar{n})$. Our ansatz is that these coefficients have the form of a discretized Gaussian distribution.

The variance is then chosen in the following way. Recalling that

$$\theta(n) = 2 \arcsin q^n \tag{A.1}$$

we can define $\Delta\bar{n}$ as

$$\Delta\bar{n} := \frac{dn}{d\theta}\Big|_{\theta(\bar{n})} \Delta\theta \,. \tag{A.2}$$

We take $\Delta\theta = \frac{\pi}{2} - \arcsin q$, which is just half of the value of the maximum angular deviation and weigh it with the rate of change of n with respect to θ, approximated as the derivative. Therefore, the value of the variance depends on the central value $\bar{n}$. This approximation becomes more and more accurate with increasing values of n for which $\theta(n)$ becomes quasi-continuous.

We then define our superposition coefficients c_n as

$$c_n = \frac{e^{-\frac{(\bar{n}-n)^2}{2\Delta\bar{n}^2}}}{\sum_{n=0}^{\infty} e^{-\frac{(\bar{n}-n)^2}{2\Delta\bar{n}^2}}} \,. \tag{A.3}$$

For computational reasons, we do not consider the full superposition going from $n = 0$ to $n = \infty$ but we truncate the series by considering the 3-σ range of our Gaussian. Namely, the sum goes from $n_{\min}$ to $n_{\max}$, where

$$n_{\min} - \bar{n} = -3\Delta\bar{n} \qquad n_{\max} - \bar{n} = 3\Delta\bar{n} \,. \tag{A.4}$$

For relatively small values of $\bar{n}$, the value for $n_{\min}$ might be negative when considering the 3-σ range. When this happens, we simply truncate the Gaussian and start the series from $n = 0$. We have explicitly verified that this doesn't affect our results in a significant way.

We have used this algorithm to construct the states used for the numerical analysis of table 4.1. In what follows, we show the results for the computation of the expectation values of the matrix elements $(R_q)_{ij}$ with their relative uncertainties for states centered around $n = 95, 34, 7, 0$, corresponding to angles $\theta = 45.275°, 90.560°, 137.518°, \theta = 180°$.

- $n = 95$, $\theta = 45.275°$

$$\begin{aligned} \langle\psi(45.275°)|R_q|\psi(45.275°)\rangle &= \begin{pmatrix} 0.997 & 0.000 & 0.000 \\ 0.000 & 0.695 & 0.708 \\ 0.000 & -0.708 & 0.698 \end{pmatrix} \\ \Delta R_q &= \begin{pmatrix} 0.005 & 0.071 & 0.030 \\ 0.071 & 0.073 & 0.069 \\ 0.030 & 0.069 & 0.073 \end{pmatrix} \end{aligned} \tag{A.5}$$

- $n = 34$, $\theta = 90.560°$

$$\begin{aligned} \langle\psi(90.560°)|R_q|\psi(90.560°)\rangle &= \begin{pmatrix} 0.990 & 0.000 & 0.000 \\ 0.000 & -0.015 & 0.990 \\ 0.000 & -0.990 & -0.005 \end{pmatrix} \\ \Delta R_q &= \begin{pmatrix} 0.015 & 0.100 & 0.100 \\ 0.100 & 0.099 & 0.004 \\ 0.100 & 0.004 & 0.100 \end{pmatrix} \end{aligned} \tag{A.6}$$

- $n = 7$, $\theta = 137.518°$

$$\langle\psi(137.518°)|R_q|\psi(137.518°)\rangle = \begin{pmatrix} 0.982 & 0.000 & 0.000 \\ 0.000 & -0.739 & 0.663 \\ 0.000 & -0.663 & -0.721 \end{pmatrix}$$
$$\Delta R_q = \begin{pmatrix} 0.025 & 0.067 & 0.173 \\ 0.067 & 0.067 & 0.074 \\ 0.173 & 0.074 & 0.067 \end{pmatrix} \tag{A.7}$$

- n=0, $\theta = 180°$

$$\langle\psi(180°)|R_q|\psi(180°)\rangle = \begin{pmatrix} 0.99 & 0 & 0 \\ 0 & -0.99 & 0 \\ 0 & 0 & -0.99 \end{pmatrix}$$
$$\Delta R_q = \begin{pmatrix} 0.014 & 0.014 & 0.140 \\ 0.014 & 0.014 & 0.140 \\ 0.140 & 0.140 & 0 \end{pmatrix} . \tag{A.8}$$

To obtain the states describing q-deformations of rotations of negative angles $\zeta < 0$, we just have to consider the same states but with $\phi = -\frac{\pi}{2}$. It is straightforward to show that for states of the form (4.41) with $\chi = 0$ having real superposition coefficients like (A.3), the map $\phi \mapsto -\phi$ exchanges $(R_q)_{23}$ with $(R_q)_{32}$, leaving all the other elements unchanged, and yields the same uncertainty matrix. Therefore the aperture of the cone in table 4.1 is the same for opposite angles.

For the $\theta = 0$ case, we use the state in the representation ρ which gives the identity matrix in computing the expectation values which is simply given by $|\chi = 0\rangle \in \mathcal{H}_\rho$. From (4.40) we thus have

$$\langle\psi(0°)|R_q|\psi(0°)\rangle = \mathbb{1}_{3\times3} \qquad \Delta R_q = \mathbf{0}_{3\times3} . \tag{A.9}$$

A.2 Representation ρ as limit of representation π

By adding a phase to the representation π discussed in the mathematical literature [91] we have

$$\rho(a)\,|\chi\rangle = e^{i\chi}\,|\chi\rangle \qquad \rho(a^*)\,|\chi\rangle = e^{-i\chi}\,|\chi\rangle \qquad \rho(c)\,|\chi\rangle = \rho(c^*)\,|\chi\rangle = 0 \tag{A.10}$$

$$\pi(a)\,|n,\phi,\epsilon\rangle = e^{i\epsilon}\cos\left(\frac{\theta(n)}{2}\right)|n-1,\phi,\epsilon\rangle \tag{A.11}$$

$$\pi(c)\,|n,\phi,\epsilon\rangle = e^{i\phi}\sin\left(\frac{\theta(n)}{2}\right)|n,\phi,\epsilon\rangle \tag{A.12}$$

$$\pi(a^*)\,|n,\phi,\epsilon\rangle = e^{-i\epsilon}\sqrt{1-q^2\cos^2\left(\frac{\theta(n)}{2}\right)}\,|n+1,\phi,\epsilon\rangle \tag{A.13}$$

$$\pi(c^*)\,|n,\phi,\epsilon\rangle = e^{-i\phi}\sin\left(\frac{\theta(n)}{2}\right)|n,\phi,\epsilon\rangle$$

with our definition of quantized angle, $\theta(n) = 2\arcsin q^n$. Looking at these equations, it may seem that we have four Euler angles in the representations of $SU_q(2)$, namely the aforementioned $(\chi,\epsilon,\phi,\theta(n))$. This is a subtlety solved by observing that, with the additional ϵ phase that we introduced in the π-representation, the representation ρ can be obtained as a somewhat trivial limit of representation π. Therefore, we have three physical degrees of freedom, with the angles χ and ϵ linked by this limit operation, so that we can ultimately set $\epsilon = \chi$.

To see this, we need to find a class of states such that

$$\pi(a)\,|\psi(\chi)\rangle \to e^{i\chi}\,|\psi(\chi)\rangle \qquad , \qquad \pi(c)\,|\psi(\chi)\rangle \to 0 \tag{A.14}$$

in this limit. We can show that states of the type (with the identification $\epsilon = \chi$)

$$|\psi_n\rangle = \frac{1}{\sqrt{n+1}}\sum_{k=n}^{2n}|k,\phi,\chi\rangle \tag{A.15}$$

from the π-representation satisfy requirement (A.14) for $n \to \infty$.

In fact, for the operator c we can immediately see that

$$\pi(c)\,|\psi_n\rangle = e^{i\phi}\frac{1}{\sqrt{n+1}}\sum_{k=n}^{2n}q^k\,|k,\phi,\chi\rangle \tag{A.16}$$

and therefore, since q is slightly less than one

$$\langle\psi_n|\pi(c^*)\pi(c)|\psi_n\rangle = \frac{1}{n+1}\frac{q^{2n}\left(1-q^{2n+2}\right)}{1-q^2} \to 0, \qquad n\to\infty. \tag{A.17}$$

Hence, $\pi(c)\,|\psi_n\rangle \xrightarrow{n\to\infty} 0$. The limit for the operator a is more subtle; in this case we have that

$$\pi(a)\,|\psi_n\rangle = \frac{e^{i\chi}}{\sqrt{n+1}}\sum_{k=n}^{2n}\sqrt{1-q^{2k}}\,|k-1,\phi,\chi\rangle \tag{A.18}$$

and we consider the difference

$$|\psi_n'\rangle = \pi(a)\,|\psi_n\rangle - e^{i\chi}\,|\psi_n\rangle\ . \tag{A.19}$$

To show that the limit $\pi(a)\,|\psi_n\rangle \to e^{i\chi}\,|\psi\rangle$ holds we will show that the succession of the norms of the states in (A.19) has 0 limit. We have that

$$\begin{aligned} 0 \ &\leq\ \langle\psi_n'\rangle = \langle\psi_n|\pi(a^*)\pi(a)|\psi_n\rangle + \langle\psi_n\rangle - 2\,\mathrm{Re}\big\{e^{i\chi}\,\langle\psi_n|\pi(a^*)|\psi_n\rangle\big\} = \\ &=\ 1+\frac{1-q^{2n}}{n+1} - \frac{1}{n+1}\sum_{k=n+1}^{2n}\left[2\sqrt{1-q^{2k}} - \left(1-q^{2k}\right)\right] \leq \\ &\leq\ 1+\frac{1}{n+1} - \frac{1}{n+1}\sum_{k=n+1}^{2n}\left(1-q^{2k}\right) = \frac{1}{n+1}\left[2-q^{2n+2}\frac{1-q^{2n}}{1-q^2}\right] \xrightarrow{n\to\infty} 0. \end{aligned} \tag{A.20}$$

This observation that representation π converges for certain states to representation ρ can be extended to generic functions of operators. In general, such functions can be written as a sum of powers of the operators $\pi(a)$, $\pi(a^*)$, $\pi(c)$ and $\pi(c^*)$. We now prove that these functions acting on a class of states in representation π give, in a certain limit, the value that the same function yields in the limit of these sates with $\pi(a)$ replaced by $\rho(a)$ and so on.

In order to do so, we consider a slightly different class of states than the one in (A.15). In particular we consider

$$|\Psi_n\rangle = \frac{1}{\sqrt{n!+1}}\sum_{k=n!}^{2n!}|k,\phi,\chi\rangle\ . \tag{A.21}$$

The reason why we make this choice with the factorial will be clear in the following.

Consider first the case in which we have an operator of the form $\pi(c)^m\pi(a)^l$. If we act with this operator on the state (A.21) and we compute the norm of the state obtained in this way we get

$$0 \leq \langle \Psi_n | \pi(a^*)^l \pi(c^*)^m \pi(c)^m \pi(a)^l | \Psi_n \rangle \leq \frac{q^{2m(n!-l)}\left[1 - q^{2m(n!+1)}\right]}{(1-q^{2m})(n!+1)} \xrightarrow[m\neq 0]{n\to\infty} 0\,. \tag{A.22}$$

The same argument holds if we have only powers of the operator $\pi(c)$ (i.e, $l = 0$) or other combinations involving $\pi(a^*)$, $\pi(c^*)$ and different orderings. The case with $m = 0$, in which the limit above is 1, corresponds to a power of $\pi(a)$ which will be handled slightly differently in the following.

Now we turn to powers of the operator $\pi(a)$, i.e $\pi(a)^m$. We do something analogous to the argument used for $\pi(a)$, namely we define the difference state

$$|\Psi'_n\rangle = \pi(a)^m |\Psi_n\rangle - e^{im\chi} |\Psi_n\rangle \tag{A.23}$$

and show its norm goes to zero as $n \to \infty$. After some algebraic manipulations, this norm is found to satisfy

$$0 \leq \langle \Psi'_n \rangle \leq \frac{2m}{n!+1} + \frac{1}{n!+1} \sum_{k=n!+m}^{2n!} \left[q^{l(l+1)} q^{2kl} (-1)^l \left(q^{-2k}; q^2\right)_l - 1\right] \overset{n\to\infty}{\longrightarrow} 0\,, \tag{A.24}$$

where $\left(q^{-2k}; q^2\right)_l := \prod_{s=0}^{l-1} \left(1 - q^{-2k+2s}\right)$ is the q-Pochhammer symbol. The result of the limit comes from the fact that the term in the square brackets above is essentially just a sum of powers of q.

We have thus shown that a generic function of $\pi(a)$ and $\pi(c)$ operators applied to (a class of) states in the π representation converges to the same function applied to a state in ρ representation (a similar argument holds for functions of $\pi(a^*)$ and $\pi(c^*)$ operators). The reason why we considered a state of the form (A.21) is now clear: it is necessary to have a number of states in the superposition which goes to infinity faster than m does in order to properly do the limit when considering generic functions, in which case we have a series in m.

The states (A.15) can be used also to show directly for the vectorial (co)-representation that it is possible to obtain the rotations about the z-axis as a limit in the representation π. In the same way, it is possible to obtain the identity, i.e. the null rotation, in the same representation.

To obtain a rotation about the z-axis, we must have $\phi = 0$ and we have to consider the large n limit. In this limit, setting $\phi = 0$, we can approximate our π representation

as

$$\pi(a)\,|n,\phi,\chi\rangle = e^{i\chi}\,|n-1,\phi,\chi\rangle \qquad \pi(c)=\pi(c^*)=0 \qquad \pi(a^*)\,|n,\phi,\chi\rangle = e^{-i\chi}\,|n+1,\phi,\chi\rangle\ . \tag{A.25}$$

Therefore, using the states (A.15), we obtain

$$\langle\psi|R_q|\psi\rangle = \begin{pmatrix} \frac{-1+n}{1+n}\cos\chi & \frac{-1+n}{1+n}\sin\chi & 0 \\ -\frac{-1+n}{1+n}\sin\chi & \frac{-1+n}{1+n}\cos\chi & 0 \\ 0 & 0 & 1 \end{pmatrix}\ . \tag{A.26}$$

In the large n limit, we see that (A.26) approximates a rotation matrix around the z-axis with greater and greater precision and it can be shown that the variances are equal to 0. Moreover, $\chi = 0$ in (A.26) gives the identity matrix in the limit of large n.

Appendix B

B.1 Monotonicity in the curvature induced scenario

In this appendix we want to investigate the monotonicity of the time delay expression as a function of the redshift distance when we restrict our focus to the curvature induced scenario. For this purpose we must check if it is possible for the derivative of the time delay with respect to the redshift parameter z to never change sign. Starting from the expression of the time delay in the curvature induced case (5.39), that we report here for completeness:

$$\Delta t = \frac{\Delta E}{E_p}\int_0^z \frac{d\overline{z}\,(1+\overline{z})}{H\,(\overline{z})}\left[\,\eta_2\left(1-\left(1-\frac{H\,(\overline{z})}{1+\overline{z}}\int_0^{\overline{z}}\frac{d\overline{z}'}{H\,(\overline{z}')}\right)^2\right) + \eta_3\left(1-\left(1-\frac{H\,(\overline{z})}{1+\overline{z}}\int_0^{\overline{z}}\frac{d\overline{z}'}{H\,(\overline{z}')}\right)^4\right)\right]. \tag{B.1}$$

we have to impose that $\frac{d\Delta t}{dz}$, given by

$$\frac{d\Delta t}{dz} = \frac{\Delta E}{E_p}\frac{(1+z)}{H\,(z)}\left[\,\eta_2\left(1-\left(1-\frac{H\,(z)}{1+z}\int_0^{z}\frac{d\overline{z}'}{H\,(\overline{z}')}\right)^2\right) + \eta_3\left(1-\left(1-\frac{H\,(z)}{1+z}\int_0^{z}\frac{d\overline{z}'}{H\,(\overline{z}')}\right)^4\right)\right], \tag{B.2}$$

never changes sign (≥ 0 or ≤ 0 for every z).
By introducing $\left(1-\frac{H(z)}{z}\int_0^z\frac{d\overline{z}'}{H(\overline{z}')}\right) = x$ we can rewrite (B.2) as:

$$\frac{d\Delta t}{dz} = \frac{\Delta E}{E_p}\frac{(1+z)}{H\,(z)}\left(\eta_2(1-x^2)+\eta_3(1-x^4)\right) \tag{B.3}$$

which is always positive or always negative if and only if $\eta_2 = -2\eta_3$.
We can also see this by considering a numerical analysis for the ΛCDM model described in chapter 5. We illustrate this in Figure B.1 by fixing $\eta_3 = -1$. The blue area identifies the values of η_2 such that $\frac{d\Delta t}{dz} \geq 0$. We can observe that only when $\eta_2 = 2$ the derivative

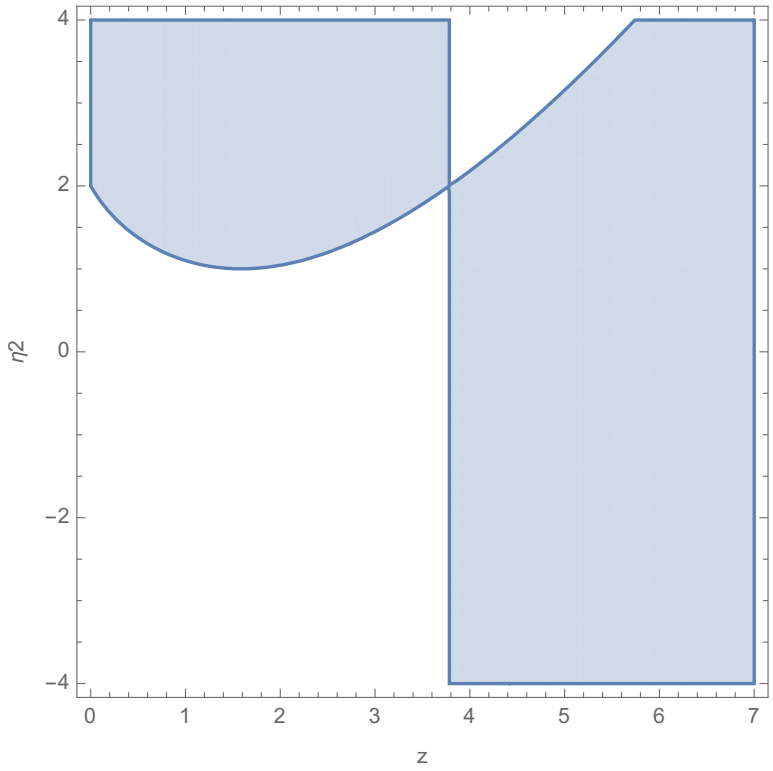

Figure B.1: The blue area identifies the values of η_2 such that $\frac{d\Delta t}{dz} \geq 0$ when $\eta_3 = -1$.

of the time delay with respect the redshift parameter z never changes sign.